Assessment of Bridge Foundations for Reuse

A Dissertation

Submitted by

Nathan T. Davis

In partial fulfillment of the requirements for the degree of

Doctor of Philosophy

in

Civil and Environmental Engineering

Tufts University

August 2018

Committee:

Dr. Masoud Sanayei (Chair)

Dr. Anil Agrawal

Dr. Babak Moaveni

Dr. Lucy Jen

Dr. Hasan Abedi

Tufts
UNIVERSITY

ARTS, SCIENCES, AND ENGINEERING

CERTIFICATE OF FITNESS

This certifies that the undersigned, appointed to determine the fitness of

Nathan Davis

for the degree of Doctor of Philosophy in Civil and Environmental Engineering

have examined the candidate's thesis/dissertation (or papers) on the subject:

Assessment of Bridge Foundations for Reuse

and have found it satisfactory.

July 12th 2018
Date of Defense

This certifies further that the candidate this day has successfully passed the customary examination.
We recommend, therefore, that the degree be awarded under the usual conditions.

SIGNATURES	NAMES
Masoud Sanayei	Dr. Masoud Sanayei
Chairperson, Examining Committee	*Chairperson, Examining Committee*
	Dr. Babak Moaveni
	Dr. Lucy Jen
Hasan Abedi	Dr. Hasan Abedi

Student Services
Dowling Hall
Medford, Massachusetts 02155
617.627.2000

Tufts
UNIVERSITY

ARTS, SCIENCES, AND ENGINEERING

CERTIFICATE OF FITNESS

This certifies that the undersigned, appointed to determine the fitness of

Nathan Davis

for the degree of Doctor of Philosophy in Civil and Environmental Engineering

have examined the candidate's thesis/dissertation (or papers) on the subject:

Assessment of Bridge Foundations for Reuse

and have found it satisfactory.

7/12/2018

Date of Defense

This certifies further that the candidate this day has successfully passed the customary examination.
We recommend, therefore, that the degree be awarded under the usual conditions.

SIGNATURES	NAMES
	Dr. Masoud Sanayei
Chairperson, Examining Committee	*Chairperson, Examining Committee*
Anil Kumar Agrawal	Dr. Anil Agrawal

Student Services
Dowling Hall
Medford, Massachusetts 02155
617.627.2000

Acknowledgements

I would like to start by thanking my family for their undying love and support of me and for always encouraging me to achieve my best. I would like to thank Kate Munson for her encouragement and patience during these last several years. To all my other friends who have supported me and listened to me rant about rebar — thank you. I would also like to thank my officemates and classmates throughout the years, who have made it a pleasure to come into work and have helped me grow as an engineer and an academic. I would like to thank Ehssan Hoomaan, with whom I worked closely throughout my PhD tenure. Ehssan, you have provided much needed insight, organization, and dedication to this project over the last several years.

I would like to thank the many professors I have had throughout my academic career at Tufts and at UMass for building my understanding of the engineering field while inspiring curiosity and interest in the field. Most importantly, my advisor, Dr. Masoud Sanayei has been a dedicated and caring advisor, teacher, and mentor to me throughout my time at Tufts. Without your belief in my abilities and constant attention, I would not have achieved what I have at Tufts or taken away as much from it as I did. To the rest of my committee — Dr. Anil Agrawal, Dr. Babak Moaveni, Dr. Lucy Jen, and Dr. Hasan Abedi, thank you for agreeing to serve on my committee and providing valuable insight into my research.

The research performed for the dissertation was funded through the Foundation Characterization Program of Federal Highway administration, contract no. DTFH61-14-D-00010/0002, under the guidance of Mr. Frank Jalinoos and PI Anil Agrawal. I would like to especially thank Mr. Jalinoos and Dr. Agrawal for their financial support, guidance, and encouragement throughout the last several years.

Contents

Certificate of Fitness ii
Acknowledgements iv
Contents v
Figures viii
Tables x
Chapter 1 Executive Summary 1
1.1 Overview 1
1.2 Societal Needs for the US Highway Bridge System 2
1.3 Foundation Reuse for Highway Bridges 2
1.4 Research Needs and Goals for Foundation Reuse 4
1.5 Roadmap to this Research 5
1.6 References 6
Chapter 2 Foundation Reuse in ABC 8
Abstract 9
2.1 Introduction 9
2.2 Definition of Foundation Reuse 12
2.3 Motivations for Foundation Reuse 16
2.4 Foundation Reuse in ABC Projects 18
2.5 Reuse Decision Model 20
2.6 Assessment 21
Desk Study 22
Integrity Assessment 22
Durability Assessment 25
Capacity Assessment 26
2.7 Foundation Strengthening 27
2.8 Innovative Materials 29
2.9 Foundation Reuse Case Histories 30
Hurricane Deck Bridge Replacement, MO (Option 1) 31
Fast-14 Replacement Project, MA (Option 3) 32
I-95 Corridor Replacement Project, VA (Option 3 and 4) 33
Huey P. Long Bridge, LA (Option 4) 34
Milton Madison Bridge, IN/KY (Option 4) 36
Mississagi River Bridge, ON, Canada (Option 4) 40
2.10 Conclusions 41
2.11 Acknowledgements 42
2.12 References 43
Chapter 3 Foundation Identification Using Dynamic Strain and Acceleration Measurements 45
Abstract 46
3.1 Introduction 46
3.2 Proposed Method for Estimation of Foundation Stiffness Parameters 49
Loading Source 49
Free Body Diagram of Foundation 50
Instrumentation Setup 51

Response of FBD to Loading 56
Foundation Modeling 59
3.3 Automated Event Selection 61
Event Separation 62
Event Frequency Selector 63
Window Selector 64
Estimation of Frequency Response Function 65
3.4 Validation of Proposed Method 68
Powder Mill Bridge 68
Sensors and Data Acquisition Equipment 70
Event Separation 72
Frequency Identification 75
Window Selection 76
Averaging Frequency Bins 78
Estimation of Foundation Stiffness Parameters 79
3.5 Conclusions 81
3.6 Future Work 82
3.7 References 83
Chapter 4 Load Rating of Existing Foundations 85
Abstract 86
4.1 Introduction 86
4.2 Background 88
4.3 Impact of Substructure Movement on Load Rating 90
4.4 Literature Review 91
4.5 Proposed Methodology 94
Superstructure Load Rating Considering Substructure Movement 96
Substructure Load Rating 97
Substructure Functionality Index (SFI) 103
Modeling Techniques 105
4.6 Field Examples 106
Three-Span Continuous Steel Girder Bridge 107
Three-Span Prestressed Concrete Simple Span Bridge 114
4.7 Conclusions and Future Work 120
4.8 Acknowledgements 121
4.9 References 121
Chapter 5 Existing Pile Capacity 124
Abstract 125
5.1 Introduction 125
5.2 Background 127
5.3 Proposed Methodology 131
5.4 Distribution of Individual Pile Capacity 133
5.5 Population Capacity Distribution 134
5.6 Updating Population Mean Capacity Distribution 136
5.7 Bayesian Updating of the Pile Capacity Distribution 137
5.8 Determining a New Resistance Factor 140

5.9 Impact of Uncertainty in Previously Applied Loading 143
5.10 Application of Findings to LRFD Code 145
5.11 Determining Capacity without prior distribution 148
5.12 Examples 152
Route 2A Bridge: Haynesville, ME 152
Jackson Road over Route 2: Lancaster, MA 154
Route 1A Viaduct, Bath ME 155
5.13 Conclusions 156
5.14 Future Work 157
5.15 Acknowledgements 157
5.16 References 157
Chapter 6 Conclusions 160
6.1 Overarching Research Conclusions for Foundation Reuse 160
6.2 Contributions of Research in Foundation Reuse 160
6.3 Future Work 162
6.4 References 163
Appendix A 164
Appendix B 167

Figures

Figure 2-1: Applications for Foundation Reuse (data from Boeckmann and Loehr 2017) 12
Figure 2-2. Foundation reconstruction options, courtesy of FHWA 14
Figure 2-3. Survey on motivations for foundation reuse (data from Boeckmann and Loehr 2017) 18
Figure 2-4: Wireline logging from willow valley bridge 24
Figure 2-5. I-95 Bridge over Overbrook Road Showing Underside after renovation, courtesy of VDOT 34
Figure 2-6: Huey P. Long Bridge with widened superstructure, courtesy of Modjeski and Masters, Inc. 35
Figure 2-7: Above water image (left) and sonar image (right) of a s bridge pier 36
Figure 2-8. Milton Madison Bridge prior to renovation, courtesy Michael Baker International . 37
Figure 2-9. (a) Coring of caisson concrete from inside of cofferdam. (b) Insertion of reinforcement, photos courtesy of Michael Baker International 39
Figure 2-10. Milton Madison Bridge after renovation, courtesy of Michael baker International 39
Figure 2-11. Micropile installation through bridge deck with casing down pier face, courtesy of CSCE 41
Figure 3-1: A free body diagram of a foundation 51
Figure 3-2: Strain gauge setup for force and moment determination from column 52
Figure 3-3: Measured (a) strains and (b) accelerations from pier column 53
Figure 3-4: Diagram of various foundations represented by spring constants 59
Figure 3-5: Powder Mill Bridge (PMB) in Barre, MA 69
Figure 3-6: Southern interior pier during construction 70
Figure 3-7: Instrumentation setup at the PMB on the (a) south and (b) north sides of the column 71
Figure 3-8: School bus crossing the PMB over the instrumented pier 72
Figure 3-9: Typical measured acceleration time history with corresponding 1-second variance. 73
Figure 3-10: Calculated (a) vertical force, (b) horizontal force, and (c) bending moment during event 74
Figure 3-11: Calculated accelerations at top of FBD for a) Vertical Acceleration, b) Horizontal Acceleration, and c) Rotational Acceleration 75
Figure 3-12: Magnitude-squared coherence for a truck recording 76
Figure 3-13: Vertical acceleration STFT during vehicle passage 77
Figure 3-14: Vertical force STFT during vehicle passage 78
Figure 3-15: Horizontal FRF data identifying selected and discarded data, as well as the average calculated for each frequency 79
Figure 3-16: Measured (a) vertical, (b) horizontal, (c), rotational, and (d) cross FRFs versus best fit analytical FRF 81
Figure 4-1: Path traveled between permanent loading and failure surface 102
Figure 4-2: Live load loading path when stress reversal is present (a) in P_U-M_U space, and (b) in M_X-M_Y space 103
Figure 4-3: (a) Google Earth image of I-275 Bridge, and (b) *CSiBridge* model of I-275 Bridge 108

Figure 4-4: Rating factors for girders with no settlement, settlement scenario 1, and settlement scenario 2 for each girder in poor condition 110
Figure 4-5: Load Rating of PC2 with no settlement 112
Figure 4-6: Load rating of PC2 during (a) settlement, and (b) settlement, rotation, and translation 112
Figure 4-7: (a) SR 595 bridge, and (b) SR 595 bridge model with piles cut off at ground elevation 115
Figure 4-8: Moment demands from various load cases 117
Figure 5-1: Distribution of ultimate pile capacity given a nominal capacity calculated using the β-method 134
Figure 5-2: Three possible population mean distributions. 135
Figure 5-3: Distribution of population mean given (a) a pile with 15% of the nominal capacity, and (b) a pile with 30% of the nominal capacity. 137
Figure 5-4: Distributions shown in Figures 3a and 3b with a past loading of 20% of the nominal capacity (a and b), and 30% of the nominal capacity (c and d). 139
Figure 5-5: Original and updated distribution for pile subjected to previous loading. 140
Figure 5-6: Updated Resistance Factor, ϕ, versus the largest load supported by pile group 142
Figure 5-7: New resistance factor using varying site COVs 143
Figure 5-8: Updated resistance factors for test loads of various biases and variances 144
Figure 5-9: Updating curve for piles with capacities calculated using alpha method (site COV = 0.15) 146
Figure 5-10: LL capacity of existing piles for various site COVs 150
Figure 5-11: LL capacity as function of proof load for various magnitudes of DL replacement 151
Figure 5-12: LL capacity of piles given changes to DL 152
Figure 5-13: New factored capacity as a function of maximum past loading 153
Figure 5-14: Updated resistance factors based on past loading 155
Figure 5-15: Capacity versus test load for Pier 5 156
Figure A0-1: Interaction diagram for uniaxial bending 165

Tables

Table 2-1: Survey responses grouped into sustainability categories 18
Table 2-2: Foundation replacement options found in FIU database 19
Table 2-3. Types of assessment and tasks involved for foundation reuse investigation (data from Agrawal et al. 2018) 22
Table 2-4. Example NDT methods for accessible concrete elements and their use (data from Agrawal et al. 2018) 23
Table 2-5. Main corehole logging technologies and their uses (data from Agrawal et al. 2018). 25
Table 2-6. Strengthening and repair options for concrete elements (data from Agrawal et al. 2018). 28
Table 2-7. Ground improvement technologies for foundation reuse (data from Agrawal et al. 2018). 29
Table 2-8: Selection of ABC Case Studies from Agrawal et al. (2018) 30
Table 2-9. Milton Madison Bridge - Tests performed, issues evaluated, extent and outcome of testing 37
Table 3-1: Values of parameters 80
Table 4-1: Empirical limits on vertical settlement (Data from Barker et al. 1991) 92
Table 4-2: Angular distortion limits in LRFD code (Data from AASHTO 2014) 93
Table 4-3: LRFD Load factors not typically used during LRFR load rating 98
Table 4-4: Load cases applicable to LRFR factors for substructures 99
Table 4-5: Girder negative moments over adjacent pier for Strength I load case including settlement loads 109
Table 4-6: Calculated factored loads without scour and with full scour 119
Table 4-7: Rating factors for the critical pile with varying scour 119
Table 4-8: Functionality index based on bearing pad deformation for three damage scenarios 120
Table 5-1: Bias and COV of load prediction 129
Table 5-2: Updated pile resistance factors for LRFD (low variability). 147
Table B0-1: Updated pile Resistance factors for LRFD (low variability) 167
Table B0-2: Updated pile Resistance factors for LRFD (medium variability) 167
Table B0-3: Updated pile Resistance factors for LRFD (high variability) 168

Chapter 1 Executive Summary

1.1 Overview

This dissertation presents research performed in support of the production of the report: *Foundation Reuse for Highway Bridges* (Agrawal et. al 2018). The production of this report was funded by an FHWA grant as part of the foundation characterization program (FCP). It provides an in-depth discussion on the state of the art for reuse of highway bridge foundations, including discussion on assessment techniques, capacity prediction, remaining service life prediction, strengthening, and planning for future reuse. While performing the research into the state of the art with foundation reuse, several unfulfilled research needs were identified related to the characterization of existing foundations and capacity evaluation for reuse applications. Novel research into load rating of existing foundations, capacity evaluation of existing driven piles, and characterization of existing pier/pile dynamic behavior was conducted and submitted for publication in peer-reviewed journals. In addition, a case study paper highlighting the advantages and challenges of foundation reuse in accelerated bridge construction (ABC) was published in a peer-reviewed article. Beyond the 4 technical journal articles published in support of this work, this work has been published in 5 conference proceedings (Agrawal et al. 2017; Davis and Sanayei 2018; Davis et al. 2017; Jalinoos et al. 2017; Sanayei and Davis 2016)and the following 9 presentations have been made at conferences:

Reliability-Based Assessment of In-Situ Pile Capacity May 2018
2018 Engineering Mechanics Institute Conference, Cambridge, MA

Identifying Bridge Foundation Systems from Operational Data for Reuse Apr. 2018
ASCE Structures Congress 2018, Fort Worth, TX

Reliability Analysis of Existing Bridge Foundations for Reuse Feb. 2018
IMAC XXXVI Conference & Exposition on Structural Dynamics, Orlando, FL

Load Assessment for Reuse (Workshop) Dec. 2017
2017 National Accelerated Bridge Construction Conference, Miami, FL

Reuse of Foundations of Existing Bridges *2017 National Accelerated Bridge Construction Conference, Miami, FL*	Dec. 2017
Reliability Analysis of Existing Bridge Deep Foundations for Reuse *ASCE Structures Congress 2017, Denver, CO*	Apr. 2017
Bridge Foundation Stiffness Identification *ASCE GeoStructures 2016, Phoenix, AZ*	Feb. 2016
Integrated Load Rating *TRB Annual Meeting 2016, Washington, D.C.*	Jan. 2016
Load Testing for Reuse of Lake Mary Bridge Foundation *TRB Annual Meeting 2015, Washington, D.C.*	Jan. 2015

1.2 Societal Needs for the US Highway Bridge System

According to FHWA statistics (FHWA 2018), at the end of 2017 there were 54,560 bridges in the United States that were either functionally obsolete or structurally deficient. Many of these deficient/obsolete bridges exist in constrained urban areas, on rural areas with a lack of alternative routes, or on important routes with significant traffic volume that cannot easily be rerouted. The backlog of obsolete and deficient bridges combined with limited DOT budgets necessitates creative solutions for renewal of the national transportation infrastructure.

1.3 Foundation Reuse for Highway Bridges

One method of reducing infrastructure costs that has emerged is the concept of foundation reuse. During foundation reuse, the superstructure is replaced while the existing foundation is reused in part or in full. Reuse of existing foundation elements allows for potential savings on foundation construction costs, limits the time associated with foundation construction and facilitates rapid renewal of infrastructure, and lowers material usage for foundation elements. Despite these benefits, there are many considerations when reusing foundation elements that are not typically considerations during new construction of elements. Due to the potential benefits and

identified challenges, the FHWA started the foundation characterization program (FCP) to address and better understand this emerging field.

The FCP was initiated in 2013 to address 3 crucial engineering issues related to the characterization of existing bridge foundations: (1) geotechnical and hydraulic hazards, (2) changes in service loads, and (3) foundation condition assessment (FHWA 2017). The FCP hosted a workshop in April/May of 2013 (Schaefer and Jalinoos 2013) that initially focused on analyzing the hydraulic hazards associated with unknown foundations, or foundations of waterways without design details such as depth, type, or materials. During this workshop, many participants cited designing for reuse and changes in service loads as driving factors behind characterizing existing foundations, and the scope of the FCP was broadened to cover all the above 3 crucial engineering issues identified.

A workshop held in January of 2014 (Colin and Jalinoos 2014) focused exclusively on the issue of foundation reuse. The workshop defined categories of reuse (replacement on new alignment, replacement on existing alignment, full reuse of existing elements, reuse of existing elements with strengthening), and provided 7 case examples of foundation reuse. This workshop identified several key areas where research is needed for foundation reuse:

- Load testing of existing foundations and better condition assessment
- Instrumenting new or existing foundations for on-demand assessment of condition
- A synthesis of common practices in foundation reuse should be developed
- Guidelines for the field evaluation of known and unknown foundations (site investigation, destructive and non-destructive testing, numerical modeling, and load testing)

Boeckmann and Loehr (2017) continued research into the current state of practice surrounding foundation reuse for highway bridges. Their report included several case studies of reuse, a survey of State Departments of Transportation (DOTs), and a literature review of available information regarding foundation reuse. Suggestions for future research included new methods for investigating existing foundations and methods for improving predictions of the load-carrying capacity of existing foundations.

1.4 Research Needs and Goals for Foundation Reuse

The research performed as part of the *Foundation Reuse for Highway Bridges* report covered various aspects of the issues documented by Schaefer and Jalinoos (2013), Colin and Jalinoos (2014), and Boeckmann and Loehr (2017). One major aspect identified by all three reports is the ability to assess the current stock of existing foundations, including unknown foundations. It was identified that the existing body of research was lacking in tools to load rate existing foundations and that new methods would be required to encompass the issues commonly encountered with bridge foundations. Another important research need identified through the reports referenced above and examination of case studies was the need for a method to improve estimation of pile capacity when no test data was available. Case studies were observed where pile capacities were estimated from driving logs or pile geometry with large capacity reductions due to the variability associated with those prediction techniques.

The goals developed based on these identified research needs were:

- Develop a method that can identify unknown foundations, verify details of known foundations, and characterize performance of existing foundations

- Develop a method for load rating of existing foundations and accounting for foundation movement in the typical load rating methodology
- Provide reliability-based recommendations for updating pile capacity when test data is not available, but there has been observed past loading on the foundation as a whole

1.5 Roadmap to this Research

Chapter 2 of this dissertation presents the manuscript for a case study paper on foundation reuse in Accelerated Bridge Construction (ABC). This chapter contains substantial background and literature review on the topic of foundation reuse for highway foundations. A discussion of the motivations behind reuse, potential benefits, and disadvantages of reusing bridge foundations is outlined. Since the manuscript in Chapter 2 is intended for publication in a special edition of the Journal of Bridge Engineering on ABC, the potential synergistic benefits between reuse of existing foundations and ABC are explored. Several case studies are discussed that highlight various aspects of reuse, including investigation, evaluation, and/or strengthening.

Chapter 3 of this dissertation proposes a method for identifying existing foundation systems through dynamic measurements. The proposed method uses a limited number of measurements taken from a bridge pier column to update a model of foundation dynamic behavior. The updated model provides increased accuracy to modeling of the foundation stiffness using only assumptions about soil and pile parameters. The parameters used to update the model correspond to real-world properties such as pile length, soil shear modulus, and pile stiffness. Monitoring of these properties can be used for unknown foundation identification, monitoring of foundations subjected to scour, or in post-hazard assessment to evaluate the integrity pile and the soil system. The proposed

method is designed to be implemented into a long-term instrumentation scheme due to the automation of foundation identification routine.

Chapter 4 of this dissertation discusses the implication of an integrated load rating of bridge superstructures and substructures. This procedure was developed to address inabilities of the current load rating paradigm to rate substructure components and to handle strength and functionality issues related to foundation movement or scour. A method is proposed to load rate pier columns on foundations subjected to movements, pile bents subjected to scour and water loads, and superstructures and bearings on foundations experiencing movements. A method for load rating biaxially eccentrically loaded columns is proposed and outlined.

Chapter 5 of this dissertation outlines a method for estimating the capacity of driven piles without static or dynamic test information available. The proposed method is intended for use of bridges with foundations without test data, but with observed past loading. The resistance factors normally required by LRFD for empirical equations and driving formulae are relatively low due to the high variability observed in those prediction methods, leading to inefficient designs. The proposed method updates the distribution of pile capacity using knowledge of previous loading to the group of piles, allowing for a more efficient design. A second method is proposed to provide a reliability-based estimate of pile capacity considering the previous loading previously applied to the group of piles and no prior estimation of pile capacity.

1.6 References

Agrawal, A.K., Davis, N.T., Hoomaan, E., Sanayei, M., Jalinoos, F. (2017) *Reuse of Foundations of Existing Bridges,* 2017 National Accelerated Bridge Construction Conference, Miami, FL, Dec 7-8, 2017

Agrawal, A.K., Jalinoos, F., Davis, N.T., Hoomaan, E., Sanayei, M. (2018) *Foundation Reuse for Highway Bridges*. FHWA Office of Research, Development, and Technology. McLean, VA 22101

Boeckmann, A.Z. and Loehr, J.E. (2017) *Current Practices and Guidelines for the Reuse of Bridge Foundations*. NCHRP Synthesis 505, Transportation Research Board of the National Academies, Washington, D.C.

Collin, J. G. and Jalinoos, F. (2014). "*Foundation Characterization Program: TechBrief #1—Workshop Report on the Reuse of Bridge Foundations*." Publication FHWA-HRT-14-072, Federal Highway Administration, Washington, D.C.

Davis, N.T., Sanayei, M. (2018) *Reliability Analysis of Existing Bridge Foundations for Reuse* IMAC XXXVI Conference & Exhibition on Structural Dynamics, Orlando, FL, Feb 12-15, 2018

Davis, N.T., Hoomaan, E., Sanayei, M., Agrawal, A.K. (2017) *Reliability Analysis of Existing Bridge Deep Foundations for Reuse* ASCE Structures Congress, 2017, Denver, CO, April 4-8, 2017

FHWA (2017). *Foundation Characterization Program (FCP)*. Federal Highway Administration. Last Accessed 6/26/2018. https://www.fhwa.dot.gov/research/tfhrc/programs/infrastructure/structures/fcp/index.cfm

FHWA (2018). *National Bridge Inventory*, Deficient Bridges by Highway System in 2017. Federal Highway Administration. Last accessed March 15, 2018, at: https://www.fhwa.dot.gov/bridge/nbi/no10/defbr17.cfm,

Jalinoos, F., Davis, N.T., Hoomaan, E., Agrawal, A.K., Sanayei, M. (2017) *Foundation Reuse in ABC Projects,* 2017 National Accelerated Bridge Construction Conference, Miami, FL, Dec 7-8, 2017

Sanayei, M., Davis N.T. (2016) *Bridge Foundation Stiffness Identification* ASCE Geotechnical & Structures Engineering Congress, 2016, Phoenix, AZ Feb. 14-17, 2016

Schaefer, V.R., Jalinoos, F. (2013). Characterization of Bridge Foundations Workshop Report, FHWA-HRT-13-101, Federal Highway Administration (FHWA), McLean, VA 22101

Chapter 2 Foundation Reuse in ABC

This chapter features the contents of a manuscript by the following authors that has been formatted for publication in a peer-reviewed manual.

Foundation Reuse in Accelerated Bridge Construction

Nathan T. Davis[1], Ehssan Hoomaan[2], Anil K. Agrawal[3], Masoud Sanayei[4] and Farrokh "Frank" Jalinoos[5]

[1]PhD Candidate, Dept. of Civil & Env. Engineering, Tufts University, Medford, MA 02155

[2]PhD Candidate, Dept. of Civil Engineering, The City College of CUNY, New York, NY 10031

[3]Professor, Dept. of Civil Engineering, The City College of CUNY, New York, NY 10031

[4]Professor, Dept. of Civil & Env. Engineering, Tufts University, Medford, MA 02155

[5]Research Structural Engineer, Federal Highway Administration, Office of Infrastructure R&D, McLean, VA 22101

Abstract

When an existing bridge is being considered for replacement due to a deteriorated or obsolete superstructure, the foundation may still have significant functional value. Reuse of these foundations during bridge replacement or widening can present significant cost and time savings over constructing new elements. The potential time savings associated with foundation reuse can reduce mobility impacts, a key goal of accelerated bridge construction (ABC), and the cost savings can increase the economic viability and sustainability of an ABC bridge replacement project. However, existing foundations may have uncertain material properties, geometry, or details that impact the risks associated with reuse. Unlike a new foundation, an existing foundation may have been damaged, may not have sufficient capacity, and may have limited remaining service life due to deterioration. Assessment of these issues, possible foundation strengthening measures, and innovative approaches to optimize loading are discussed in this paper. An analysis of an ABC database is performed to examine the current role foundation reuse in ABC projects. Six case examples are presented where foundation was reused or considered for reuse during a bridge replacement project.

Keywords: Foundation Reuse, Accelerated Bridge Construction, Maintenance, Decision-Making, Retrofitting

2.1 Introduction

As of 2017, there are 54,560 bridges in the united states that are either structurally deficient or functionally obsolete (FHWA 2018a). The renewal, widening, or replacement of these deficient bridges is putting increased financial strain on bridge owners and stakeholders. For many deficient bridges in both rural and urban areas, closure for any significant length of time can cause traffic delays, block access for emergency vehicles, impact local business interests, and create additional

costs related to traffic rerouting. In recent years, accelerated bridge construction (ABC) has gained popularity as a method for controlling the impacts on users by drastically shortening the onsite construction time and mobility impacts. ABC involves the use of innovative planning, design, materials, or construction methods to reduce construction time when constructing new bridge or replacing old bridges (Culmo 2011; FHWA 2018b). One of the most common applications for ABC is limiting mobility impacts for bridge replacement projects on high traffic or important routes where a complete or partial closure of a bridge may impact the larger transportation network. In some cases, bridges requiring rehabilitation or replacement are founded on substructures that still have significant functional value. The reuse of these substructure elements presents substantial cost and time savings due to the decreased amount of construction required.

Initial research into foundation reuse was focused on the reuse of building foundations in crowded urban sites. A European Union project called Reuse of Foundation for Urban Sites (RuFUS) produced a best practice handbook (Butcher et al. 2006) to provide technical guidance on foundation reuse. The Construction Industry Research and Information Association (CIRIA) followed a year later with a guide (Chapman et al. 2007) intended provide an overview of the risks and strategies behind foundation reuse. Strauss et al. (2007) discussed the drivers that impact the frequency of building foundation reuse in the US. This research discusses the use of SPeAR® diagrams that visually convey the favorable influence of the identified drivers.

The FHWA Foundation Characterization Program (FCP) held a workshop in early 2013 (Schaefer and Jalinoos 2013) on the characterization of bridge foundations. This workshop identified many issues surrounding the analysis of existing foundations but was not explicitly focused on reuse. In early 2014, the FCP held a workshop (Collin and Jalinoos 2014) specifically

focused on bridge foundation reuse. After the workshop, 10 transportation agencies were informally polled by NCDOT with all responding that they had either reused or retrofitted existing bridge foundations.

The first major research project to explicitly focus and formally survey agencies on the reuse of bridge foundations was NCHRP Synthesis 505, titled *Current Practices and Guidelines for the Reuse of Bridge Foundations* (Boeckmann and Loehr 2017). This synthesis sought to document the current state of foundation reuse guidelines at the State-level and identify gaps in knowledge that prevent foundation reuse from being considered. This report included survey responses from 45 US state transportation agencies and 8 Canadian transportation agencies regarding their reuse practices and guidelines. The survey was given primarily to state geotechnical engineers and not structural engineers, so respondents may not have been aware of all projects whereby foundations were reused by bridge engineers as-is (without a need for strengthening). Of the 53 responding agencies, 51 cited experience with foundation reuse. 50 respondents provided situations where bridge foundation reuse had occurred. Their answers included bridge widening, superstructure replacement, seismic retrofit, increases to clearance, bridge repurposing, as shown in Figure 2-1.

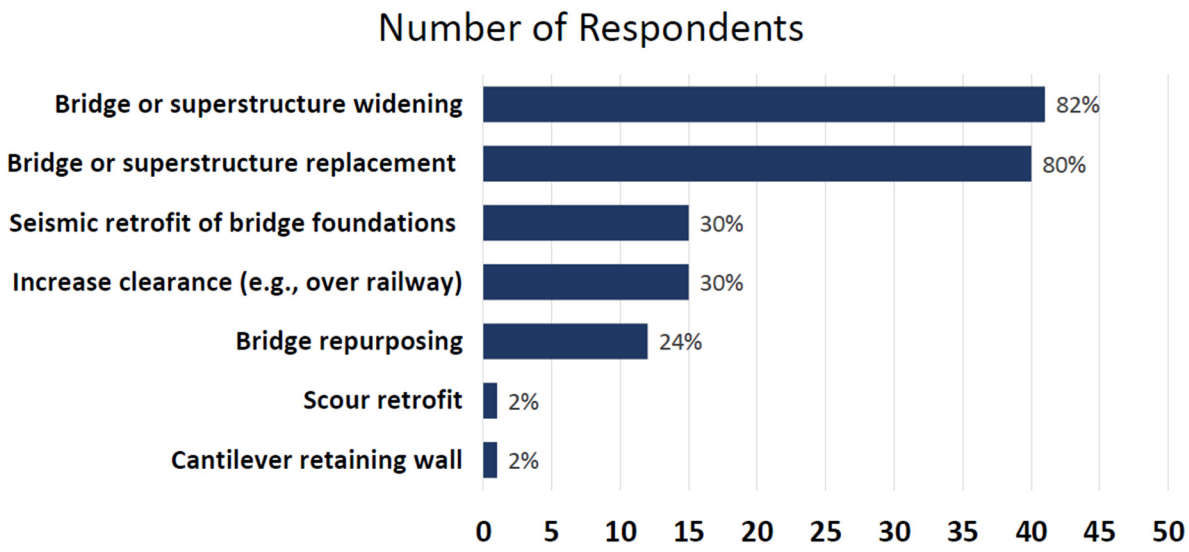

Figure 2-1: Applications for Foundation Reuse (data from Boeckmann and Loehr 2017)

The upcoming FHWA report *Foundation Reuse for Highway Bridges* (Agrawal et al. 2018) provides an in-depth discussion of the technical aspects of evaluation and potential retrofit of bridge foundations. In this manual, 15 case studies across the US and Canada are used to highlight common issues and technical solutions. The manual provides a discussion of the benefits and challenges associated with foundation reuse for ABC projects. A sample of ABC projects with substantial substructure work taken from the Florida International University (FIU) ABC database (FIU 2017) is provided that details the type of foundation work involved. Aktan and Attanayake (2015) published a manual for the Michigan Department of Transportation (MDOT) on ABC construction techniques, which included significant discussion on the installation of new foundation elements in the vicinity of existing foundation elements.

2.2 Definition of Foundation Reuse

The *Foundation Reuse for Highway Bridges* report (Agrawal et al. 2018) provides the following definition of bridge foundation reuse: ***use of an existing foundation or substructure of***

a bridge, in whole or in part, when the existing foundation has been evaluated for new loads. Where *foundation* is used to describe all substructure components below the ground level, and *substructure* describes above ground components, like piers, abutments, pier caps, and columns. This distinction is useful when discussing reuse, as available inspection methods and typical concerns can vary between above and below ground elements. This definition specifically excludes in-kind deck replacement, where an existing bridge deck is replaced while the substructure and superstructure are left in place, and loads are similar (± ~10%) to the original construction. Deck replacements are commonly performed as a mid-life overhaul when the majority of the bridge is in good shape, except the deck. ABC in the form of prefabricated elements and rapid set concrete is commonly used with deck replacement projects to limit their mobility impacts. On long bridges, deck replacement often causes longer mobility impacts than a full superstructure replacement would, as deck panels are replaced individually instead of a new superstructure being lifted, slid, or transported into place in one piece. With ABC, the mobility impacts of deck replacements can be limited to a series of off-peak hours or a shortened construction window.

Butcher et al. (2006) have considered 4 available foundation reconstruction options: complete reuse, partial reuse, complete replacement, and removal and replacement. This categorization scheme was adopted by Collin and Jalinoos (2014) to better fit with situations observed in bridge foundation reuse. Figure 2-2 (Jalinoos 2015) illustrates the foundation options available when reconstructing a bridge superstructure.

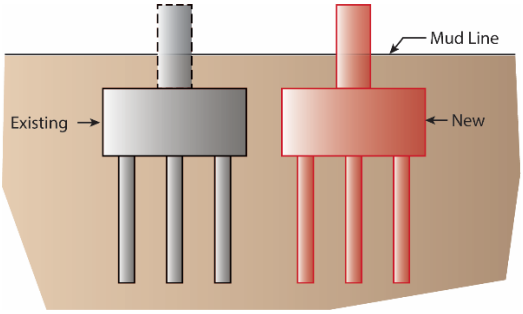

Option 1: Install new foundation on new alignment

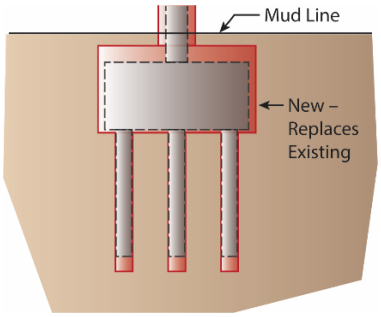

Option 2: Install new foundation on the existing alignment

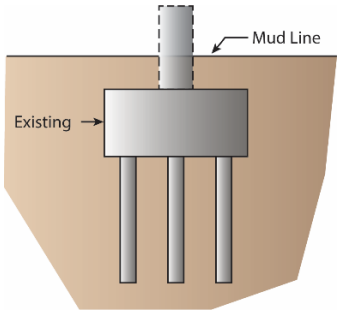

Option 3: Reevaluation and reuse existing foundation

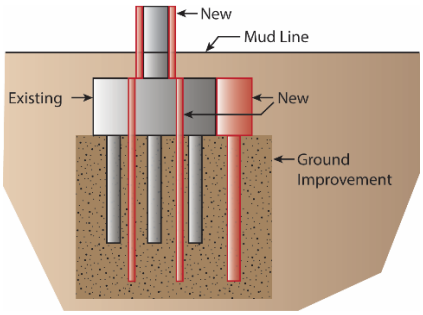

Option 4: Reuse existing foundation by strengthening it

Figure 2-2. Foundation reconstruction options, courtesy of FHWA

Options 1 and 2 are considered "foundation reconstruction" – where a new foundation is built. Options 3 and 4 are considered "foundation reuse" – where all or portions of existing foundations are reused. The options are not necessarily mutually exclusive, as one replacement project may involve multiple substructure elements with some saved and others not. A description of these 4 options is provided below:

Option 1:

Option 1 alternatives use new foundation elements constructed on an alignment that is parallel to the existing alignment. The new foundation elements can be constructed while the existing alignment is in use, with the primary traffic impacts occurring during the change from the original to the new alignment. ABC approaches are most often used with Option 1 foundations

when construction may impact an underlying roadway, there are environmental considerations that limit on-site construction, or there is a short construction season/window.

Option 2:

Option 2 alternatives use new foundation elements constructed within the existing alignment to support a new superstructure. This option preserves the existing right of way, but has the potential to cause significant mobility impacts, as the bridge needs to be closed during at least some of the construction. ABC approaches are frequently used with Option 2 bridges to limit the amount of closure required. Construction of the new foundations may interfere with the existing roadway, which may require off-peak closures during foundation installation or closure and demolition of the existing bridge prior to foundation installation. The latter scenario has the potential for the largest mobility impacts of any option, although the use of prefabricated components and rapid construction can limit these impacts.

Option 3:

Option 3 alternatives involve reuse of the existing foundation with a new superstructure that can be lifted, slid, or transported into place. This approach allows for preservation of the original right of way (ROW), the historical appearance, and reduce the amount of new materials required. Option 3 alternatives may involve patching spalls, chloride extraction, or other minor repair work to substructure elements to maintain their functionality but are more or less used in their existing condition. The primary mobility impacts for Option 3 bridges occurs during superstructure replacement, which can be limited to a very short window using conventional heavy lifting equipment (CHLE), self-propelled modular transporters (SPMT), or slide-in bridge construction (SIBC). Option 3 alternatives may be suitable for deck widening if there is sufficient

reserve capacity in the substructure/foundation for increased loads, or if innovative materials are used for the bridge deck to reduce loading on reused components.

Option 4:

Option 4 alternatives reuse the existing foundation enhanced with major repair, retrofit, or strengthening. Strengthening/retrofit can include any changes made to the system that improve the capacity or durability of existing elements, such as underpinning or strengthening with new piles or shafts, encasement of piers/piles with concrete, wrapping of elements with fiber reinforced polymer (FRP) or polyvinyl chloride (PVC), installation of new piles or shafts for a widened footprint, installation of additional reinforcement to existing concrete sections, ground improvement near existing elements to increase capacity, installation of additional piers, or installation of scour protection. These activities can be performed while the bridge is in service, limiting mobility impacts.

2.3 Motivations for Foundation Reuse

Collin and Jalinoos (2014) report the following 9 drivers for foundation reuse in bridge projects that were identified by presenters and speakers at the TRB workshop:

- **Asset Management —** Existing elements still have functional value
- **Technical Drivers —** Installation of new elements may be difficult
- **Time Savings —** Minimize bridge closure by limiting amount of construction
- **Economic Drivers —** Real cost savings and user cost savings
- **Efficiency —** Lower costs and shortened construction means more deficient bridges can be replaced
- **Past Performance —** Foundation has been load tested by past loading

- **Environmental Benefits —** Lower material usage and waste generation, lower construction impact in sensitive areas (rivers, wetlands, etc.)
- **Sustainability Issues —** Lower material usage and waste generation
- **Historic Preservation —** Reuse allows preservation of historical bridge features

One of the above drivers for foundation reuse is *sustainability issues*. Sustainability succinctly sums up many of the benefits that can be derived from foundation reuse, as many of the drivers behind foundation can be considered as contributing to a project's sustainability. Sustainability, as defined by the FHWA INVEST program (FHWA 2017), consists of a "triple bottom line" of outcomes: social, economic, and environmental. The goal of viewing projects from a sustainability perspective is to meet the continuing social needs of users at a minimum cost while minimizing the use of natural resources. In the survey performed in NCHRP 505 (Boeckmann and Loehr 2017), the 51 respondents who reported experience were also asked to provide the situations and needs that had motivated foundation reuse. The responses generally align with other drivers discussed in the workshop, as shown in Figure 2-3. The workshop responses can all be considered as contributing to at least one of the triple bottom line items, as shown in Table 2-1.

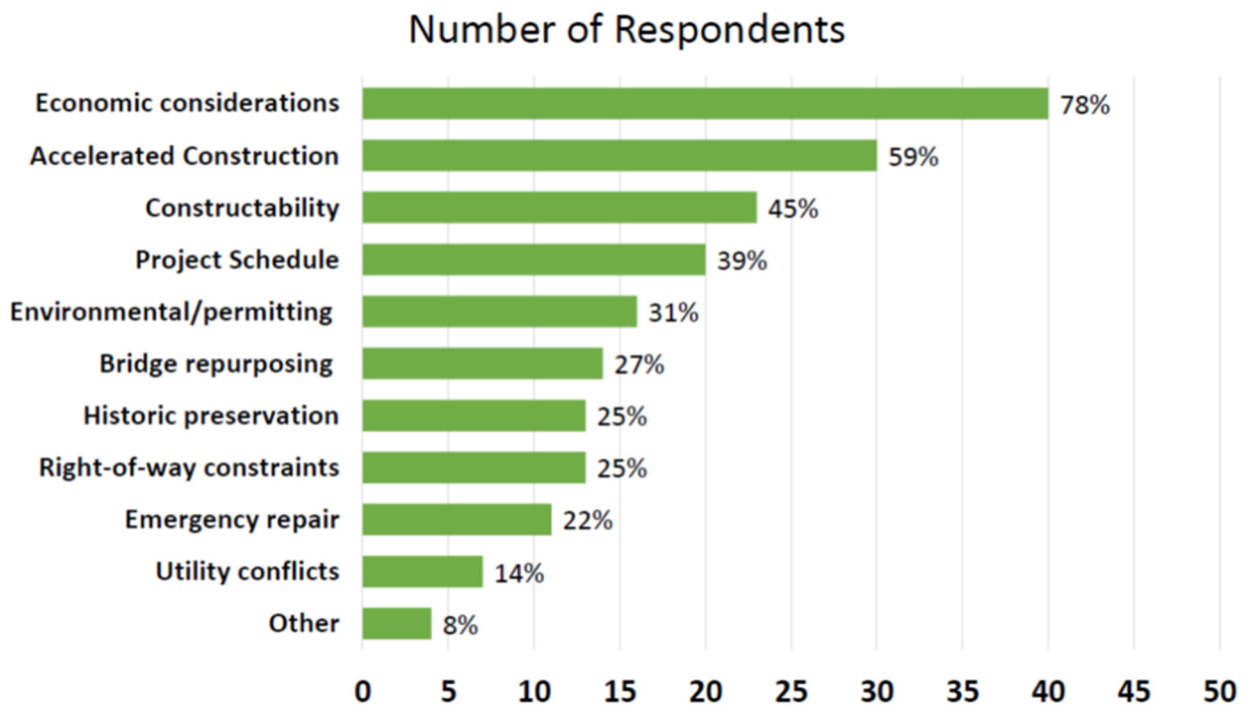

Figure 2-3. Survey on motivations for foundation reuse (data from Boeckmann and Loehr 2017)

Table 2-1: Survey responses grouped into sustainability categories

Social	Economic	Environmental
Accelerated construction	Economic considerations	Environmental/ permitting
Project Schedule	Constructability	Bridge Repurposing
Right of Way constraints	Historic Preservation	
Emergency Repairs	Utility Conflicts	

2.4 Foundation Reuse in ABC Projects

The decision to use ABC is typically driven by a desire to lessen impacts on traffic, deal with constructability issues, avoid use of temporary structures, avoid weather related delays, and utilize short construction seasons (Culmo 2011). Since mobility impacts and construction time are the key concerns when pursuing ABC construction projects, ABC projects are gauged by 2 different time metrics: onsite construction time and mobility impact time. ABC projects are frequently categorized by mobility impact time, with projects assigned one of 5 tiers (Culmo 2011; FHWA 2018b; FIU 2017). Tier 1 projects have the shortest traffic impacts (less than a day) and Tier 5 having the largest mobility impacts (greater than 3 months). FIU (2017) uses a similar 6-

tier system, with an additional differentiation between less than 1 month of impacts and 1 to 3 months of impacts. For clarity, this system is adapted to have a Tier 4a and Tier 4b in this paper, so that it aligns with the conventions of Culmo (2011) and FHWA (2018b).

The FIU UTC ABC project database (FIU 2017) provides a database of 111 ABC projects from around the country. This database provides information on the superstructure type, installation method used, closure time (and corresponding tier), and cost information for select projects. The case examples that make up the database are provided to the database by owners, stakeholders, and design engineers, so they are not a random sample of ABC projects. Table 2-2 presents a summary of the foundation replacement options used for the 111 case examples in the ABC database (FIU 2017). This information is not directly provided by the database and was assembled from the descriptions provided of the construction sequence. Fourteen of the case examples in the FIU database represent new construction, where there was no existing bridge or foundations to consider for reuse. Another 9 of the case examples represent a deck replacement. The remaining 88 case examples in the database represent reconstruction of an existing bridge.

Table 2-2: Foundation replacement options found in FIU database

ABC Tier (length of impact)	Replacement Option					
	NC	**DR**	**1**	**2**	**3**	**4**
Tier 1 (< 1 day)	3	1	3	6	3	1
Tier 2 (1 to 3 days)	0	2	0	7	5	2
Tier 3 (<2 weeks)	1	0	0	8	2	2
Tier 4a (2 weeks to 1 month)	0	3	0	3	2	1
Tier 4b (1 to 3 months)	5	2	5	14	0	0
Tier 5 (>3 months)	5	1	6	16	0	2
Total	14	9	14	54	12	8

NC = New Construction
DR = Deck Replacement
1,2,3,4 = Replacement options 1-4 (Figure 2-2)

It can be noted from Table 2-2 that 54 of the 88 (61%) reconstruction projects were Option 2 projects, where the original alignment was maintained without reuse. Twenty (20) of the 88 (23%) reconstruction projects involved foundation reuse, with (Option 4) or without (Option 3) strengthening. Greater than half of the Option 2 case examples took longer than a month to complete, with many of the longer projects requiring demolition of the existing bridge prior to installation of new abutment walls, piles, drilled shafts, footings, micropiles, etc. Thirteen of the Option 2 case examples, however, were performed in under 3 days using rapid foundation construction, construction of the foundation while bridge was in service, or construction of the foundation during off-peak lane closures. Overall, it can be noted from the database that many Option 2 bridges saw significant on-site construction time and mobility impacts associated with replacement foundation installation. Some Option 1 examples avoided large mobility impacts by constructing the new bridge prior to closing the existing one, but many of these bridges also saw significant mobility impacts during construction. On the other hand, only 2 of the 20 reuse examples impacted user mobility for greater than three months, with both being Option 4 projects where the bridge was closed during foundation strengthening. It is unclear if foundation reuse was feasible or considered for many of the Option 1 or Option 2 case examples.

2.5 Reuse Decision Model

A reuse decision model was proposed by Agrawal et al. (2018) that considered the major portions of the decision-making process for projects considering foundation reuse. The components of the decision-making process suggested by Agrawal et al. (2018) are:

- Desk study

- Assessment of the existing foundation integrity, durability, and capacity
- Analysis of scour and hazard vulnerability
- Assessing constructability of proposed alternatives
- Environmental impacts assessment (EIA)
- Risk analysis of proposed alternatives
- Life-cycle cost analysis (LCCA) of available options.
- Alternative Selection

The "desk study" and integrity, durability, and capacity assessments are the aspect of the decision model that relate to evaluating the existing bridge conditions and are discussed in the next section. Analysis of scour and hazard vulnerability and the EIA are standard components of bridge foundation construction and are applicable to reuse investigations as well. Agrawal et al. (2018) outlines a risk management process (RMP) that has 4 phases: identification of risks, assessment of identified risks, and monitoring of identified risks. A life cycle cost estimation procedure is outlined that converts future costs to present costs using the discount rate, and accounts for uncertain and probabilistic costs. An important part of the LCCA that is extremely important for ABC projects is accounting for both user and agency costs. Agency costs refer to direct outlays related to construction, while user costs provide a monetary measure of the impact that construction has on the community and typical bridge users. The important user cost to consider is the impact of construction on user travel times.

2.6 Assessment

Agrawal et al. (2018) divided the assessment of bridge foundations into 4 primary components: the desk study, the integrity assessment, the durability assessment, and the capacity assessment. These investigations are not meant to be mutually exclusive, independent or sequential, but rather refer to an overall grouping of the assessment. Table 2-3 provides a summary of the types of tasks performed during the desk study and assessments.

Table 2-3. Types of assessment and tasks involved for foundation reuse investigation (data from Agrawal et al. 2018).

Assessment Portion	Tasks
Desk Study	Collect and review design drawings, installation records, soil boring history, soil test data, QA/QC records, inspection history, hazard history, and other reports.
Integrity Assessment	Determine material properties of foundation structures. Assess component damage and deterioration. Identify uncertain details, such as pile length and subsurface dimensions. Evaluate geotechnical performance, including settlement, geo-hazards, slope stability, and other changes to geotechnical system.
Durability Assessment	Assess current state of the bridge and level of deterioration. Assess environmental factors at the bridge that may lead to future deterioration of elements. Estimate remaining service life. Identify potential life cycle costs of durability issues identified and the life cycle costs of repair measures identified.
Capacity Assessment	Determine new loads on the foundation. Determine capacity of existing components, accounting for integrity and durability assessments. Determine capacity of footings and deep foundations, performing load testing if necessary.

Desk Study

The desk study consists of gathering available and easily identifiable information on the existing foundation and comparing the initial findings with the requirements of the project. Important details that are considered during the desk study include: in-situ geometry, compatibility between new and existing footprints, past performance, identification of alternatives. The desk study allows for proper planning of the subsequent assessment steps, as well as the identifying important issues at an early stage so that reuse can be planned accordingly.

Integrity Assessment

Agrawal et al. (2018) detail the various types of testing readily available to assess the integrity of above ground and below ground portions of in-situ foundations. For above-ground portions, three main types of testing are identified: visual/physical inspection, material sampling

with laboratory testing, and non-destructive testing (NDT). Visual and physical inspection are important parts of normal bridge maintenance, as they provide a firsthand look at the state of the foundation under consideration for reuse. Material sampling and testing is most commonly employed with concrete structures (and on a more limited basis with masonry and timber members), as removal of test samples allows for compressive strength testing, petrographic testing, modulus testing, and testing of the reinforcement strength. NDT technologies are widely used for evaluating concrete structures, and a summary of available technologies is provided in Table 2-4. NDT technologies are also commonly employed with steel, masonry and timber elements to look for cracking decay, or measure moisture content.

Table 2-4. Example NDT methods for accessible concrete elements and their use (data from Agrawal et al. 2018).

NDT Method	Issues Investigated
Ground Penetrating Radar	Rebar layout, voids, cover depth and delamination
Ultrasonic Pulse Velocity and tomography	Location of voids, weak zones, honeycombing, and cracks
Infrared Thermography	Location of voids and delaminations
Electrical Resistivity (ER)	Presence of water, chlorides, and salts and likelihood of corrosion
Radiography	Location of voids and condition of tendons and strands
Impact Echo	Location of grout voids and delaminations
Ultraseismic / Parallel Seismic	Location of defects and voids in buried piles

Wireline logging, an important new development, has the ability to provide a wealth of information on foundation elements below the ground surface. Wireline logging runs are typically conducted from coreholes drilled from the top of the foundation, carried through the foundation elements, and into the underlying soil or rock. These coreholes also allow for direct sampling of the foundation element at any elevation, the foundation/soil interface, and the soil directly underneath the existing foundation. Wireline logging provides a continuous record of foundation

properties surrounding the corehole wall, as can be seen in Figure 2-4. Some important wireline technologies that can be deployed are listed in Table 2-5.

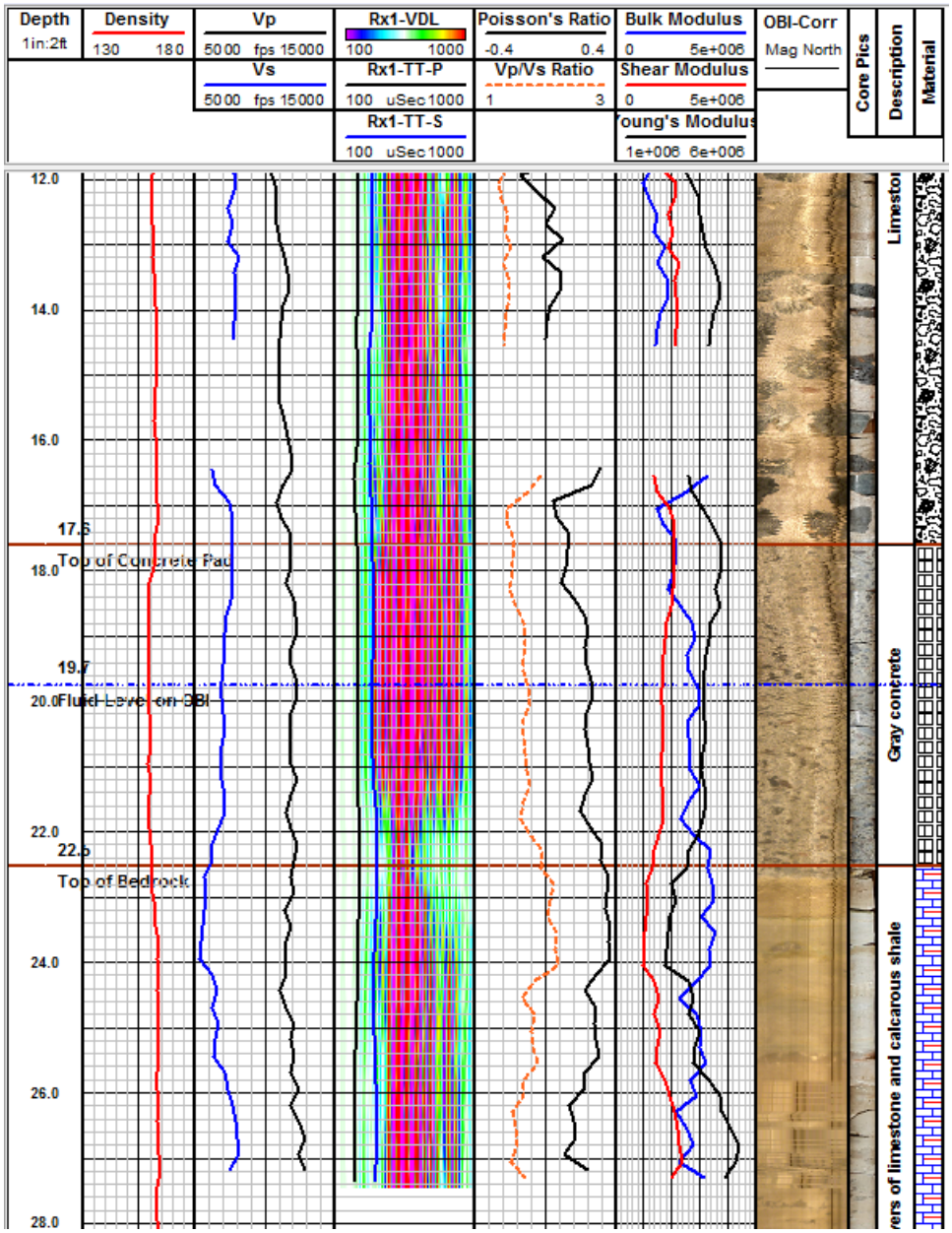

Figure 2-4: Wireline logging from willow valley bridge

Table 2-5. Main corehole logging technologies and their uses (data from Agrawal et al. 2018).

Logging Technology	Measured Parameters	Notes
Optical televiewer (OTV)	Digitally images the inside of corehole wall using optical camera. Records an oriented 360° unwrapped and 3D image of the corehole wall or a "digital core."	Ideal for air filled coreholes. For water-filled holes, clear water is required. It can pick the orientation of micro-cracks in structural elements or bedrock
Acoustic televiewer (ATV)	Oriented images inside of the fluid filled corehole using acoustic transducer. Provides similar imagery as Optical televiewer.	Requires fluid filled holes and works in muddy (unclear) water.
Caliper logs (mechanical and acoustic)	Measure the corehole diameter and any change due to voids or washout zones in soil or bedrock.	Determines the change in the diameter of the corehole wall and the depth of voids
Full waveform sonic (FWS) log	Measures compressional (p), shear (s) Stoneley, and tube wave arrivals and amplitude.	Along with density logs, elastic (mechanical) properties logs can be derived to display shear, bulk, Young's moduli and Poisson ratio as a function of depth.
Density log (compensated and 4-pi)	Determines material density.	Compensated density measures density values as a function of depth. 4-pi density is mostly used to detect defects.
Electrical resistivity logs	Determines electrical resistivity of material at different radius of investigation as well as single point resistance (SPR) and spontaneous potential (SP).	Can identify areas of high conductivity in concrete / masonry, and possibly rebar corrosion in rebars in concrete
Electromagnetic Induction logs	Measure electromagnetic conductivity at typically 2 radii of investigation	Can measure areas of high conductivity and steel.
Thermal neutron log	Measures the amount of hydrogen atoms in a formation.	Its main use is in the determination of porosity or presence of moisture.
Gamma log	Measures the amount of gamma radiation produced mainly by isotopes of potassium, thorium, and uranium.	Can identify differing concrete mix or concrete deterioration.

Durability Assessment

The durability assessment focuses on issues that may impact the longevity of the substructure after reuse. For steel structures, the primary consideration during this assessment is the amount of

observed corrosion and section loss, the performance and intactness of any coatings present, and estimation of the future rates of corrosion. For timber elements, it is important to identify sources of decay (insects, fungus, etc.), as well as identifying the elevation of the ground water and how that changes over time. Timber elements can achieve an indefinite lifespan as long as the elements remain permanently submerged. For concrete elements, the most important consideration when determining future service life is the corrosion of reinforcement steel. Reinforcement corrosion is typically triggered by the loss of cover concrete, the presence of chloride ions, or the presence of carbonation in the cover concrete. Determining the extent of chloride exposure and the amount of carbonation present is crucial to understanding the longevity of the substructure. After these measurements have been made, the remaining service life can be estimated following the work of Sohanghpurwala (2006).

Capacity Assessment

The capacity assessment is where the capacity of the existing foundation is determined using the information obtained in the integrity and durability assessments. Typically, this stage involves modeling of the foundations using finite element software, analytical equations, or other methods. Agrawal et al. (2018) present a methodology developed by Davis et al. (2018) that allows the capacity of existing in-situ pile foundations to be determined in an LRFD context by identifying the amount of load that the foundation as a whole can support. Four situation of pile foundation reuse are identified:

- Design drawings and original test data are available
- Design drawings are available, but no test data is
- Testing is performed on the entire foundation

- Testing is performed on individual piles

2.7 Foundation Strengthening

Agrawal et al. (2018) discuss various strengthening measures that are available for Option 4 bridges where greater capacity is required. Strengthening measures can include strengthening of above ground elements, installation of additional below ground elements, and ground improvement. Scour countermeasure protection can be used to ensure soil providing resistance is not lost during an extreme flood. Repair technologies for steel elements generally consist of encasement with concrete, installation of cathodic protection, application or reapplication of paint or coatings, or removal and replacement of subpar members. Repair technologies available for timber elements include concrete encasement, PVC wrapping (to inhibit further decay), FRP wrapping (to strengthen and inhibit further decay) grout/epoxy injection (to fill in internal decay), or posting/splicing in new elements to replace areas of decay. Reinforced concrete is the predominant material found in above ground portions of foundation elements (piers, columns, abutments, etc.), and presents the largest array of potential issues and repair solutions, as shown in Table 2-6.

Addition of new geotechnical elements can allow for a wider bridge deck and additional geotechnical and structural capacity. Available technologies for addition of new elements includes: micropiles, jacked piles, driven piles, drilled shafts, continuous flight auger (CFA) piles, and tiebacks/ soil nailing. In practice, the addition of micropiles and drilled shafts is most commonly observed, as they produce very little soil displacement and ground vibrations. These technologies are frequently deployed while the original bridge remains in service.

Table 2-6. Strengthening and repair options for concrete elements (data from Agrawal et al. 2018).

	Identified Issue	Strengthening Measures Available
Integrity Issues	Concrete Damage	Replacement of impacted concrete
	Alkali Silica Reactivity (ASR), Delayed Ettringite Formation (DEF)	Removal and replacement of impacted concrete, replacement of ASR/DEF impacted members
	Corroded Reinforcement (loss of rebar area)	Removal/replacement of cover concrete with new rebar, doweling, external rebar, FRP wrapping
Durability Issues	Chloride Ingress	Removal/replacement of affected concrete, cathodic protection, ECE, expansion joint elimination
	Spalling/delaminations	Patching of spalls, galvanic anodes to prevent corrosion, FRP wrapping, addressing primary issue causing spalling
	Freeze-Thaw	Removal/replacement of susceptible concrete, wrapping of susceptible concrete with moisture barriers
	Carbonation	Removal/replacement of carbonated concrete, wrapping with moisture barriers, cathodic protection
Capacity Issues	Increased Loads	Addition of new elements, encasement of existing concrete sections, addition of external reinforcement cage, FRP wrapping, doweling of additional bars,
	Low Concrete Strength	Replace/add elements, encase with new concrete
	Under-reinforcement, detailing issues	Doweling, encasement with additional reinforcement cage, FRP wrapping of low capacity sections

When existing foundations are suitable for reuse, but issues with the surrounding soil exists, employment of ground improvement technologies can enable reuse. Agrawal et al. (2018) discuss the following ground improvement technologies, along with a list of potential uses and how the technology is deployed, as shown in Table 2-7.

Table 2-7. Ground improvement technologies for foundation reuse (data from Agrawal et al. 2018).

Technique	Uses	Description
Compaction Grouting	• Liquefaction mitigation • Bearing Capacity • Improve passive resistance • Settlement Reduction	Densifies soil by injecting grout volume that displaces original soil. Most effective in sandy soils, can cause ground heave and soil displacement near injection
Jet Grouting	• Liquefaction mitigation • Bearing Capacity • Settlement Reduction	Soil is jetted out of ground in columns and replaced with grout mixture. Can lead to ground displacement when elements are loaded during installation. Can be used on sandy and fine-grained soils
Permeation Grouting	• Liquefaction mitigation • Bearing Capacity • Settlement Reduction	Grout is injected into soil and allowed to permeate into the void space of soil to improve soil performance. Most effective on cohesionless soils
Soil Mixing	• Liquefaction mitigation • Bearing Capacity • Settlement Reduction • Improve passive resistance • Decrease active earth pressure	Rotary tool advanced as grout injected into ground. Results in a column of mixed soil and grout with improved properties
Stone Columns	• Liquefaction mitigation • Bearing capacity • Soil densification • Settlement Reduction	Provides some lateral stability to soil and some compaction during installation. Can allow for excess pore pressures to dissipate. Some methods of installation densify the surrounding soil to increase stiffness and reduce settlements.
Dynamic Compaction	• Liquefaction mitigation • Bearing Capacity • Settlement Reduction	Densifies soils by repeatedly dropping large weight from crane. Improves soil properties where applied.

2.8 Innovative Materials

When analyzing a bridge replacement project where foundation reuse is considered, innovative bridge deck solutions can become much more viable. These solutions that generally revolve around lowering the weight of the bridge deck may actually increase the cost of the bridge deck, preventing them from being considered during normal foundation construction. When employed to limit dead loads on the foundation and enable reuse, the increased deck cost can be more than offset by the reduced necessity for installation or repair of foundation elements. One of the most commonly employed technologies is the use of lightweight concrete. This technology was employed by VDOT during the I-95 corridor bridge replacement to lower foundation loading

by up to 7%. More innovative technologies include the use of lightweight materials to construct decks rather than concrete. Gangarao et al. (2007) describe the use of honeycomb FRP decks when replacing short 2 span bridges. By drastically lowering the weight of the deck, the replacement superstructure could be a single span, eliminating the need for the center pier. While the case studies discussed by Gangarao et al. (2007) involved new foundation elements, this approach can be adapted to reduce loading on reused foundation elements.

2.9 Foundation Reuse Case Histories

As part of *Foundation Reuse for Highway Bridges* (Agrawal et al. 2018), various case studies were compiled where existing foundations were investigated for reuse. All but one of the case studies considered were Option 3 or 4. The Hurricane Deck Bridge, included in this paper, was investigated for possible reuse, but ultimately replaced with a new bridge on a new alignment. Five ABC case studies from that report (Table 2-8) are discussed in this paper.

Table 2-8: Selection of ABC Case Studies from Agrawal et al. (2018)

Bridge	Owner	Drivers for reuse	Drivers for ABC	ADT
Hurricane Deck	MO	• Potential for cost savings	Lack of alternative routes during construction	8,166
Fast-14	MA	• Cost savings • Preserving alignment • Enabling ABC	Important route that could never be fully closed, lane restrictions only possible on weekends	200,000
I-95	VA	• Cost savings • Preserving alignment • Enabling ABC	Important route that could never be fully closed, lane restrictions only possible on weekends	150,000
Huey P. Long	LA	• Cost savings • Preserving historical appearance	Important road and rail route, bridge widened while left in service	45,000
Milton Madison	KY/ IN	• Cost savings • Preserving historical appearance • Preserving alignment	Nearest crossing a 80 km (50-mile) detour	10,000
Mississagi River	ON, CA	• Cost Savings	Important route	3,920

Hurricane Deck Bridge Replacement, MO (Option 1)

The Hurricane Deck Bridge was a 5-span under truss bridge spanning the Lake of the Ozarks in Camden County, MO (Axtell et al. 2004). There were four center piers consisting of pneumatic caissons that were believed to bear directly on bedrock. The bridge was originally opened in the early 1930s, and the deck and truss elements were in need of replacement. Since the foundation elements appeared to be in good shape, the bridge owner (MoDOT) anticipated that significant cost savings could be realized through reuse of the existing foundations. The proposed baseline alternative reused the existing foundations with a new delta frame supported 5-span bridge deck. The existing bridge deck would be slid to a temporary foundation to maintain traffic during construction of the new superstructure on the existing foundation elements. An investigation on the existing foundation elements was performed to assess the feasibility of foundation reuse.

The existing caissons were primarily investigated using vertical borings taken from the deck surface. At least two holes were drilled into each caisson with core barrels to allow for examination core recovery, rock quality designation (RQD), testing of removed samples, downhole wireline logging with an acoustic televiewer, and crosshole sonic logging (CSL) between the completed holes. The CSL performed on these foundations was of limited value, believed to be due to the large spacings between coreholes (Axtell et al. 2004). The tests did not identify any major issues with the pier; however, the winning bid was an alternative technical concept (ATC) that involved construction of a new bridge parallel to the existing alignment (Option 1). This proposal increased the number of piers in the lake from 4 to 7, allowing the superstructure to be a steel girder bridge rather than a delta truss. The wining proposal was 1% cheaper than the cheapest bid that reused the existing foundations. While the Option 1 alternative was ultimately chosen for this project, the

reuse (Option 3) alternatives were of similar economic value but may have provided additional benefits such as lower material usage, longer span openings, and historical value.

Fast-14 Replacement Project, MA (Option 3)

The I-93 corridor is the primary interstate connection between Boston, MA and its northern suburbs and carries over 200,000 vehicles per day over four traffic lanes in either direction (Moran 2012; Jalinoos et al. 2016). The 14 bridges in this corridor (7 in each direction) had all deteriorated since their original construction and required increased patching and repair work. Due to the high traffic volumes and lack of feasible alternate routings, closure of this interstate for any period of time was impossible, and closure of any lanes during weekday operation would have led to massive delays and traffic impacts. An ABC approach was used where the bridge superstructures were replaced throughout 10 summer weekend closures, when traffic volumes were lowest. During construction, bridges on one direction of travel were closed, demolished and replaced while traffic was diverted to 2 lanes each way on the opposite side of the highway. The new bridge decks were prefabricated composite girder decks that were lifted into placed using conventional heavy lifting equipment. After the weekend closure, traffic was restored to normal until the following weekend, when the process was repeated for other bridges.

The existing substructures had experienced some deterioration, primarily from deicing runoff through overhead joints in the old decks (Moran 2012). The observed deterioration was repaired, and the new superstructure design eliminated the expansion joints over the piers to prevent further damage. No significant investigation was performed into the capacity of the substructure, as no major performance issues had been observed, and there were no substantial

changes to the loading. This project is a prime example of how Option 3 bridges can substantially reduce the time, cost, and technical limitations of a bridge replacement project.

I-95 Corridor Replacement Project, VA (Option 3 and 4)

The I-95 corridor replacement project involved replacement of 11 aging and deteriorated bridges located near the junction of I-95 and I-64 (LeGrand 2015; Jalinoos et al. 2016). These bridges were subjected to very high traffic volumes that could not be accommodated through diversion to local roads or other highways. Bridge closure for any significant period was highly undesirable due to high traffic volumes. In additional 3 of the bridges considered were widened during the reconstruction process. ABC using preconstructed bridge units was chosen as it could deliver the project while only requiring bridge/lane closures on weekday nights between 8pm and 6am. The preconstructed bridge units were constructed off-site and transported to each of the 11 bridge sites. Upon arrival, the original bridge superstructure was demolished, and the new deck was placed on the existing substructure elements, which were reused without requiring any strengthening. These substructures had undergone varying amounts of damage during their original lifespan and were repaired appropriately prior to the deck replacement.

The prefabricated bridge decks were constructed of lightweight concrete that reduced the dead load by 7% (LeGrand et al. 2015). For the 3 bridges that required widening, 50 additional drilled shafts were installed on either side of the existing piers to support the additional width. In general, the substructures were found to be in relatively good condition, although almost all of them had undergone at least some chloride-related corrosion. The main source of damage was chloride intrusion, which had led to reinforcement corrosion, cracking, and spalling. A combination of patching of spalls, cathodic protection with an aluminum-zinc-indium galvanic

anode, removal of expansion joints over piers, and electrochemical extraction (ECE) were used to provide additional service life to the piers (Sharp 2016). A photo of the repaired foundation with a replacement superstructure is provided in Figure 2-5.

Figure 2-5. I-95 Bridge over Overbrook Road Showing Underside after renovation, courtesy of VDOT

Huey P. Long Bridge, LA (Option 4)

The Huey P. Long Bridge, in Jefferson Parish, Louisiana is a major crossing of the Mississippi River that was originally built in 1935 and is a registered National Historic Civil Engineering (Modjeski and Masters 2013). The bridge carries both rail and vehicular traffic over the Mississippi river with five main spans (and several smaller approach spans). The original superstructure was functionally obsolete, and widening was required to provide adequate lane width and an additional travel lane and shoulder in each direction. The bridge was widened using a parallel truss widening scheme, which placed new truss elements outside of the existing truss elements, preserving the original appearance of the superstructure. The new widened

superstructure, now with 4 parallel trusses connected by cross-bracing, was substantially heavier and wider than the original bridge. To accommodate the additional width of the bridge deck, a steel W-frame (Figure 2-6) was constructed on the upper portion of each pier to transfer the loads to lower portion, which was encased in additional concrete. Significant reserve geotechnical capacity was identified, finding that the foundations could easily support double their previous loading with an additional 2.5 cm (1 in) to 3.8 cm (1.5 in) of settlement expected. Test breaks of the pier concrete from the original construction indicated that the concrete was of significantly higher strength than the design. The 28-day strengths from the original test data were extrapolated to present day strengths following findings by ACI (1992) and Neville (1995). Diving inspections and sonar imaging were performed to evaluate the condition of the below water portions of the pier and the extent of scour, finding scour around the piers of up to 7.9 m (26 ft) deep. This scour had not undermined the foundation and the design did not rely on soil resistance from scoured or scour-prone depths. The results of a sonar imaging survey showing scour is shown in Figure 2-7.

Figure 2-6: Huey P. Long Bridge with widened superstructure, courtesy of Modjeski and Masters, Inc.

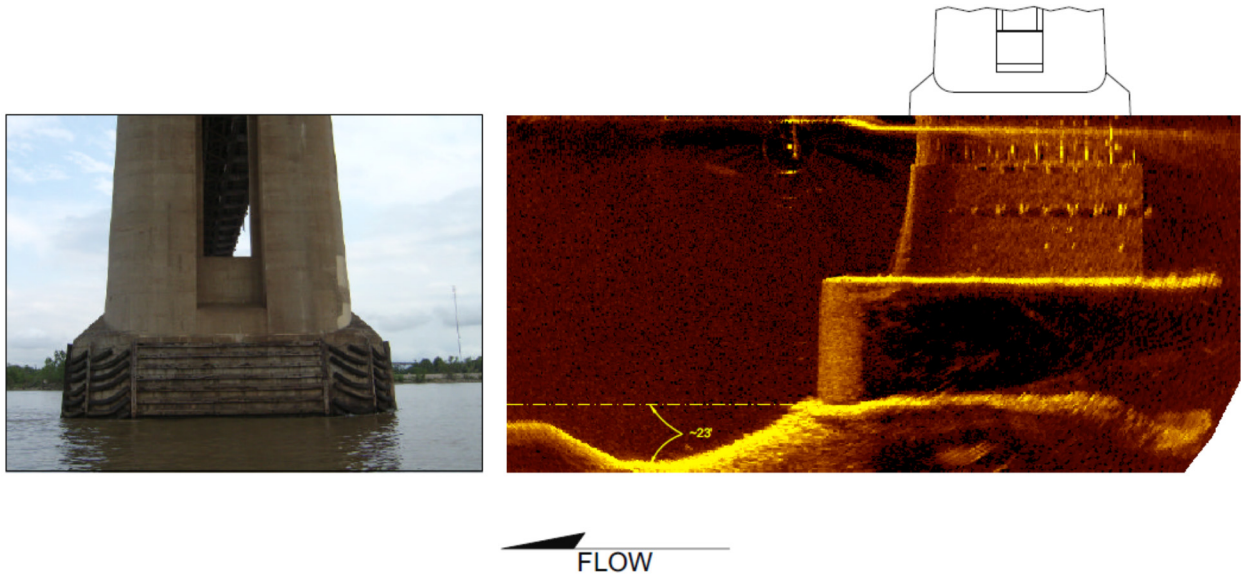

Figure 2-7: Above water image (left) and sonar image (right) of a bridge pier

Milton Madison Bridge, IN/KY (Option 4)

The Milton Madison Bridge (Figure 2-8) is a major crossing of the Ohio River between Indiana and Kentucky that was originally constructed in 1928 (Jalinoos 2015; Jalinoos et al. 2016; Tiberio 2015; Ligozio 2009). The bridge was a signature 5-span through truss that had significant historical value and overlooked a historical district in neighboring Madison, Indiana. In addition, closure of the crossing would have resulted in an approximate 80 km (50 mile) detour to cross the Ohio River. The original superstructure was structurally deficient and had no shoulders and narrow lanes that were insufficient by modern standards. The existing piers showed some signs of cracking and deterioration but appeared to be in generally good condition. To address these issues, the superstructure was replaced using a slide-in-place deck that had 3.7 m (12 ft) wide traffic lanes, 2.4 m (8 ft) wide shoulders on either side, and a 1.5 m (5 ft) wide sidewalk. Two replacement (Option 1) alternatives were considered alongside a strengthening and reuse (Option 4) alternative. The Option 4 alternative that reused four of the original piers was chosen as it presented an approximate $50 million cost savings (Tiberio 2015).

Figure 2-8. Milton Madison Bridge prior to renovation, courtesy Michael Baker International

The substructure consisted of 9 piers, including 4 founded on pneumatic caissons in the river, and 5 approach piers. Most of the existing piers appeared to be in reasonable shape considering their advanced age, but did show cracking on the pier faces, delaminated sections, lift lines from the original construction, and areas of paste erosion. Piers 4 and 5 (the leftmost piers in Figure 2-8) had been exposed to deicing chemical runoff and were considered to be in too poor of shape to be salvageable. Some major uncertainties that existed with the salvageable piers included: rebar location and depth, concrete strength, concrete integrity/deterioration, and chloride penetration A thorough investigation program was carried out to assess the integrity of the original piers, as shown in Table 2-9.

Table 2-9. Milton Madison Bridge - Tests performed, issues evaluated, extent and outcome of testing

Test Performed	Issues Evaluated with Testing	Extent of Testing	Outcome
GPR	Cover depth, Rebar layout	135 scans performed along 3 reused piers and 1 pier not reused	Drilling locations were chosen to avoid rebar. GPR survey confirmed very low reinforcement ratio.
Impulse Response	Extent of delamination, check for indications of honeycombing and subsurface voids	Performed along 3 reused piers and 1 pier not reused	Area of higher reflectivity corresponded to delaminated areas of concrete.
Down-Hole Camera in Core Hole	Integrity of interior concrete	1 core on each of 4 salvageable piers	No significant voids observed, ineffective below water line

Single hole sonic logging (SSL) on Core drilled through pier	Determine if voids or defects are present in pier	1 core on each of 4 salvageable piers	Anomalies reported just above caisson/soil interface, few other minor anomalies
Petrography	Mix properties; damage from freeze/thaw, erosion, ASR, carbonation penetration	Performed on 15 core samples, some extracted from exterior face, some from vertical coring through center of pier	Mix properties verified, minimal freeze/thaw or ASR noted, little carbonation penetration
Compression Tests	Compressive Strength	58 compression tests; 54 on 5 cm (2") cores, 4 on 10 cm (4")	Compressive strength taken as 1.5 standard deviations below average of the 54 tests on 5 cm (2") cores
Modulus Tests	Modulus of elasticity for concrete	Performed on 2 10 cm (4") dia. cores, also taken from concrete strength found from compression testing	Modulus used was from strength-based calculations
Chloride testing	Level of chloride penetration	138 powder samples extracted for 5 different piers. 4 samples taken at each location at 2.5 cm (1") intervals (up to 11.4 cm (4.5") deep)	4 of 5 piers did not have significant chloride exposure, even at surface. 1 pier had chloride levels higher than threshold (0.3% by wt) at rebar level

After the test program was completed, it was determined that 4 piers (Piers 6 through 9) could be salvaged, although they required encasement in 61 cm (24") of new high-performance concrete (HPC) to achieve a design life of 75 years. The new concrete was reinforced with epoxy-coated rebar and designed to carry all the new loads, bypassing the original pier stems, even though they had functional capacity. One major issue identified during evaluation was the presence of unreinforced caissons below the water and ground level. Analysis showed that the unreinforced portions would be subjected to tensile stresses that required reinforcement. The solution involved installing a temporary cofferdam so that drilling could be performed though the existing foundation (Figure 2-9a) and epoxy coated rebar installed in the completed holes (Figure 2-9b).

Figure 2-9. (a) Coring of caisson concrete from inside of cofferdam. (b) Insertion of reinforcement, photos courtesy of Michael Baker International

Additional geotechnical stability (due to overturning) issues were found during analysis due primarily to large design scour depth of up to 12.5 m (41.1 ft) deep. Due to the large potential scour, water and wind forces were able to generate significant moment at the base of the foundation, which cause the loading eccentricity to exceed the foundation width. When the foundation was analyzed with the scourable soil present, overturning was not an issue, so scour prevention measures in the form of rip rap and geotextiles were installed alongside the foundation to prevent scour and overturning forces. A rendering of the final rehabilitated bridge piers is provided in Figure 2-10.

Figure 2-10. Milton Madison Bridge after renovation, courtesy of Michael baker International

Mississagi River Bridge, ON, Canada (Option 4)

The Mississagi River Bridge in Iron Bridge, Ontario, Canada, carries Provincial Highway over the only major crossing of the Mississagi River for dozens of miles in either direction (Li et al. 2014). Originally constructed in 1943, the bridge deck had suffered from corrosion and deterioration and was in generally poor condition. Since acquisition of adjacent rights of way (ROW) was not possible, a plan that maintained the existing alignment while reusing the existing piers. These piers were constructed by driving steel sheet piling into the river bed, excavating soil to the desired bearing surface, and filling the cofferdam with concrete. It was believed that all piers were founded directly on bedrock. Vertical coreholes were drilled through the piers into the underlying soil and bedrock, finding that 3 of the original piers had been founded on soil instead of bedrock. Deterioration of the steel sheet piling was observed through visual and ultrasonic inspection, the existing was measured through visual observations. In some spots, the existing scour was beneath the footing bottom, and there was concern that the soil-supported piers would become unstable as the cofferdams continued to deteriorate. The foundation was underpinned using micropiles drilled through the existing footings, the underlying soil, to bedrock. This approach allowed underpinning of the existing foundation without complete closure of the bridge, as micropiles were installed from the existing bridge deck (Figure 2-11)

Figure 2-11. Micropile installation through bridge deck with casing down pier face, Source: CSCE SMSB Conference 2014

The new micropiles were connected to the existing bridge using a new pile cap poured around the existing pier wall. Steel rails were used as compression struts that connected a pair of micropiles on either side of the pier to the new pile caps and old piers. A threaded bar was used a tension tie below the tops of the micropiles to prevent the new pile cap from separating from the pier. The new cap was poured in multiple sections and continued to the top, so that the existing pier was encased. The new piers were provided with ice nosing to prevent the buildup of ice and associated loading. Rip-rap (loose stones) large enough to resist scour at the expected flood velocities was placed around the piers to fill in old scour and prevent new scour from eroding lateral resistance of the pier.

2.10 Conclusions

The reuse of existing foundations during ABC projects presents many possible benefits in terms of direct cost savings, faster construction, lower user impacts, and reduced environmental impacts. Still, reuse can present new challenges to designers and bridge owners that complicates the risk analysis and decision-making process. Recent research in the area of foundation reuse

presents methodologies for mitigating or controlling the risks associated with foundation reuse. Presented case studies herein indicate that consideration of foundation reuse in ABC projects can make ABC cost competitive or cheaper (in terms of direct costs) with conventional bridge construction techniques. ABC options that reuse foundation can also obtain the benefits of lower construction times, reduced material usage, lower user impacts, and historical preservation. To aid owners and stakeholders in decision-making for foundation reuse for ABC projects, databases of completed ABC projects can include specific information on the existing and replacement foundation type as well as the foundation reconstruction option.

2.11 Acknowledgements

The research presented in this paper has been supported through the foundation characterization program of Federal Highway administration, contract no. DTFH61-14-D-00010/0002. Any opinions, findings, and conclusions or recommendations expressed in this paper are those of the authors and do not necessarily reflect the views of the Federal Highway Administration. The authors would like to thank Aaron Stover of Michael Baker International, David Kangar of Modjeski and Masters, John Moran, Mahmoud Lardjane of CSCE, and Andrew Zickler of the Virginia DOT for providing case study photos.

2.12 References

ACI. (1992). ACI 209R-92: *Prediction of Creep, Shrinkage, and Temperature Effects in Concrete Structures.* Report of ACI Committee 209, American Concrete Institute, Farmington Hills, MI.

Agrawal, A.K., Jalinoos, F., Davis, N.T., Hoomaan, E., Sanayei, M. (2018) *Foundation Reuse for Highway Bridges*. FHWA Office of Research, Development, and Technology. McLean, VA 22101

Aktan, H. and Attanayake U. (2015). *Research on Evaluation and Standardization of Accelerated Bridge Construction Techniques*. Report: RC-1618A. Michigan Department of Transportation, Research Administration, Lansing, MI.

Axtell, P.J. and Siegel, T.C., Brown, D. (2014). "Sustainability and Reuse of Foundations for Hurricane Deck Bridge." Proceedings of the 39th Annual Conference on Deep Foundations, Deep Foundation Institute, Atlanta, GA.

Boeckmann, A.Z. and Loehr, J.E. (2017) *Current Practices and Guidelines for the Reuse of Bridge Foundations*. NCHRP Synthesis 505, Transportation Research Board of the National Academies, Washington, D.C.

Butcher, A.P., Powell, J.J.M., and Skinner, H.D. (2006). *Reuse of Foundations for Urban Sites: A Best Practice Handbook*, IHS BRE Press, Hertfordshire, United Kingdom.

Chapman, T., S. Anderson, and J. Windle. (2007). Reuse of Foundations, Report C653, CIRIA, London, United Kingdom.

Collin, J. G. and Jalinoos, F. (2014). "*Foundation Characterization Program: TechBrief #1—Workshop Report on the Reuse of Bridge Foundations.*" Publication FHWA-HRT-14-072, Federal Highway Administration, Washington, D.C.

Culmo, M.P. (2011) *Accelerated Bridge Construction — Experience in Design, Fabrication and Erection of Prefabricated Bridge Elements and Systems* FHWA-HIF-12-013, Federal Highway Administration, Washington, D.C.

Davis, N.T., Sanayei, M., Agrawal, A.K. Jalinoos, F. (2018) "*Determining the Capacity of Reused Bridge Foundations from Limited Information"*, ASCE Journal of Bridge Engineering, in press

FHWA. (2017). "**I**nfrastructure **V**oluntary **E**valuation **S**ustainability **T**ool (INVEST)," Federal Highway Administration, Washington, DC. Last accessed February 15, 2017, at www.sustainablehighways.org.

FHWA (2018a), *National Bridge Inventory*, Deficient Bridges by Highway System in 2017. Federal Highway Administration. Last accessed March 15, 2018, at https://www.fhwa.dot.gov/bridge/nbi/no10/defbr17.cfm,

FHWA (2018b), *Accelerated Bridge Construction*, Federal Highway Administration. Last accessed March 15, 2018, at https://www.fhwa.dot.gov/bridge/abc/

Florida International University (FIU). (2017) *ABC Project Database*. Accelerated Bridge Construction University Transportation Center. Florida International University. Last accessed on 3/15/2018 at http://utcdb.fiu.edu/

Gangarao, H., Shekar, V., Lasiriphong, K. (2007). *Engineering and Monitoring Services for Market Street Bridge.* IBRCP-1 West Virginia Dept. of Transportation, Charleston, WV 25305

Jalinoos, F. (2015). Reusing Bridge Foundations. Public Roads, Vol. 79, No. 3. Last accessed February 15, 2017, at https://www.fhwa.dot.gov/publications/publicroads/15novdec/05.cfm

Jalinoos, F., Mulla, M., Schaefer, V.R. (2016). Foundation Reuse and Enhancement: A Viable Option for Bridge Widening and Replacement Projects. Geo-Strata—Geo Institute of ASCE, Vol. 20, Issue 3, Pg. 52-57.

Jalinoos, F., Agrawal, A.K., Hoomaan, E., Crowder, R. E., Descour, J., and Olson, L. (2018) *Assessment of Substructures of Willow Valley Creek Bridge in Arizona.* Federal Highway Administration

LeGrand, L. (2015) *Keeping Virginia Moving* FHWA-HRT-15-005, Public Roads, Vol. 79, No. 1, Federal Highway Administration

Li, E., Morozevych, S., and Lo, C. (2014). "Underpinning of Existing Foundations of a Major River Crossing Using Micropiles in Ontario, Canada," Proceedings of the 9th International Conference on Short and Medium Span Bridges, Calgary, AB, Canada.

Ligozio, C.A., and Villalobox-Chapa, S. (2009). Evaluation of Milton Madison Bridge Substructures, a Report for Wilbur Smith and Associate. CTL Group Project No. 210727. Louisville, Kentucky.

Modjeski and Masters, Inc. (2013). Widening of the Huey P. Long Bridge. Final Report to Louisiana Department of Transportation and Development. Baton Rouge, LA.

Moran, J. (2012). "The Fast 14 Project." Public Road Magazine, FHWA-HRT-12-004. Vol. 75 No. 6. Federal Highway Administration. Washington, DC

Neville, A. M. (1995). *Properties of concrete*. Pearson. Edinburgh Gate, Essex, England

Sohanghpurwala, A. A. (2006). NCHRP 558 *Manual on service life of corrosion-damaged reinforced concrete bridge superstructure elements* NCHRP Report No. 558. Transportation Research Board, Washington DC

Schaefer, V.R., Jalinoos, F. (2013). Characterization of Bridge Foundations Workshop Report, FHWA-HRT-13-101, Federal Highway Administration (FHWA), McLean, VA 22101

Sharp, S.R. (2016). "Use of Electrochemical Chloride Extraction and Associated Repairs to Extend the Beneficial Life of Reinforced Concrete Substructures." FHWA/VTRC 16-R16. Virginia Transportation Research Council. Charlottesville, VA.

Strauss, J., R. Nicholls, T. Chapman, and S. Anderson. (2007). "Drivers Affecting Frequency of foundation Reuse and Relevance to U.S. Cities," GSP 158 Contemporary Issues in Deep Foundations, American Society of Civil Engineers, Reston, Va.

Tiberio, T. (2015). Reuse of Milton Madison Bridge Piers presentation to the 94th Annual Meeting of the Transportation Research Board, Washington, D.C.

Chapter 3 Foundation Identification Using Dynamic Strain and Acceleration Measurements

This chapter features the contents of a manuscript by the following authors that has been formatted for publication in a peer-reviewed manual.

Foundation Identification Using Dynamic Strain and Acceleration Measurements

Nathan T. Davis[1] and Masoud Sanayei[2]

[1] PhD Graduate, Dept. of Civil & Environmental Engineering, Tufts University, Medford, MA 02155
[2] Professor, Dept. of Civil & Environmental Engineering, Tufts University, Medford, MA 02155

Abstract

This paper proposes a method to characterize bridge foundations using live load dynamic strain and acceleration measurements taken from substructure elements during operational loading. These measurements are used to assemble frequency response functions (FRFs) that describe the load-response behavior of the tested foundation element as a function of frequency. This method only requires that a limited number of measurements be performed on exposed portion of the bridge substructure (piers, columns piles, etc.), and can be performed during daily operational bridge traffic. The direct result of this analysis is an updated boundary condition that be used for modeling of the superstructure in place of the fixed conditions typically used. Furthermore, this method can be used to identify foundation depth and type, verify design parameters, and update finite models of pile and drilled shaft behavior. A case study is presented where dynamic measurements were taken from an in-service drilled shaft.

Keywords: Bridge Foundation Identification, Measured Strains and Accelerations, Short-Time Fourier Transform (STFT), Frequency Response Function (FRF), Optimization

3.1 Introduction

As of December 2017, there were 26,727 bridges in the United States over waterways or tidal areas with unknown foundations (FHWA 2018). There is also a substantial amount of bridges over land with unknown foundations, though this number is not tracked (Schaefer and Jalinoos 2013). The lack of information on these bridge foundations inhibits evaluation of geo-hydraulic hazards impacting the foundation such as scour, or liquefaction. To address this potential hazard, the FHWA launched the foundation characterization program (FCP) (Schaefer and Jalinoos 2013; Collin and Jalinoos 2014), which also identified changes in service loads (foundation reuse), and foundation condition assessment as essential applications of foundation characterization (FHWA

2017). Schaefer and Jalinoos (2013) identified the following areas for foundation characterization: foundation type, pile type, embedment depth, geometry and material, integrity, and load carrying capacity. While Colin and Jalinoos (2014) identify various destructive and non-destructive testing/evaluation options for identifying many of the above parameters, it was stated that "Additional research into methods of assessing the integrity and capacity of existing foundations should also be pursued."

Maser et al. (1998), Maser and Sanayei (1999), and Sanayei and Maser (1999) proposed using estimated foundation stiffness as a means of detecting foundation type. Foundation stiffness referred to a boundary condition consisting of a 3 by 3 stiffness matrix at the ground surface. A 2D plane-strain finite element model (FEM) of the foundation system was used to estimate the 2D response of the system and component of the stiffness matrix in 2D. Maser et al. (2001) compared the results of a static 3D FEM of the foundation system with the stiffness coefficients obtained following the work of Novak (1974). It was found that the predicted dynamic stiffness entries ranged from 1.38% to 10.85% different from modeled static stiffness values.

Maser et al. (1998), Maser and Sanayei (1999), and Sanayei and Maser (1999) proposed that foundation stiffness be extracted from static strain, displacement, and rotation measurements from a bridge. A 2D frame model of the bridge was used to update the foundation stiffness parameter based on these measurements. While force and displacement patterns from truck crossings roughly matched expectations, parameter estimation did not accurately identify the foundation boundary condition.

Santini et al. (1999) extended the foundation stiffness concept to be used with dynamic data for foundation identification. This approach attempted to update a 2D FEM of a bridge subjected

to dynamic loading. The foundation was modeled as a boundary condition that provided stiffness and inertial effects. The parameter estimation approach used was incapable of identifying the stiffness components of the foundation boundary condition

Sipple et al. (2014) used acceleration measurements from a bridge superstructure to identify the boundary conditions for a bridge deck. The authors did not model the substructure and updated a single boundary condition at the bearings along with structural parameters. This approach did not attempt to identify the individual behavior of the foundation, pier columns, and bearing pads. Since measurements were performed only on the bridge deck, the authors believe it will be difficult to separate foundation behavior from bearing and substructure behavior.

This paper proposes a method for measuring foundation behavior and estimating many of the parameters identified by Collin and Jalinoos (2014) important to foundation characterization for known and unknown foundations. The proposed method requires only a limited number of measurements from the foundation element under consideration and does not require information regarding the superstructure or knowledge of the input excitation. Measurements are taken from a pier column or foundation wall during daily operational bridge traffic without bridge closure or special traffic considerations. The dynamic response measurements are aggregated and averaged after sufficient responses have been measured to determine the frequency response function (FRF) of the foundation. The calculated FRF is compared with an empirical model of foundation behavior to determine foundation parameters such as depth, soil properties, and foundation structural properties that govern the foundation FRF.

3.2 Proposed Method for Estimation of Foundation Stiffness Parameters

A major novel aspect of the proposed method is that it is an output-only method that solely relies on live load excitation generated by operational bridge traffic consisting of cars, trucks, and busses. This approach allows the method to be used on in-service bridges where closure is not possible, and/or the weight of the passing vehicles are unknown. Many output-only methods (e.g., Sipple and Sanayei 2014; Reynders et al. 2013; Ubertini et al. 2016) still require detailed models that predict the natural mode shapes and fundamental frequencies of the structure in order to extract information from the observed differences. This method instead creates a free body diagram (FBD) of the foundation using force and acceleration time histories at the top of the FBD calculated from strain and acceleration measurements performed on the pier column. From the response of the FBD to excitation, the foundation behavior can be ascertained following the method presented below.

Loading Source

While operational traffic imparts primarily vertical loads onto the substructure, the dynamic response of the bridge deck generates vertical forces, lateral forces, and moments in the pier columns in a range of frequencies. As a vehicle crosses midspan, the girders underneath the vehicle deflect downwards. Since the bottom girder fiber is far below the neutral axis, this deflection causes the bottom girder fibers to expand longitudinally away from the passing vehicle, inducing a lateral force onto the bridge piers. This force is secondary (and therefore expected to be smaller in magnitude) to the vertical forces directly caused by the vehicle weight. The lateral forces act on the bridge piers at a distance above the foundation, generating a moment along with any moments generated by rotation of the girders. The passing vehicles will often excite fundamental modes of

the bridge deck, transferring loads onto the foundations at these frequencies. The proposed method allows this broad-spectrum forcing function to be utilized without modeling of the bridge deck and bearings with their associated fundamental frequencies and mode shapes.

Free Body Diagram of Foundation

The proposed method examines a free body diagram (FBD) that contains a limited portion of the substructure and the foundation system. Shown in Figure 3-1, the FBD consists of a lower portion of a pier column being acted upon by external forces and moments. The above-lying superstructure is not explicitly considered in this analysis and is instead replaced by a time history of internal forces and moments acting on the top of the FBD. This approach significantly reduces the amount of modeling required, reducing complexity of the model, and the potential for modeling errors associated with the bridge deck, bearings, and loading source.

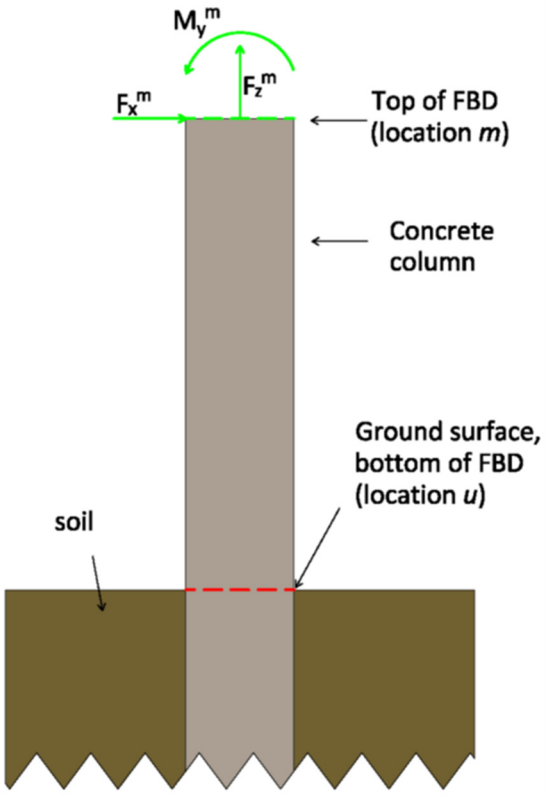

Figure 3-1: A free body diagram of a foundation

For a single foundation element, a total of 3 forces, 2 moments, and a torsional force will be imparted on the top of the FBD from the superstructure in a 3D reality. Figure 3-1 is a 2D representation of this FBD, where out of plane forces and moments are neglected. Neglecting these DOFs is possible when there is no coupling between forces and moments acting in orthogonal directions. Torsion is neglected in this study as it is uncoupled from other DOFs, not expected to have a significant response, and difficulties associated with measuring torsion in a foundation column.

Instrumentation Setup

Measuring the 2D operational live load-induced forces (vertical, shear) and bending moment in a foundation pier column requires a total of 4 strain gauges arranged in 2 pairs, with the top of

the FBD centered between the two pairs. In 3D, to measure 5 DOF (neglecting torsion), 2 orthogonal pairs at each elevation could be used, but as few as 3 strain gauges can find both moments and the axial force. It is desirable for accurate shear force estimation to maximize the distance between the pairs of strain gauges. To avoid issues with stress concentrations, the gauges should be placed at least 1 diameter away from the top or bottom of the column pier. To measure the 3 accelerations required for 2D analysis, a setup using 4 accelerometers is proposed, with one pair of accelerometers (one vertical and one horizontal) placed on either side of the column. In reality, only a single horizontal accelerometer would be required, but the use of two accelerometers with averaging can improve the quality of the data. A schematic of the proposed test setup is shown in Figure 3-2.

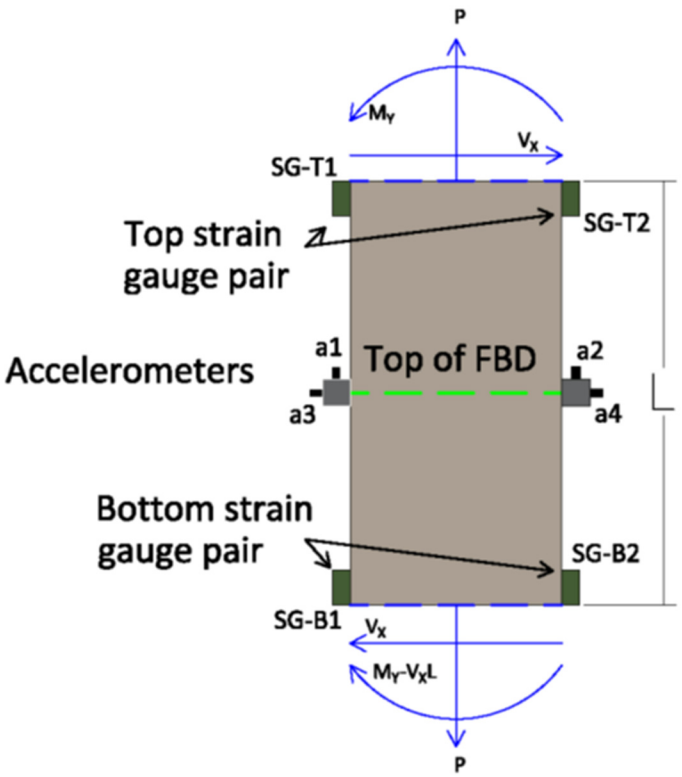

Figure 3-2: Strain gauge setup for force and moment determination from column

Figure 3-3 shows a typical strain and acceleration recording taken during vehicular passage. From the strain measurements, it can be observed that there is significant low-frequency (<0.5Hz) loading on the pier column as the vehicle passes over the instrumented pier column. Some higher frequency (5Hz - 20Hz) excitations are visually identifiable in the raw strain measurements. The strain measurements are zeroed by setting the first sample for each recording to 0, but some drift is evident in the time history if each strain signal. This drift is believed by the authors to be due to the combination of strain gauge selection and environmental effects such as sunlight and temperature changes. Drift is frequently removed from measurement time histories by baseline correcting (detrending) the signal, but since the proposed method is frequency-based and the majority of thermal drift is at low frequencies not considered in this analysis, thermal drift is not removed from the data.

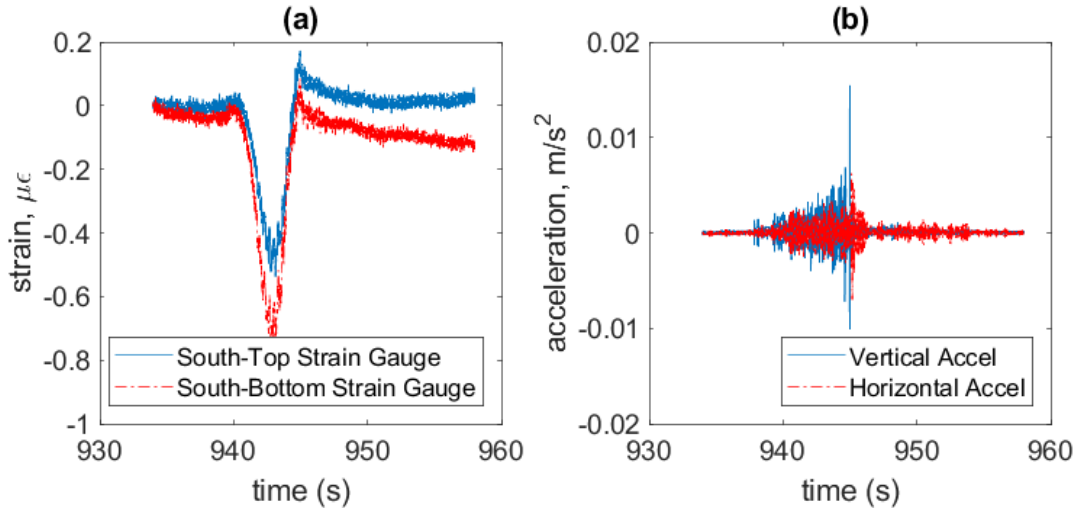

Figure 3-3: Measured (a) strains and (b) accelerations from pier column

At each pair of strain gauges, the axial force and bending moment due to live loading can be determined using Eq.(3-1) and Eq.(3-2),

$$P = AE(\varepsilon_1 + \varepsilon_2) \tag{3-1}$$

$$M_Y = \frac{EI}{2r}(\varepsilon_1 - \varepsilon_2) \tag{3-2}$$

where A = transformed cross sectional area, E = modulus of elasticity of concrete, I = transformed moment of inertia, and ε_1 and ε_2 are the measured strains on the left and right side of the column in Figure 3-2, respectively.

Since the axial force due to live loading is constant throughout the section between the strain gauge pairs, the axial force at the top of the FBD can be calculated by averaging the axial force obtained in Eq.(3-1) for the top and the bottom pair, as shown in Eq.(3-3). While this step is in theory not necessary, it can improve the quality of the data by virtue of averaging,

$$P^m = \frac{P^b + P^t}{2} \tag{3-3}$$

where the superscript m represents the top of the FBD, the superscript b represents the bottom strain gauge pair, and the superscript t represents the top strain gauge pair. Likewise, the shear force induced by live loads will be constant throughout the section. This shear force can be calculated from the moments measured at the top and bottom pair of strain gauges by dividing the difference in moments by the length (L) between the center of the two strain gauge locations, as shown in Eq.(3-4).

$$V_X^t = V_X^b = V_X^m = \frac{-(M_Y^t - M_Y^b)}{L} \tag{3-4}$$

Due to the constant shear throughout the section, the live load moment is expected to vary linearly between the two strain gauges. Since increasing the distance between the two pairs of strain gauges will increase the moment difference caused by constant shear, increasing the distance between the strain gauge pairs will provide a shear estimate that is more tolerant to sensor noise.

The moment at the top of the FBD (location *m*) can be calculated by taking the average of the top and bottom moments (when the top of the FBD is halfway between the strain gauge pairs), as shown in Eq.(3-5).

$$M_Y^m = \frac{(M_Y^t + M_Y^b)}{2} \tag{3-5}$$

In practice, the top of the FBD (location *m*) is not required to be halfway between the strain gauge pairs, as the moment can be estimated at any point in the column assuming this linear relationship and a constant shear and vertical force, but this convention makes physical sense in most cases and allows the simplification presented in Eq.(3-5).

To isolate the dynamic effects created by traveling vehicles or other live loading sources, the strain gauge time histories for each event are zeroed by subtracting the first sample from all the samples in the recording. It can be observed that there is some drift in the strain gauge time histories. This drift is a product of thermal sensor drift and is generally of low frequency in comparison to the frequencies of interest. Thermal drift in strain gauges is frequently accounted for by detrending or a baseline rotation of the strain time histories so that the signal begins and ends at approximately 0. Since the proposed method is performed in frequency domain and the low frequencies most affected by thermal drift are not used for updating, each strain gauge time history is zeroed, but no detrending or baseline rotation is performed.

The four measured accelerations are then converted in time domain into accelerations acting at the top of the FBD to be used in analysis. Since the top of the FBD is at the centroid of the column and the vertical acceleration measurements are performed at a distance away from the centroid, each vertical accelerometer is influenced by the vertical and rotational accelerations at the top of the FBD. The vertical acceleration is calculated as the average of the 2 vertical

accelerations. The rotational acceleration is the difference between the two vertical accelerations, divided by the distance between the two sensors, as shown in Eq.(3-6) and Eq.(3-7),

$$\ddot{Q}_v = \frac{\ddot{Q}_1 + \ddot{Q}_2}{2} \tag{3-6}$$

$$\ddot{Q}_\theta = \tan^{-1}\left(\frac{\ddot{Q}_1 - \ddot{Q}_2}{2(r + d_s)}\right) \approx \frac{\ddot{Q}_1 - \ddot{Q}_2}{2(r + d_s)} \tag{3-7}$$

where $\ddot{Q}_1$ and $\ddot{Q}_2$ are the vertical accelerations measured at accelerometers *1* and *2*, respectively, *r* is the column radius, and d_s is the distance from the column edge to the measurement location. Rotational acceleration is defined as $\ddot{Q}_\theta$. In practice, the measured angles of rotation in radians will be small enough that the angle will be equal to its tangent, so the simplification shown in Eq.(3-7) can be used. The horizontal acceleration is calculated as the average of 2 accelerometer measurements, as shown in Eq.(3-8),

$$\ddot{Q}_h = \frac{\ddot{Q}_3 - \ddot{Q}_4}{2} \tag{3-8}$$

where $\ddot{Q}_3$ and $\ddot{Q}_4$ are the horizontal accelerations measured at accelerometers *3* and *4*, and the negative sign accounts for the different accelerometer orientations.

Response of FBD to Loading

The general equation of motion (in discrete time) for the foundation element shown on the right side of Figure 3-4 is given by Eq. (9),

$$[\boldsymbol{F}] = [\boldsymbol{K}][\boldsymbol{Q}] + [\boldsymbol{C}][\dot{\boldsymbol{Q}}] + [\boldsymbol{M}][\ddot{\boldsymbol{Q}}] \tag{3-9}$$

where $\boldsymbol{F}$, $\boldsymbol{Q}$, $\dot{\boldsymbol{Q}}$, and $\ddot{\boldsymbol{Q}}$ are matrices of forces, displacements, velocities, and accelerations at all degrees of freedom (DOF) in the model. These four matrices are all size *2n* by *m*, with *n* being the

number of DOF considered at the top of the FBD (3 for 2D, 5 for 3D when torsion is excluded), and *m* being the number of samples measured. ***K***, ***C***, and ***M*** are the stiffness, damping, and mass matrices, respectively and are all size *2n* by *2n*. In frequency domain, Eq.(3-9) can be rewritten in terms of measured forces, $\boldsymbol{F}$, and measured accelerations, $\ddot{\boldsymbol{Q}}$, by expressing velocities and displacements as the first and second integrals of acceleration, as shown in Eq.(3-10),

$$[\boldsymbol{F(\omega)}] = -\frac{1}{\omega^2}[\boldsymbol{K}]\left[\ddot{\boldsymbol{Q}}(\boldsymbol{\omega})\right] + \frac{1}{i\omega}[\boldsymbol{C}]\left[\ddot{\boldsymbol{Q}}(\boldsymbol{\omega})\right] + [\boldsymbol{M}]\left[\ddot{\boldsymbol{Q}}(\boldsymbol{\omega})\right] \tag{3-10}$$

where $\boldsymbol{F(\omega)}$ and $\ddot{\boldsymbol{Q}}(\boldsymbol{\omega})$ are matrices of Fourier transforms of the force and acceleration measurements, respectively. Both matrices are of size *2n* by *nfft/2*, with *n* being 3 for 2D measurements and *nfft* being the length of the Fourier transform. ω is the frequency expressed in radians and *i* is the imaginary operator, $\sqrt{-1}$. ***K***, ***C***, and ***M*** are identical to the matrices in Eq.(3-9), and can be condensed into an FRF matrix as shown in Eq.(3-11).

$$[\boldsymbol{D}(\boldsymbol{\omega})] = -\frac{1}{\omega^2}[\boldsymbol{K}] + \frac{1}{i\omega}[\boldsymbol{C}] + [\boldsymbol{M}] \tag{3-11}$$

Since measurements are only performed at the top of the FBD (half of the total FBD DOFs), it is useful to partition the matrices in Eq.(3-11) as shown in Eq.(3-12),

$$\begin{bmatrix} \boldsymbol{F(\omega)_m} \\ \boldsymbol{F(\omega)_u} \end{bmatrix} = \begin{bmatrix} \boldsymbol{D(\omega)_{mm}} & \boldsymbol{D(\omega)_{mu}} \\ \boldsymbol{D(\omega)_{um}} & \boldsymbol{D(\omega)_{uu}} \end{bmatrix} \begin{bmatrix} \ddot{\boldsymbol{Q}}(\boldsymbol{\omega})_m \\ \ddot{\boldsymbol{Q}}(\boldsymbol{\omega})_u \end{bmatrix} \tag{3-12}$$

where the subscripts *m* and *u* denote the measured and unmeasured DOFs, respectively. $\boldsymbol{F(\omega)_m}$, $\boldsymbol{F(\omega)_u}$, $\ddot{\boldsymbol{Q}}(\boldsymbol{\omega})_m$, and $\ddot{\boldsymbol{Q}}(\boldsymbol{\omega})_u$ are all size *n* by *nfft/2*. The proposed method models the unmeasured DOFs as being supported by a set of foundation springs with no other external forces being applied at that location, so $\boldsymbol{F(\omega)_u} = 0$ for all the entire *n* by *nfft/2* matrix. The FRF matrix ***D*** is then

invertible and is comprised of the stiffness components of the modeled portion of column and supporting soil springs, as shown in Eq.(3-13),

$$\boldsymbol{D(\omega)} = \begin{bmatrix} \boldsymbol{D_c(\omega)_{mm}} & \boldsymbol{D_c(\omega)_{mu}} \\ \boldsymbol{D_c(\omega)_{um}} & \boldsymbol{D_c(\omega)_{uu} + D_F(\omega)_{uu}} \end{bmatrix} \tag{3-13}$$

where the $\boldsymbol{D_c}$ entries are components of the FRF matrix for the column between the top and bottom of the right ride of Figure 3-4, and $\boldsymbol{D_F}$ is the FRF matrix of the foundation, as discussed in the following section. Eq.(3-12) can be rearranged as shown in Eq.(3-14):

$$\begin{bmatrix} \boldsymbol{F(\omega)_m} \\ \boldsymbol{0} \end{bmatrix} = \begin{bmatrix} \boldsymbol{D(\omega)_{mm}\ddot{Q}(\omega)_m + D(\omega)_{mu}\ddot{Q}(\omega)_u} \\ \boldsymbol{D(\omega)_{um}\ddot{Q}(\omega)_m + D(\omega)_{uu}\ddot{Q}(\omega)_u} \end{bmatrix} \tag{3-14}$$

From the bottom row of Eq.(3-14), the following equality shown in Eq.(3-15) can be obtained.

$$\boldsymbol{\ddot{Q}_u = -D_{uu}^{-1} D_{um} \ddot{Q}_m} \tag{3-15}$$

Eq.(3-15) can be substituted into the top row of Eq.(3-14) to provide the equality in Eq.(3-16)

$$\boldsymbol{F(\omega)_m = \left(D(\omega)_{mm} - D(\omega)_{mu} D(\omega)_{uu}^{-1} D(\omega)_{um}\right)\ddot{Q}(\omega)_m} \tag{3-16}$$

For convenience, Eq.(3-16) can written in a condensed format, as shown in EQ.(3-17),

$$\boldsymbol{F(\omega)_m = D(\omega)^{FBD}\ddot{Q}(\omega)_m} \tag{3-17}$$

where D^{FBD} is an $n*n$ matrix whose entries in 2D are given by Eq.(3-18),

$$\boldsymbol{D(\omega)^{FBD}} = \begin{bmatrix} D(\omega)_{VV}^{FBD} & D(\omega)_{VH}^{FBD} & D(\omega)_{V\theta}^{FBD} \\ D(\omega)_{HV}^{FBD} & D(\omega)_{HH}^{FBD} & D(\omega)_{H\theta}^{FBD} \\ D(\omega)_{\theta V}^{FBD} & D(\omega)_{\theta H}^{FBD} & D(\omega)_{\theta\theta}^{FBD} \end{bmatrix} \tag{3-18}$$

where for symmetrical foundations, the entries $D(\omega)_{VH}^{FBD}$, $D(\omega)_{V\theta}^{FBD}$, $D(\omega)_{HV}^{FBD}$, and $D(\omega)_{\theta V}^{FBD}$ are generally 0, unless the substructure is angled or the foundation produces an off-centered response. In general, the proposed method is not restricted to this assumption, although off-diagonal terms that are of a different order of magnitude than the diagonal terms may be difficult to recover.

Foundation Modeling

The bottom of the FBD is modeled as a boundary condition that represents the foundation behavior. The boundary condition isn't assumed to impose external loading on the FBD, only react to loading applied at other DOFs. The boundary condition consists of a frequency-dependent stiffness and damping commonly modeled as a spring and dashpot. This representation is a commonly used approach for modeling many types of foundations, including foundations with complicated subsurface geometry, as shown in Figure 3-4.

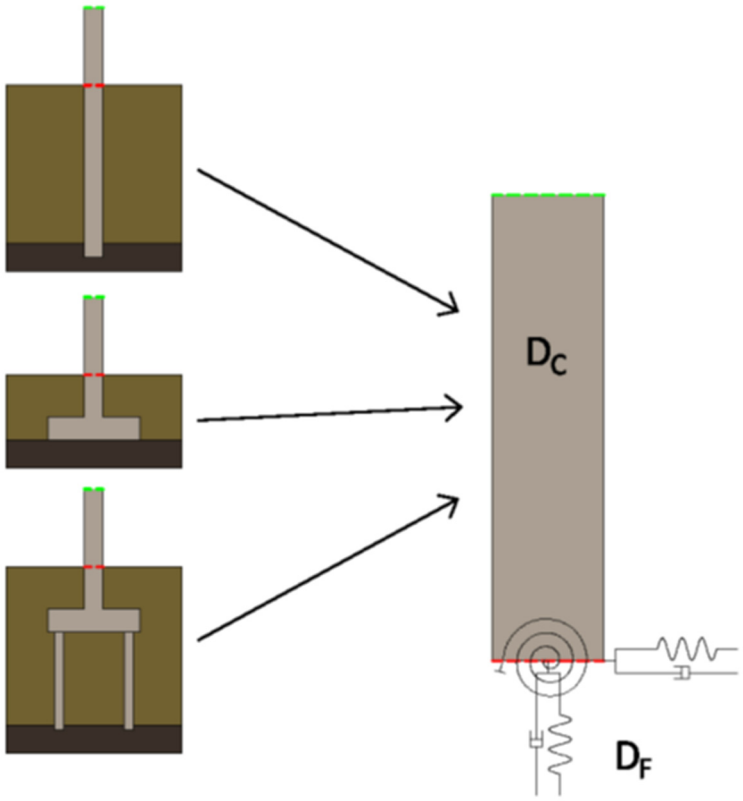

Figure 3-4: Diagram of various foundations represented by spring constants

Gazetas (1983) and Dobry and Gazetas (1986) discusses the then state-of-the-art in modeling of foundation behavior for various foundation types during dynamic loading. Novak (1974) and Novak and Aboul-Ella (1978) outlined a procedure to estimate the frequency-

dependent response of a pile foundation subjected to vertical, horizontal, and rotational loading. Gazetas and Dobry (1984) describe a method for estimating the lateral response of piles in layered soils that includes hysteretic damping to describe non-linear behavior. Beredugo and Novak (1972), Kausel-Bolt (1974), Gazetas (1981), and Gazetas and Roessett (1979) describe procedures for estimating the boundary condition provided by rigid plates on soil. Elsabee and Morray (1977) and Dobry and Gazetas (1982; 1986) estimate the response of embedded shallow foundations. Gerolymos and Gazetas (2005) and Assimaki and Gazetas (2008) provide a method for calculating the dynamic response of caisson foundations, which are deeper than embedded shallow foundations, but shallower than pile foundations.

In general, these methodologies describe the relationship between force applied to the foundation and displacement of the top of the foundation. Since they are developed using simplified models of foundation behavior, it is assumed that no coupling exists between the vertical and rotational DOFs. The stiffness and damping components obtained using one of the above-mentioned methodologies can be arranged into a frequency-response function (FRF) matrix that represents the foundation, $\boldsymbol{D_F}$, as shown in Eq.(3-19).

$$\boldsymbol{D_F(\omega)} = \begin{bmatrix} -\frac{K_{VV}(\omega)}{\omega^2} + \frac{C_{VV}(\omega)}{i\omega} & 0 & 0 \\ 0 & -\frac{K_{HH}(\omega)}{\omega^2} + \frac{C_{HH}(\omega)}{i\omega} & -\frac{K_{H\theta}(\omega)}{\omega^2} + \frac{C_{H\theta}(\omega)}{i\omega} \\ 0 & -\frac{K_{\theta H}(\omega)}{\omega^2} + \frac{C_{\theta H}(\omega)}{i\omega} & -\frac{K_{\theta\theta}(\omega)}{\omega^2} + \frac{C_{\theta\theta}(\omega)}{i\omega} \end{bmatrix} \quad (3\text{-}19)$$

The matrix shown in Eq.(3-19) is the foundation FRF and is used in Eq.(3-13) as the boundary condition at the bottom (*location u*) of the free body diagram. Once identified, this boundary condition can be placed into a dynamic model of the entire bridge to simulate the appropriate

boundary condition and improve the accuracy of that model. The division by $-\omega^2$ and $i\omega$ in the stiffness and damping terms (respectively) follows from Eq.(3-11), where integration is performed to relate forces and accelerations. Since the validation model used for the research is a drilled shaft with a slenderness ratio of about 11, it is most appropriate to model the foundation as a pile (Gerolymos and Gazetas 2005), following the approach discussed by Novak (1974) and Novak and Aboul-Ella (1978).

3.3 Automated Event Selection

A major novel aspect of the proposed method is that it can be paired with a long-term instrumentation setup to provide a continual snapshot of foundation behavior. As part of this research selection criteria have been devised so that foundation behavior can be automatically extracted from ambient data acquired from a long-term instrumentation setup. The automated procedure allows determination of foundation behavior from a limited set of data (in the range of several hours to days) automatically with no human intervention. Such a system could potentially identify changes to the foundation, such as scour, deterioration, or seismic damage. The procedure for automatic data collection are as follows:

- Recordings are performed for a long segment of time (e.g., several hours or days)
- Events (passage of one or several vehicles) are separated from the extended recording
- A time history of forces and accelerations is calculated for the selected windows
- The magnitude-squared coherence between forces and accelerations is used to identify frequencies in each event with good signal to noise (SNR)

- Short-time Fourier transforms (STFT) are made of each event to identify short time windows (~4 seconds) where the force and acceleration measurements exceed background noise by a defined amount
- The foundation FRF is extracted from data from the selected windows

The MSC and STFT selection criteria are necessary for use in the proposed method, as the recordings observed at an in-service bridge indicate that much of the data observed is at low SNRs, necessitating advanced processing to identify portions of recordings with the best SNR. The advanced signal processing techniques demonstrated in this paper are not typically employed on monitoring of civil structures. These techniques allow for extraction of meaningful data from signals that might otherwise provide highly variable results.

Event Separation

Periods of increased dynamic loading on the foundation from the extended recording, referred to here as events, are separated from the extended recording for further analysis. Event selection is performed on the basis of variance in the acceleration signal measurements, as the signal variance is a simple calculation that provides a measure of the total power in a signal (Smith 1997). Truck crossings, vehicular traffic, and other operational excitations will impart dynamic loading on the foundation resulting in higher recorded power in the accelerometer signals. The event separator reduces hours of continuously sampled data into a limited number of high energy events where further analysis is performed.

The variance of all accelerometer time histories is calculated in 1-second increments and summed together for all recorded time intervals. Two thresholds are set: a peak threshold that must be crossed for an event to be identified, and a secondary threshold that specifies the data

surrounding the peak to be retained. An additional 3 seconds of samples on either side of every event is retained during this step. It is desirable to use easily exceeded thresholds at this stage as the goal of the first selector is to select a reasonable amount of data for further analysis.

Event Frequency Selector

Once events have been separated, time histories of the forces, moments, and accelerations at the top of the FBD are calculated, as described in the proposed method section. The second selector is applied to these calculated time histories to distinguish which frequencies contain usable data for each separated event. The basis of selection for this selector is the magnitude-squared coherence (MSC) between the calculated force and vertical acceleration time histories, as well as the multiple-input multiple-output MSC between the horizontal force, moment, horizontal acceleration, and rotational time histories. For a single-input single-output system (as is the assumed case for vertical motion), the MSC is calculated by dividing the cross-power spectral density of the two signals by the product of each signal's power spectral density, as described by digital signal processing books, such as Alessio (2015). The result is a function of frequency with each frequency bin containing a value ranging from 0 to 1. If the two signals are perfectly correlated and noise free, the MSC will be 1 for all frequencies. Uncorrelated signals or situations where the output is a function of multiple inputs will produce a lower MSC, though it may not be 0. In the presence of noise, the MSC will tend to be reduced by the random nature of signal, therefore use of a threshold MSC when selecting data helps ensure that a high SNR is maintained (Alessio 2015). This concept can be extended to multiple-input, multiple-output systems (Matlab 2018) where the MSC relates each output to all considered inputs.

Window Selector

Once an excitation event has been identified and frequencies of interest have been chosen for that event, localized windows are selected within each event where the calculated force and accelerations at the top of the FBD exceed the background noise in a specific frequency bin by a specified amount. The selection of windows is performed using short-time Fourier transforms (STFT) taken of the separated events that allow for determination of the location higher signal energy in both time and frequency domains. This allows each frequency considered during the analysis to be calculated from short period of time where that specific frequency was being excited by live loading and bridge dynamics.

The STFT (Jauregui 2014) consists of Fourier transforms taken over successive windowed time segments, with the same window length and type used as was used to construct the periodogram of background noise. Both the periodogram of background noise and the STFT values are converted to units of power by dividing by the number of samples in the window. The magnitude selector then considers the frequencies identified by the coherence selector for each event and identifies individual windows where the power/frequency exceeds the thresholds mentioned earlier. Each individual window that exceeds the threshold is stored separately and used for estimation of FRFs.

A power spectral density of the background force and acceleration measurements was taken using Welch's averaged periodogram method (Proakis and Manolakis 2007), using a 512-sample (4-second) long Hann window, and an overlap of 50%. The choice of window length and window function controls frequency resolution, signal leakage, and scalloping loss (Proakis and Manolakis 2007). These are important characteristics to control, as the proposed method is inherently based

on frequency-domain information taken from short windows where excitation was observed. There is a tradeoff between resolution in time domain and frequency domain, as shorter windows provide lower resolution in frequency domain. A 4-second-long window provides a frequency resolution of 0.25 Hz. For this research, a Hanning window is chosen to be consistent with the window used to find the background periodogram. The choice of a Hanning window was compared with various other windows (rectangular, Hamming, Blackman, Blackman-Harris, Tukey, etc.). The major benefits of the Hann window include a narrow main lobe, decent attenuation of the closest side lobe, and continual roll off of other side lobes. The continual roll off helps ensure little power from the low frequencies is leaked into the frequencies under consideration. Further discussion on windows and the frequency related impact of windowing is given by Proakis and Manolakis (2007).

Estimation of Frequency Response Function

After all identified windows have been extracted from the complete data set, they are sorted by frequency. Since the vertical DOFs are assumed to be uncoupled from the horizontal and rotational DOFs, they can be extracted without any assumptions about the behavior of the remaining DOFs. Eq.(3-20) shows the equation proposed to provide a weighted average of the FRF for a specific frequency bin,

$$\overline{FRF}(\omega)_{VV} = \frac{\sum_{i=1}^{nWin(\omega)_{VV}} 20 * \log_{10}\left|\frac{F_V(i)}{\ddot{Q}_V(i)}\right| * \left|F_V(i)\right| * \left|\ddot{Q}_V(i)\right|}{\sum_{i=1}^{nWin(\omega)_{VV}} \left|F_V(i)\right| * \left|\ddot{Q}_V(i)\right|} \tag{3-20}$$

where F_V and $\ddot{Q}_V$ are the FFTs of the i[th] window of measured vertical forces and accelerations at frequency ω, respectively. $nWin(\omega)_{VV}$ is the number of vertical measurement windows selected at

frequency ω, and $\overline{FRF}(\omega)_{VV}$ is the average measured vertical frequency response function for the FBD.

Since the remaining 4 non-zero DOFs are coupled, they must be solved for simultaneously. Therefore, it is necessary to provide an initial estimate of the $\boldsymbol{D^{FBD}}$ shown in Eq.(3-8), Eq.(3-9), and Eq.(3-10). The initial estimate of this matrix is calculated using the equations outlined in Novak (1974) using estimated values of the soil and foundation parameters. Eq.(3-21) through Eq.(3-24) provide the proposed equations for calculating the weighted frequency bin average for the remaining non-zero FRF terms.

$$\overline{FRF}(\omega)_{HH} = \frac{\sum_{i=1}^{nWin(\omega)_{HH}} 20*\log_{10}\left|\frac{F_H(i) - D(\omega)_{H\theta}^{FBD}\ddot{Q}_\theta(i)}{\ddot{Q}_H(i)}\right| * \left|F_H(i)\right| * \left|\ddot{Q}_H(i)\right|}{\sum_{i=1}^{nWin(\omega)_{HH}} \left|F_H(i)\right| * \left|\ddot{Q}_H(i)\right|} \tag{3-21}$$

$$\overline{FRF}(\omega)_{\theta\theta} = \frac{\sum_{i=1}^{nWin(\omega)_{\theta\theta}} 20*\log_{10}\left|\frac{F_\theta(i) - D(\omega)_{\theta H}^{FBD}\ddot{Q}_H(i)}{\ddot{Q}_\theta(i)}\right| * \left|F_\theta(i)\right| * \left|\ddot{Q}_\theta(i)\right|}{\sum_{i=1}^{nWin(\omega)_{\theta\theta}} \left|F_\theta(i)\right| * \left|\ddot{Q}_\theta(i)\right|} \tag{3-22}$$

$$\overline{FRF}(\omega)_{H\theta} = \frac{\sum_{i=1}^{nWin(\omega)_{H\theta}} 20*\log_{10}\left|\frac{F_H(i) - D(\omega)_{HH}^{FBD}\ddot{Q}_H(i)}{\ddot{Q}_\theta(i)}\right| * \left|F_H(i)\right| * \left|\ddot{Q}_\theta(i)\right|}{\sum_{i=1}^{nWin(\omega)_{H\theta}} \left|F_H(i)\right| * \left|\ddot{Q}_\theta(i)\right|} \tag{3-23}$$

$$\overline{\mathrm{FRF}}(\omega)_{\theta H} = \frac{\sum_{i=1}^{nWin(\omega)_{\theta H}} 20*\log_{10}\left|\frac{F_\theta(i) - D(\omega)_{\theta\theta}^{FBD}\ddot{Q}_\theta(i)}{\ddot{Q}_H(i)}\right| * \left|F_\theta(i)\right| * \left|\ddot{Q}_H(i)\right|}{\sum_{i=1}^{nWin(\omega)_{\theta H}} \left|F_\theta(i)\right| * \left|\ddot{Q}_H(i)\right|} \tag{3-24}$$

where $\overline{FRF}(\omega)_{HH}$, $\overline{FRF}(\omega)_{\theta\theta}$, $\overline{FRF}(\omega)_{H\theta}$, and $\overline{FRF}(\omega)_{\theta H}$ are the average frequency response function for the horizontal, rotational, and 2 cross-rotational DOFs, respectively. $nWin(\omega)_{HH,H\theta,\theta\theta}$

are the number of horizontal/rotational windows identified for each frequency, equal because these DOFs are solved simultaneously. F_H^i and F_θ^i are the FFT of the horizontal forces and moments for the ith window of frequency ω, respectively. $\ddot{Q}_H^i$ and $\ddot{Q}_\theta^i$ are the FFT of the horizontal and rotational accelerations for the ith window of frequency ω, respectively. The $\boldsymbol{D}^{\boldsymbol{FBD}}$ terms in Eq.(3-21) through Eq.(3-24) are components of the matrix in Eq.(3-18). Since this matrix is symmetrical, an average of the 2 cross terms, as shown in Eq.(3-25) is used.

$$\overline{FRF}(\omega)_C = \frac{\overline{FRF}(\omega)_{H\theta} + \overline{FRF}(\omega)_{\theta H}}{2} \tag{3-25}$$

After the FRF frequency bin averages for each DOF are obtained, outliers are removed from the data to limit their impact on the analysis. Very few outliers were identified for vertical FRF estimation, and most horizontal/rotational outliers observed were in cases where the horizontal and rotational excitations were of differing orders of magnitude. Presently, outliers are considered to be all points where the FRF would be greater than 10 dB away from the calculated mean, with the horizontal data being rejected if any measurement is outside the range of ±10 dB of the mean. After this process is performed, the average is calculated again without the outlier data present. A more sophisticated method of outlier data rejection is to remove measured data points outside the range of ±2 standard deviations away from the mean, although this is not possible for all frequency points as some did not have enough data collected to determine a standard deviation. Approximately 4% of the total windows obtained in the validation case were discarded as outliers, in line with the 95% interval covered by ±2 standard deviations.

The differences between the average FRF calculated from data and the $\boldsymbol{D}(\omega)^{\boldsymbol{FBD}}$ matrix calculated as shown in Eq.(3-19) are then minimized. To perform this minimization, an objective

function that minimizes the difference between the estimated FRFs and the assumed FRF is proposed in Eq.(3-26),

$$J\left(G, L_p, E_p\right) = \sum_{DOF} \sum_{\omega=1}^{Ny} \frac{nWin(\omega)_{DOF} * \left(\overline{FRF}(\omega)_{DOF} - D_{DOF}^{FBD}\right)^2}{sum(nWin(\omega)_{DOF})} \tag{3-26}$$

where *Ny* is the frequency bin corresponding to the Nyquist frequency (half of the sampling rate), and there are half as many frequency bins as sample length. Only frequency bins where data was selected using the preceding procedure are considered in the objective function. Eq.(3-26) weighs each frequency bin by the number of observations in that bin, so that bins with a greater number of observations have a higher weight factor than bins with a low number. For this research, the fmincon routine in MATLAB (MathWorks 2016) was employed to find the $\boldsymbol{D}(\omega)^{\boldsymbol{FBD}}$ matrix that minimizes Eq.(3-26). Typical or expected values of input parameters are used to develop the analytical $\boldsymbol{D}(\omega)^{\boldsymbol{FBD}}$ curves found from literature. Lower and upper bounds were supplied to the routine to ensure convergence at the global minimum. It was observed that very wide bounds following reasonable assumptions about foundation parameters were suitable.

3.4 Validation of Proposed Method

To validate the proposed method, an instrumentation scheme was implemented on a test bridge with a known foundation. Measurements of the dynamic response of the foundation were performed during operational traffic and parameter selection was performed with the resulting data obtained.

Powder Mill Bridge

The Powder Mill Bridge (PMB), shown in Figure 3-5, is a 3-span continuous steel girder bridge located in Barre, MA. The PMB has 6 girders and is approximately 47 m long and 11.8 m

wide with two 5 m wide travel lanes and a 1.8 m wide sidewalk. The northern span (on the left side of the figure) contains two additional girders to accommodate a wider deck with turning lanes.

Figure 3-5: Powder Mill Bridge (PMB) in Barre, MA

The two interior pier bents each consist of a 1.2 m wide by 1.0 m deep concrete pier cap supported by 3 920 mm diameter columns, each supported by 1.07 m diameter drilled shafts. The drilled shafts are surrounded by a medium to stiff overconsolidated clay and terminated in bedrock approximately 11.5 m below ground surface, and overlain by riprap for scour protection. The southern interior bent (shown during construction in Figure 3-6) is located near an electrical junction installed alongside long-term monitoring equipment during the bridge's construction (Sanayei et al. 2012). The bridge experiences moderately frequent truck traffic, in part due to a nearby landfill. The PMB was chosen as a test case due to its accessibility, the long pier columns that allow for easy instrumentation, and the commonality of the bridge type.

Figure 3-6: Southern interior pier during construction

Sensors and Data Acquisition Equipment

The equipment used for the PMB validation test consisted of 4 BDI ST350 strain transducers (BDI 2012), 4 Wilcoxon 731A/P31 seismic accelerometers and amplifiers (Wilcoxon 2017), and an NI BNC 2110 data acquisition system (DAQ). The strain transducers were installed on the left column of the southern pier in Fig.(8) with accompanying extension bars (BDI 2012) to allow strains to be measured over a distance of 0.457 m (18”). Since the ST350 functions as a load cell with an output controlled by the amount of force applied to the transducer, the use of an extension bar provides an amplified signal that can be correlated to the average strain over the measurement distance. As the shear due to live load is expected to be constant over the measurement distance, a linear strain profile will be expected and the output of ST350 is taken to be the strain at the midpoint of the sensor and extension bar. This style of strain gauge transducer allows for extremely precise strain measurements but is prone to thermal drift as changes in the temperature of the extension bar will cause elongation and shortening that impacts the measurements.

The strain transducers were connected to a Micro-Measurements 2120B dynamic strain gauge signal amplifier and conditioner. Figure 3-7 shows a view of two sides of the instrumented pier column during testing. Figure 3-8 shows a school bus crossing the PMB during testing, with the instrumentation setup visible on the column beneath the bus in the lower left corner.

Figure 3-7: Instrumentation setup at the PMB on the (a) south and (b) north sides of the column

Figure 3-8: School bus crossing the PMB over the instrumented pier

Event Separation

Approximately 8 hours of recordings were performed at the PMB with the instrumentation setup proposed in this research. The event extraction routine was applied to the recorded data to separate periods of increased excitation. The two variance thresholds used to extract events were $2*10^{-6}$ Volts^2/sample for the peak threshold $2*10^{-7}$ Volts^2/sample for the lower threshold. Three seconds on either end of the lower threshold were extracted along with the portions that exceeded the variance threshold. The appropriate threshold will be specific to the bridge being investigated, the background noise level, and the expected level of excitation. Figure 3-9 shows an accelerometer signal alongside the calculated average variance of accelerometer signals for a typical traffic event.

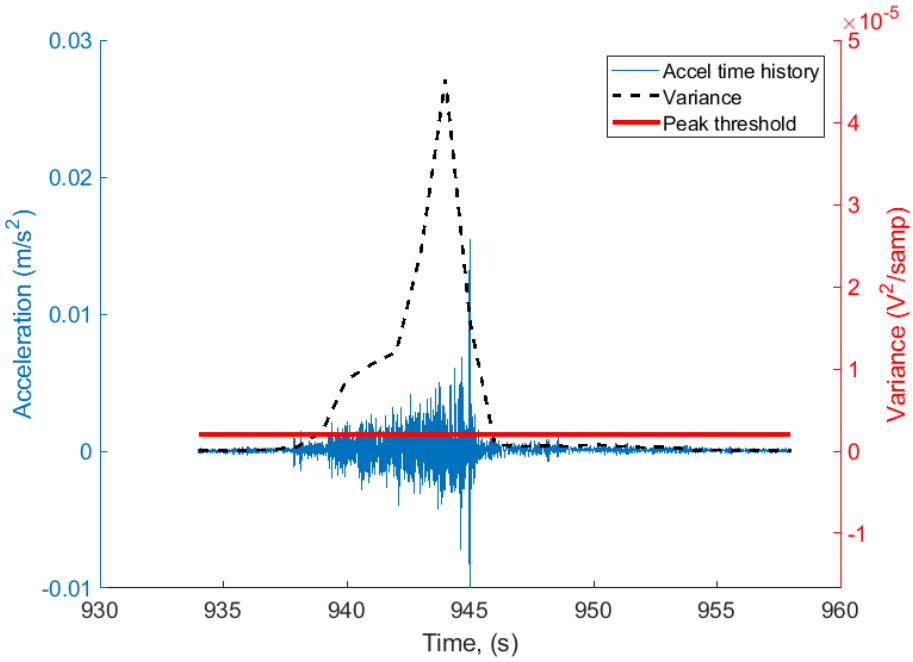

Figure 3-9: Typical measured acceleration time history with corresponding 1-second variance

Figure 3-10 shows a time history of forces acting on the top of the FBD, calculated from strain measurements taken during this event using Eq.(3-1) through Eq.(3-5). It can be observed that the vertical force loading on the foundation is of significantly greater magnitude than the horizontal force loading. The noise in the horizontal force and moment time histories appear to be greater in comparison to the signal than with the vertical force time history. This is expected, as the horizontal and moment loading is largely secondary effects for the vertical loading, and the horizontal time history is calculated without any of the spatial averaging performed for the moment and vertical force time histories.

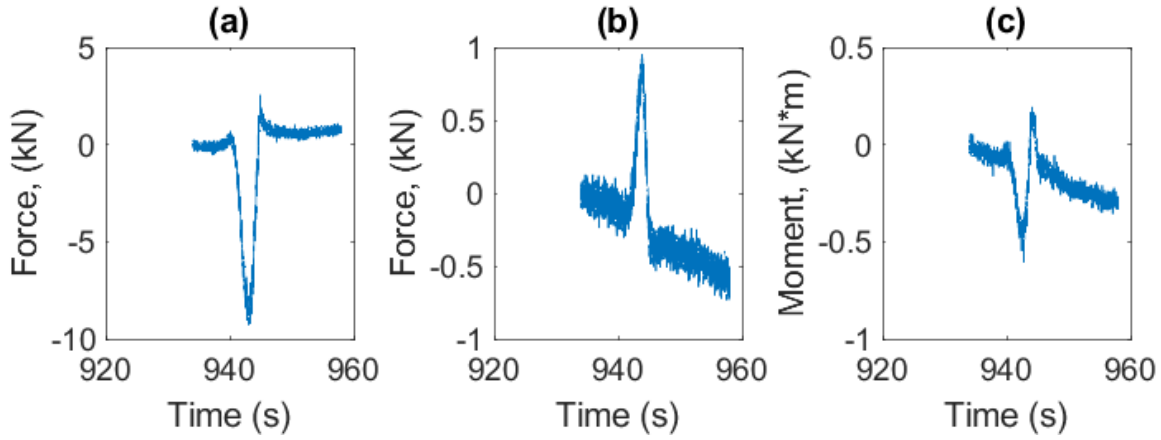

Figure 3-10: Calculated (a) vertical force, (b) horizontal force, and (c) bending moment during event

As can be seen in Figure 3-10, the drift observed in the strain gauge time histories (Figure 3-3a) is carried into the force and moment time histories. As mentioned earlier, low frequency drift is commonly corrected using linear detrending or high-pass filtering which is not needed since the low frequencies where interference is observed can simply be neglected. Figure 3-11 shows the accelerations at the top of the FBD calculated using Eq.(3-6) through Eq.(3-8) for a selected event.

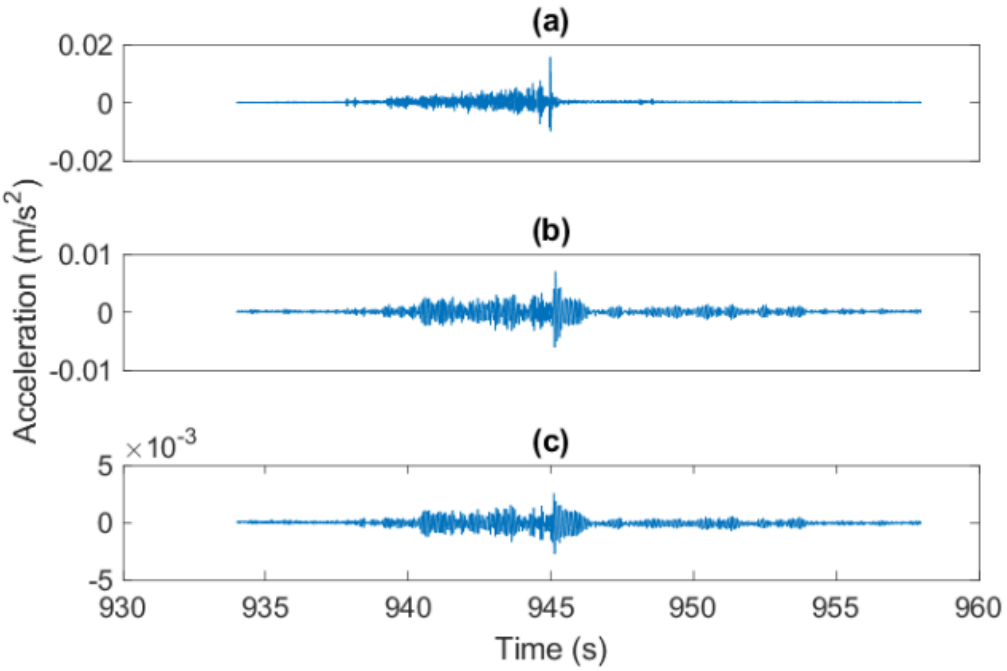

Figure 3-11: Calculated accelerations at top of FBD for a) Vertical Acceleration, b) Horizontal Acceleration, and c) Rotational Acceleration

Frequency Identification

After separation of events and calculation of the force and acceleration time histories, the MSC selector is used to identify the frequencies for each event that meet a minimum level of coherence (0.90 for this research). Only the frequencies which exhibit high coherence over the length of the event are considered. If no frequencies exceeded this threshold, no data from the event selected is utilized. Due to the random nature of the induced excitation, the relatively low signal levels, and the lack of forcing at frequencies not excited by the bridge deck, many frequencies from each recording are not selected during this step. As can be observed from Figure 3-12, for a selected event, only a small portion of frequencies in the lower range meet the coherence

threshold. Of the 303 events isolated during the previous step, 255 of them had at least one frequency meet the MSC threshold criteria.

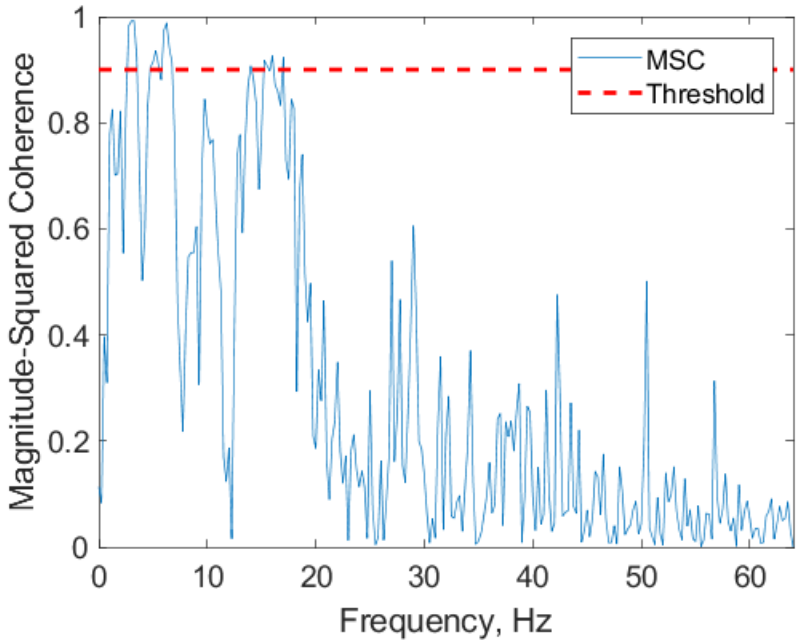

Figure 3-12: Magnitude-squared coherence for a truck recording

Window Selection

For this research, two thresholds were chosen as criteria for window selection: 6 dB for horizontal/rotational forces/moments/accelerations, and 12 dB for vertical forces/accelerations. The vertical and horizontal windows were considered separately so that windows that exceeded the vertical criterion were retained for vertical analysis, and windows that exceeded the horizontal criterion were retained for horizontal/rotational analysis. Only windows where both the force and acceleration measurements exceed their background by the threshold were considered. The lower threshold for horizontal rotational DOFs was selected due to the relatively lower amount of excitation caused by a passing truck in these directions. The background noise is determined by taking a periodogram of the measurements when no traffic or other discernable and significant

external excitations were overserved. Forces and accelerations were calculated from measurements obtained during a 70-second long excitation-free period at 256 samples per second. The thresholds considered for this example are very low (corresponding to ~2x and 4x the noise level). In practice, a higher threshold would be desired, but this was not possible due to the low SNR observed in the strain gauges. Newer strain gauges than used for this example are commercially available with lower electronic noise and higher sensitivity. Also, many bridge types with slenderer columns and heavier traffic loads will experience higher strains in the strain gauges.

A visualization of the STFTs for a typical event is given in Figure 3-13 for vertical force and (b) vertical acceleration measurements. The same process is applied to horizontal and rotational DOFs, with only measurements where both exceed the criteria considered.

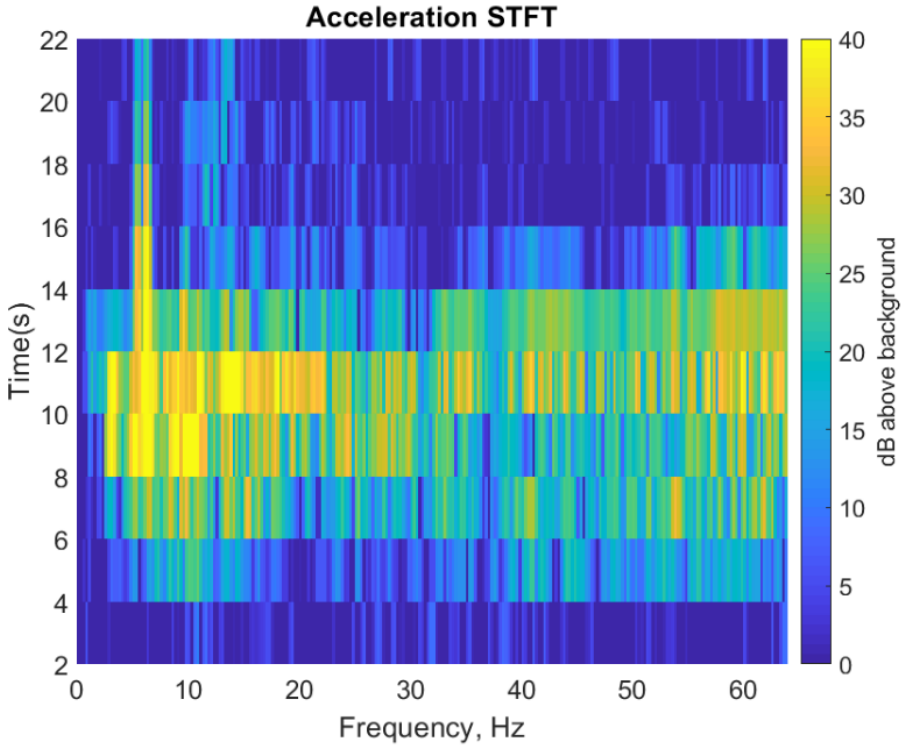

Figure 3-13: Vertical acceleration STFT during vehicle passage

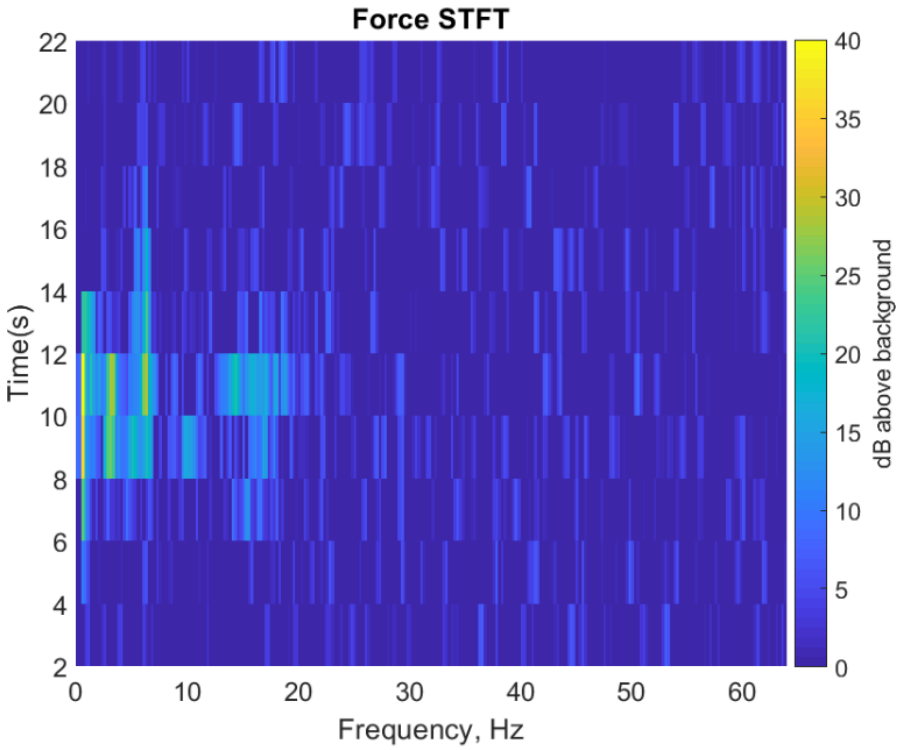

Figure 3-14: Vertical force STFT during vehicle passage

For the event shown above, a total of 17 frequency bins (out of 257) were considered on the basis of the MSC. Of the 255 events with had at least some frequencies meeting the MSC threshold criterion, 202 events had at least 1 window meet the magnitude selection criterion. From these 202 events, a total of 1600 vertical excitation windows were extracted, and 437 horizontal/rotational excitation windows were extracted. It should be noted that a new window is created for each time and frequency, so some points in time have several windows stored correlating to different frequencies.

Averaging Frequency Bins

As described in the automated event selection section, outliers were automatically removed after initial determination of the average for each frequency. A total of 17 horizontal windows out of 436 were discarded. Figure 3-15 shows a plot of all 419 horizontal FRF windows that were

selected for analysis (circles), along with the averages for each frequency bin where windows were identified (stars).

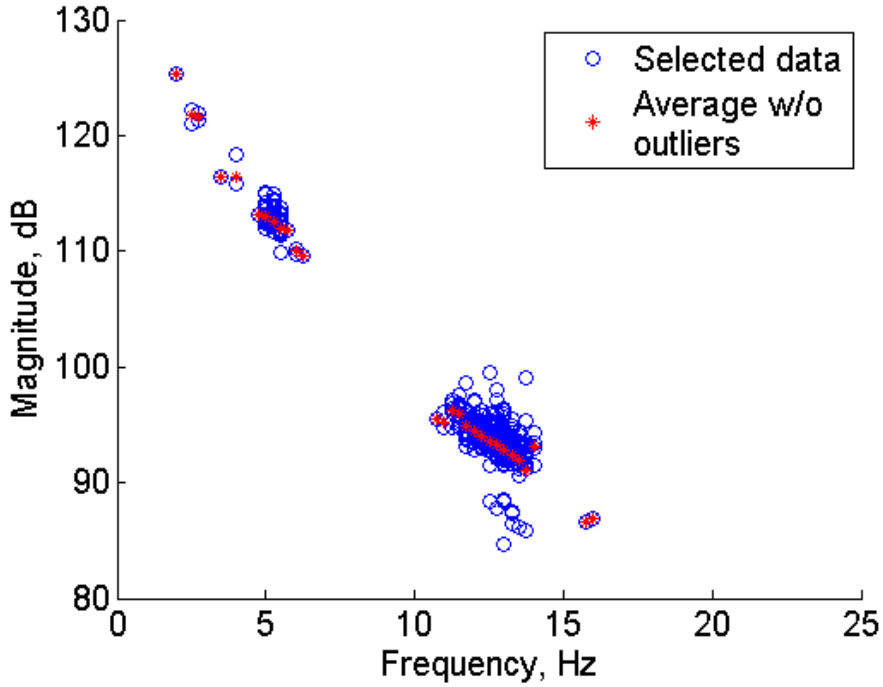

Figure 3-15: Horizontal FRF data identifying selected and discarded data, as well as the average calculated for each frequency

Estimation of Foundation Stiffness Parameters

Three foundation stiffness parameters were considered during updating for the validation model: the depth of the foundation below grade, the shear modulus of the soil, and the modulus of elasticity of the pile. These three parameters were chosen as their selection will greatly impact the behavior of the foundation, they are expected to be important parameters to estimate for unknown foundations, and they are known with a relative degree of confident for the validation case. Table 3-1 provides the parameters which provide the optimal curve fit for the validation model.

Table 3-1: Values of parameters

Parameter	Expected Value	Converged Value
Pile Length (Lp)	11.5 m	12.0 m
Pile Stiffness (Ep)	25.7 GPa	20.6 MPa
Soil Shear Modulus (G)	8-20 MPa	11.1 MPa

The initial value chosen for the pile length and stiffness are based on construction design plans with bedrock elevations (from nearby borings), and compression test breaks of the concrete cylinders used to form the pier columns. The soil shear modulus for the hard clay present at the bridge typically ranges from 8 to 20 MPa. Convergence to the global minimum, was examined by starting from various initial values. It was found that parameter identification converged to identical values when the pile length, soil shear modulus, or pile stiffness was varied by an order of magnitude. The updated parameters returned from the parameter estimation routine at global convergence also were in very good agreement with the initially expected values, as shown in Table 3-1. For the PMB validation case, the proposed method appears to have high predictive capability. Plots of the obtained FRFs versus the best fit curves are provided in Figure 3-16.

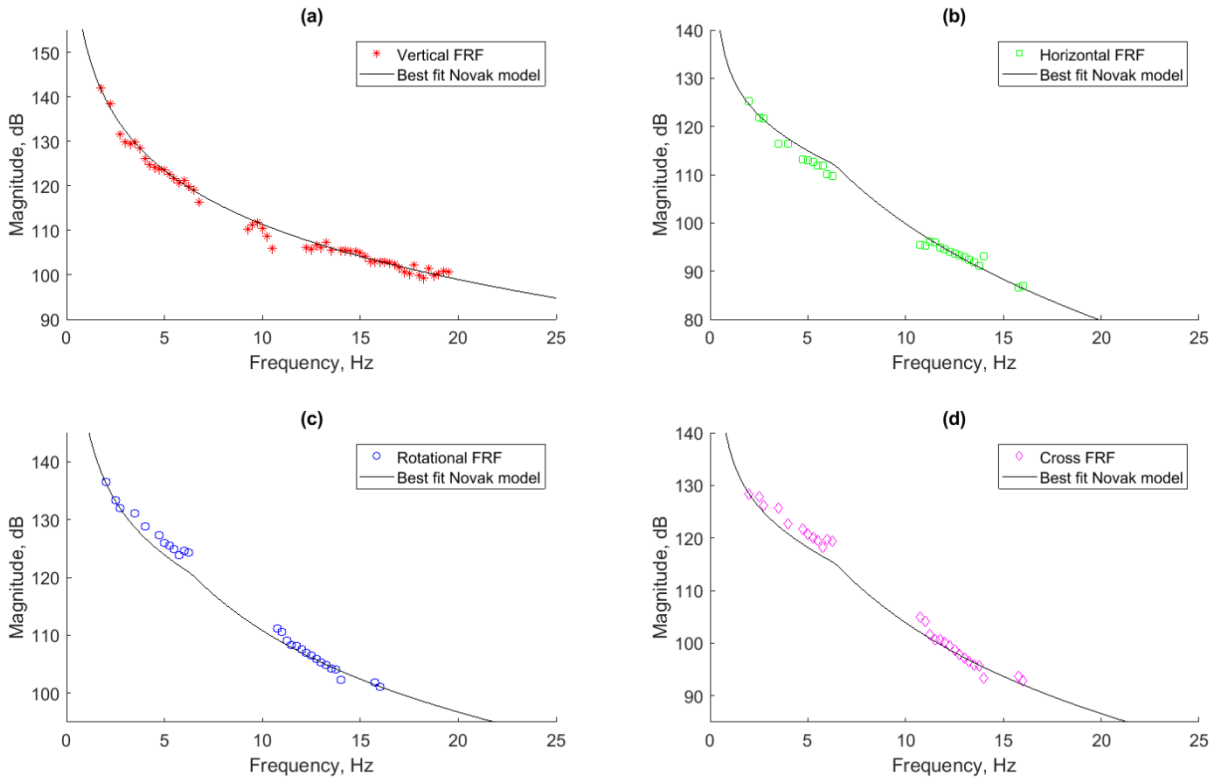

Figure 3-16: Measured (a) vertical, (b) horizontal, (c), rotational, and (d) cross FRFs versus best fit analytical FRF

As can be seen, the fitting routine finds a set of physical parameters that well matches the expected behavior of the foundation to the observed behavior. Some divergence between the measured FRF and the analytical FRF can be observed in Figure 3-16(a), however those are in frequency bins where few observations (as low as 1) were observed. Due to the low number of observations, a high variance in the results is expected, and these bins are weighted lower following Eq.(3-26). Some divergence is seen around 5 Hz for the horizontal, rotational and cross terms. This is also in frequency bins where relatively few observations were made, so these results are expected to be more variable and weighted lower.

3.5 Conclusions

A method has been presented that allows for foundation behavior to be accurately modeled following anticipated empirical formulae. The method was employed in a validation example to

verify that the proposed measurements could be performed, that the automated setup would be capable of extracting foundation information, that the calculated foundation behavior matched observed behavior, and to validate the predictive capabilities of the model. It was determined through testing that the required measurements were able to be performed with commercially available and practical sensors, and that the required excitation level could be achieved through arbitrary excitation related to normal, operational vehicle traffic. The automated method was capable of parsing an entire day of data and extracting useful information with minimal computational overhead. The proposed method estimated a pile length nearly identical to the expected pile length, a soil shear modulus within expectations, and a pile modulus of elasticity approximately 80% of the expectation. The soil modulus is normally highly variable. Overall the predictions reasonably validated the proposed method.

3.6 Future Work

The automated collection approach allows this method to be adapted for programs designed to provide continuous or intermittent monitoring of foundation performance. Some important issues that can potentially be identified include scour monitoring and monitoring of pile deterioration. Preliminary work shows that a foundation undergoing scour or loss of cross-sectional area will produce a detectable change in the foundation frequency response function. For a long-term monitoring system, the sensors would need to be placed in an area relatively protected from the elements and above potential water elevations during a scour event. Future work to enable this usage would require identifying the statistical sensitivity of the method to changes in important parameters such as pile length, soil stiffness, pile modulus, and elevation of soil surrounding the pile. The work in the paper can be extended beyond drilled shafts and single piles and be applied to various types of foundation systems with other dynamic stiffness formulations.

3.7 References

Alessio, S.M. (2015). Digital Signal Processing and Spectral Analysis for Scientists: concepts and applications. Springer

Atkinson, J. (2000). GeotechniCAL reference package. Last accessed on 7/11/2018 at http://environment.uwe.ac.uk/geocal/SoilMech/basic/stiffness.htm

BDI (2012). ST350 Operations Manual Rev. 2.2 Bridge Diagnostics Incorporated, Louisville, CO 80027

Beredugo, Y. O., & Novak, M. (1972). Coupled horizontal and rocking vibration of embedded footings. *Canadian Geotechnical Journal*, 9(4), 477-497.

Collin, J. G. and Jalinoos, F. (2014). "*Foundation Characterization Program: TechBrief #1—Workshop Report on the Reuse of Bridge Foundations.*" Publication FHWA-HRT-14-072, Federal Highway Administration, Washington, D.C.

Dobry, R., & Gazetas, G. (1982). Stiffness and Damping of Arbitrary shaped Embedded Foundations. Research Rep. CE-82, 4.

Dobry, R. and Gazetas, G. (1986). Dynamic response of arbitrarily shaped foundations. *Journal of Geotechnical Engineering*, 112(2), 109-135.

Dobry, R. and Gazetas, G. (1988). Simple method for dynamic stiffness and damping of floating pile groups. *Geotechnique,* 38(4), 557-574.

FHWA (2017). Foundation Characterization Program (FCP). Webpage. Last Accessed 6/26/2018. https://www.fhwa.dot.gov/research/tfhrc/programs/infrastructure/structures/fcp/index.cfm

FHWA (2018), *National Bridge Inventory*, Deficient Bridges by Highway System in 2017. Federal Highway Administration. Last accessed March 15, 2018, at https://www.fhwa.dot.gov/bridge/nbi/no10/defbr17.cfm,

Gazetas, G. (1981). Strip foundations on a cross-anisotropic soil layer subjected to dynamic loading. *Geotechnique*, 31(2), 161-179.

Gazetas, G. (1983). "Analysis of machine foundation vibrations: state of the art." *Soil Dynamics and Earthquake Engineering, 2(1)*

Gazetas, G. and Dobry, R. (1984). Horizontal response of piles in layered soils. *Journal of Geotechnical Engineering,* 110(1), 20-40.

Gazetas, G. and Roesset, J. M. (1979). Vertical vibration of machine foundations. *Journal of Geotechnical and Geoenvironmental Engineering,* 105

Jauregui, J.C. (2014) Parameter Identification and Monitoring of Mechanical Systems Under Nonlinear Vibration. Woodhead Publishing. Sawston, Cambridge, UK

Kausel Bolt, E. A. M. (1974). *Forced vibrations of circular foundations on layered media* (Doctoral dissertation, Massachusetts Institute of Technology).

Maser, K. R., Sanayei, M., Lichtenstein, A., and Chase, S. B., (1998). "Determination of Bridge Foundation Type from Structural Response Measurements," SPIE, Proceedings of the Nondestructive Evaluation Techniques for Aging Infrastructure & Manufacturing, March 31-April 2, 1998, San Antonio, TX, SPIE Vol. 3400, pp 55-67. DOI: 10.1117/12.300125.

Maser, K. R., and Sanayei, M. (1999). "Evaluation of Bridge Foundation Type and Condition Using Static Response Measurements," The Proceedings of the 8th International Conference on Structural Faults and Repair, London, July 13-15, 1999.

Maser, K., Sanayei, M., Klimkewicz, L., Abedi, H. and Edgers, L., (2001). "Unknown Foundation Identification Using Stiffness Data from Field Measurements," Proceedings of Transportation Research Board, 80th Annual Meeting, TRB ID Number: 01-3388, January 7-11, 2001.

MathWorks, Inc. (2016) MATLAB and Statistics Toolbox Release 2016b, Natick, Massachusetts

Novak, M. 1974. "Dynamic Stiffness and Damping of Piles." *Canadian Geotechnical Journal Vol. 11 No. 4*, pp 574-598.

Novak, M., & Aboul-Ella, F. (1978). Impedance functions of piles in layered media. *Journal of the Engineering Mechanics Division, Vol. 104 No. 3*, 643-661.

Proakis, J.G., Manolakis, D. (2007). Digital Signal Processing: Principles, Algorithms, and Applications. Fourth Edition. Pearson Prentice Hall. Upper Saddle River, New Jersey 07458

Reynders, E., Wursten, G., & De Roeck, G. (2014). Output-only structural health monitoring in changing environmental conditions by means of nonlinear system identification. Structural Health Monitoring, 13(1), 82-93.

Sanayei, M. and Maser, K. R. (1999). "Bridge Foundation Stiffness Identification Using Static Field Measurements," ASCE, Proceedings of the 1999 Structures Congress, April 18-21, 1999, New Orleans, LA, pp. 316-319.

Sanayei, M., Phelps, J.E., Sipple, J.D., Bell, E.S., and Brenner, B.R. (2012). "Instrumentation, nondestructive testing, and FEM updating for bridge evaluation using strain measurements." *Journal of Bridge Engineering. Vol. 17, No. 1*, January/February 2012, pp. 130-138.

Santini, E. M., Sanayei, M., Liu M., and Olson, L. D. (1999). "Bridge Foundation Stiffness Identification Using Dynamic Field Measurements," ASCE, Proceedings of the 1999 Structures Congress, April 18-21, 1999, New Orleans, LA, pp. 320-323.

Sipple, J., Sanayei, M. (2014). "Full Scale Bridge Finite Element Model Calibration Using Measured Frequency Response Functions," *ASCE, Journal of Bridge Engineering, Vol. 20, No. 9*,

Smith, S.W. (1997) The scientist and Engineer's Guide to Digital Signal Processing, 1st Edition. California Technical Publishing, Poway, CA 92064

Ubertini, F., Comanducci, G., & Cavalagli, N. (2016). Vibration-based structural health monitoring of a historic bell-tower using output-only measurements and multivariate statistical analysis. Structural Health Monitoring, 15(4), 438-457.

Wilcoxon (2017) Seismic Accelerometer and power amplifier 731A/P31 system. Wilcoxon Sensing Technologies. Germantown, MD 20876

Chapter 4 Load Rating of Existing Foundations

This chapter features the contents of a manuscript by the following authors that has been formatted for publication in a peer-reviewed manual.

Integrated Superstructure-Substructure Load Rating for Bridges with Foundation Movements

Nathan T. Davis[1], Ehssan Hoomaan[2], Masoud Sanayei[3], Anil K. Agrawal[4] and Farrokh "Frank" Jalinoos[5]

[1]PhD Candidate, Dept. of Civil & Env. Engineering, Tufts University, Medford, MA 02155

[2]PhD Candidate, Dept. of Civil Engineering, The City College of CUNY, New York, NY 10031

[3]Professor, Dept. of Civil & Env. Engineering, Tufts University, Medford, MA 02155

[4]Professor, Dept. of Civil Engineering, The City College of CUNY, New York, NY 10031

[5]Research Structural Engineer, Federal Highway Administration, Office of Infrastructure R&D, McLean, VA 22101

Abstract

Superstructures of highway bridges are load rated regularly as a part of the National Bridge Inspection Standards (NBIS). It is well known that the load carrying capacity of a superstructure is affected by foundation movements; however, the current load rating framework does not explicitly include these effects. In the current framework, foundation movement could be treated as structural condition change and considered as a permanent load. In this paper, we propose an integrated framework for load rating of superstructures and substructures in the presence of continuing foundation movements and geo-hydraulic hazards. The approach is based on the modification of the load rating equation to include foundation movements and effects of loads other than dead and live loads that can affect the load capacity of a bridge. A methodology for load rating elements loaded in biaxial moment and axial load, commonly experienced by piers, columns and piles, has also been proposed. The term "Substructure Functionality Index" (SFI) has been proposed to account for the effect of foundation movement on the functionality of critical elements such as bearings. Applications of the proposed integrated superstructure-substructure load rating and SFI have been demonstrated through two examples of actual bridges. It has been demonstrated that the load rating produced can be non-conservative if the effects of foundation movement are neglected.

Keywords: Bridge Load Rating, Superstructure, Substructure, Settlement, Foundation

4.1 Introduction

Load rating of superstructure components is a procedure commonly used in the USA to evaluate the operational capacity of bridge components carrying dead and live loads (Mertz 2005; Chajes et. al 1997; Sanayei et. al 2016). Load rating of all bridges ("bridge" is defined as any structure that carries a highway load and has a total length greater than 20 ft) is required in

compliance with National Bridge Inspection Standards (NBIS) and is carried out by bridge owners to better maintain the existing inventory and to ensure safe usage of aging infrastructure. Typical load rating of bridge superstructures is carried out by developing analytical models using approximate load distribution methods and structural and geometrical details from design drawings or on-site inspections (Gao 2013). Load rating based on field testing is carried out when analytical models are not reliable because of the presence of physical damages to bridge components or because of unreliable / insufficient information on structural or geometrical details of bridge components (Cai and Shahawy 2003). The result of a traditional load rating is a "rating factor" that defines the maximum safe carrying load for a component as a multiple of the design or rating truck load.

In general, load rating procedures have been limited to superstructure elements, although substructures are routinely evaluated for capacity when deterioration of structural elements or the soil system is noted. The 2011 AASHTO Manual for Bridge Evaluation (MBE), (AASHTO 2011) provides the following guidance on the consideration of substructures in load rating procedures: "Where deemed necessary by the owner, load rating of substructure elements and checking stability of substructure components such as abutments, piers, and walls should be done using all permanent loads and loads due to braking and centrifugal forces, but neglecting other transient loads such as wind or temperature." State DOTs provide varying requirements with limited guidance on the load rating of substructure elements. For example, MassDOT (2013) requires pile bents to be load rated. FDOT (2016) states that the substructure, specifically "rotted piles, settlement, excessive scour, and distressed pile caps" should be considered. IDOT (2014) requires

a reevaluation of substructures with condition factors below 4. MaineDOT (2015) states that substructures need not routinely analyzed as part of the load rating procedure.

The main objective of the research presented in this paper is to investigate and propose a methodology for load rating bridges including the effects of foundation movements such as vertical settlement, horizontal translation, or rotation. This approach uses integrated modeling of the superstructure-substructure system to perform load rating of both superstructure and substructure elements considering foundation movement and other foundation loads. The superstructure and substructure load rating process return a rating factor in the same way as the conventional load rating approach. Additionally, an index, referred to as the "Substructure Functionality Index" (SFI) is also proposed to quantify the functionality of bridges after foundation movement. This index is similar to the condition rating commonly applied to bridge components during routine bridge inspections. It ranges from zero to 10, with 10 indicating no foundation movement, and zero indicating loss of functionality.

4.2 Background

Bridge load rating provides an assessment of the live load carrying capacity of superstructure components and is commonly carried out for two levels of loads: (i) Inventory rating that corresponds to loads that can be safely carried by the bridge for an indefinite period and (ii) operating rating that corresponds to the maximum permissible live load that can be placed on the bridge, though with potential adverse effects on lifespan. AASHTO guidelines on Load and Resistance Factor Rating (LRFR) seek to achieve a reliability index (β) of 3.5 for inventory load rating and 2.5 for operating load rating, achieved by using factors of 1.75 and 1.35 on the live load for inventory and operational load rating, respectively. Load rating is initially performed with an

HL-93 load-rating vehicle at the inventory or operating level. If the rating factor for the design truck is below 1.0, load rating is then performed with state legal loads, which more closely match the operating condition. Evaluation at these load levels is performed with different live load factors prescribed in the MBE (2011). If the load rating is below 1.0 for state legal loads, the bridge is posted at the value that is the product of the rating factor and the gross vehicle weight of the rating truck. Load rating can also be performed for permit vehicles that exceed the normal truck size and weight limits to ensure they do not overstress bridges along the routes they propose to operate over.

The MBE (2011) presents a detailed guideline on load rating of bridges. The following general expressions are used to determine the load rating factor (RF) of each element subjected to a single load effect using the LRFR method,

$$RF = \frac{C - \gamma_{DC} DC - \gamma_{DW} DW \pm \gamma_p P}{\gamma_{LL}\left(LL + IM\right)} \tag{4-1}$$

$$C = capacity = \begin{cases} \varphi_c \varphi_s \varphi R_n & \text{Strength Limit State} \\ f_R & \text{Service Limit State} \end{cases} \tag{4-2}$$

where f_R = Allowable stress specified in AASHTO (2014) or as stated, R_n = Nominal member resistance (as calculated), DC = Dead load effect due to structural components and attachments, DW = Dead load effect due to wearing surface and utilities, P = Permanent loads other than dead loads, LL = Live load effect, IM = Dynamic load allowance, γ_{DC} = LRFD load factor for structural components and attachments, γ_{DW} = LRFD load factor for wearing surfaces and utilities, γ_P = LRFD load factor for permanent loads other than dead loads, γ_{LL} = LRFD load factor for live load factor (different for operating and inventory levels), φ, φ_c, and φ_s are the LRFD resistance factor, condition factor, and system factor, respectively

The Resistance factors, φ, φ_c, and φ_s in Eq.(4-2) are applied to account for the uncertainty in calculating the capacity, uncertainty due to deterioration, and a decrease in reliability for less redundant systems, respectively. Typical values of the system factor, φ_s range from 0.85 to 1.0, and are provided in Table 6A.4.2.4-1 of the MBE, while LRFR values for the condition factor, φ_c, are provided in Table 6A.4.2.3-1 of the MBE.

The only permanent loads specifically mentioned in the MBE are the secondary effects from post-tensioning. Other transient, semi-permanent, or permanent loads that can impact a bridge during operation (e.g. wind, water, earth pressure, or settlement) are typically neglected during load rating. The proposed methodology in this paper will consider some of these additional permanent loads in the rating equation.

The load factors used in LRFR have been derived from load factors and load combinations common to LRFD design. The load combinations that need to be applied during LRFR depend on the type of superstructure and common design checks for the component being rated. The load cases considered for LRFR are presented in Table 6A.4.2.2-1 of the MBE (2011), and include Strength, Service, and Fatigue load cases. The Strength load cases use factors of 1.25, 1.50, and 1.75 for the dead loads, wearing surface loads, and live loads, respectively.

4.3 Impact of Substructure Movement on Load Rating

Regardless of the underlying cause, vertical foundation settlement will result in force and moment redistribution in girders, bearings, and other superstructure elements. The magnitude of force and moment created by foundation movement is affected by details and characteristics of the bridge superstructure, such as the type of girders present, the layout of the superstructure (vertical and horizontal curves, skew, and super-elevation), and the details of their connection to the pier or

abutment undergoing movement. Only differential movements from one foundation element to the next one or across a foundation element will induce forces or moments in superstructure elements. Simple span bridges provide a discontinuity in the girders over the piers, allowing rotation that reduces load redistribution resulting from differential settlement. Continuous girders will experience positive moment demand over settling piers and negative moment demand over the adjacent pier or abutment during differential settlement. Abutments often undergo a combination of vertical settlements, horizontal translation, and rotation. These movements can induce forces and moments in the girders, though the magnitude will depend on the details of the girder to abutment connection.

Since the current load rating procedure does not regard the forces and moments resulting from settlement, the load rating for some superstructure elements may not be conservative for bridges that have undergone substantial foundation movements. The approach presented in this paper incorporates these effects in the standard load rating procedure. It should be noted that the proposed research is not recommended to be applied to all bridges. Rather, the proposed approach is recommended to be used only for bridges where substantial foundation movement that may lower the load rating is observed during inspection.

4.4 Literature Review

Sayed et al. (2013) proposed a method for load rating bridge piers subjected to scour. A rating factor was assigned to the individual piers by determining the amount of live load that could be carried without the pier undergoing excessive settlement. To represent the ultimate condition at failure, the dead and live loads were factored by 2.5 and applied to a model created in FB-Pier (FB Pier 2015). P-Y curves were used to represent soil behavior and were removed to simulate scour.

This methodology only considered foundations in their worst-case scoured condition, and not necessarily their current condition, as is typical with load rating practice. Only vertical settlements were considered, and limits were based on empirical findings from literature (Bozozuk 1978; Grover 1978; Wahls 1990; Walkinshaw 1978). These limits were summarized by Barker et al. (1991) and are shown in Table 4-1.

Table 4-1: Empirical limits on vertical settlement (Data from Barker et al. 1991)

Settlement Magnitude	Basis for recommendation	Reference
50 mm	Not harmful	Bozozuk (1978)
60 mm	Ride quality	Walkinshaw (1978)
> 60 mm	Structural distress	Walkinshaw (1978)
100 mm	Ride quality and structural distress	Grover (1978)
100 mm	Harmful but tolerable	Bozozuk (1978)
> 100 mm	Usually intolerable	Whals (1990)

These settlement limits are based on studies of large populations of bridges and may not represent conditions for a particular bridge that is being load rated. Wang et al. (2011) studied the changes in positive and negative moments due to support settlements for continuous span steel girder, concrete girder, and slab bridges. It was shown that the reliability indices for pre-stressed concrete girder and slab bridges undergoing foundation movement are significantly lower than those for steel girders due to the increased stiffness of slab bridges, indicating that these bridges are more sensitive to foundation movement.

It is well known that the differential movement of foundations (including settlement or rotation) not only causes ride quality and serviceability issues but can also cause damage—including damage to abutments, piers, railings, curbs, sidewalks, bearings, anchor bolts, and can result in significant stresses and cracking in concrete components (DiMillio et al. 1981; Moulton

et al. 1985). The acceptable limit on movements depends on the characteristics of the bridge being analyzed. Furthermore, these criteria ignore horizontal movement and rotation, whereas it was noted by Moulton et al. (1985) that "most types of structural damage appear to occur for those bridges with both vertical and horizontal movements occurring simultaneously." Moulton et al. (1985) proposed limits on differential vertical settlement rather than total settlement, which were adapted by AASHTO (2014), as shown in Table 4-2.

Table 4-2: Angular distortion limits in LRFD code (Data from AASHTO 2014)

Tolerable settlement (δ)	Type of bridge
0.004L*	Continuous-span bridges
0.008L	Simple-span Bridges

* L is span length

Andrawes and Caiza (2012) presented a method for load rating the structural capacity of eccentrically loaded timber piles by subtracting the dead load stresses from the total stress capacity and dividing by the stresses induced by the live load. Kim and Andrawes (2017) have extended this methodology to include Fiber-Reinforced Polymer (FRP) retrofitted timber piles.

Dupont and Allen (2002) studied the causes and effects of approach settlement and effectiveness of construction techniques in mitigating this issue. Paikowsky and Lu (2006) examined the reliability of serviceability criteria in the LRFD code, considering the observations from Moulton et al. (1985), to propose new settlement criteria for various bridge types. Modjeski and Masters (2015) examined serviceability requirements for bridges, including settlement criteria for shallow and deep foundations. Changes to the LRFD code were proposed that included appropriate γ_{SE} terms for settlement predicted using various methods. Proposed γ_{SE} factors ranged from 1.0 to 1.25 depending on the prediction technique used. The primary source of uncertainty in these calculations was related to the prediction of settlement prior to it occurring. Factors for

measured settlement were not proposed. Moon et al. (2018) studied the impacts of foundation movement on bridge superstructures, finding pier and abutment settlement can cause superstructures to exceed Strength or Service limit criteria, especially for continuous multispan steel girder and prestressed concrete bridges. The worst-case movements were found to be differential settlement between adjacent piers/abutments, and differential settlements across single elements.

4.5 Proposed Methodology

As discussed previously, the MBE leaves the evaluation of substructure elements, including the evaluation of stability of substructure components such as abutments, piers, and walls up to the discretion of the bridge owners. The MBE also does not require the consideration of transient loads such as wind or temperature. While permanent loading on superstructure elements is generally limited to prestressing forces, "permanent" loading on abutments is present in the form of vertical or horizontal earth pressures. Water loads are typically regarded as transient loads, but bridge foundations that see significant water loading during daily operational traffic should have these loads included as well. The water loads to be used during load rating should not represent a flood or abnormal condition, but rather the loads present on a semi-permanent basis.

Since the load rating procedures outlined in the MBE are centered on the rating of superstructure components, the procedure for load rating members in eccentric axial loading is not explicitly specified. Instead, the rating equation shown in Eq.(4-1) defines the rating factor as the capacity minus the dead load and wearing surface demands, divided by the anticipated live load demand. For a structural component in uniaxial bending, the capacity is the factored nominal moment/shear capacity and the demands are the factored moment/shear demands on the

component for each load case. Similarly, axially loaded components are rated based on the factored axial capacity and factored axial demands. For both types of loading, the rating factor is the percentage of the factored live load demand on the remaining capacity after the permanent loading has been accounted for.

Unlike superstructure components, many substructure components, especially pier columns and long piles, must be designed to resist significant simultaneous axial force and bending moment demands (eccentric axial loading). While pier columns are primarily comprised of reinforced concrete, piles can be made of reinforced concrete, prestressed concrete, steel, or timber. Piles and columns can be square, rectangular, or circular in shape.

For many bridges undergoing foundation movements, the most prominent concern is not the strength of superstructure components, but the rideability and functionality of the bridge. Excessive settlement can result in damage to bearings that can lead to unseating of girders from bearings, discontinuities in bridge decks, cracking of deck or girder concrete, or girders contacting abutments. In these circumstances, the primary concerns are independent from the magnitude of live load applied. A load rating procedure intended to provide the maximum load permissible does not aid in the evaluation of these issues. While the concept of load rating does not fully apply to rideability and functionality concerns, there is an ongoing necessity to document the performance of these substructures in a consistent manner.

The proposed integrated load rating methodology has three main components: i) superstructure load rating considering the effects of substructure movement, ii) load rating of substructure elements; and, iii) defining the functionality of the structure concerning an observed settlement. The superstructure and substructure load rating procedures return a rating value in the

same way as current load rating procedures. The functionality of the bridge considering settlement is quantified through the newly developed "Substructure Functionality Index" (SFI). This value should not be interpreted as a load rating, but rather as akin to a condition rating commonly applied to components during routine bridge inspections. The SFI can range from zero to 10, with 10 indicating no foundation movement, and zero indicating loss of functionality.

Superstructure Load Rating Considering Substructure Movement

For superstructure elements, the primary difference between traditional load rating and the proposed integrated load rating is the addition of a settlement term to the rating equation. The settlement term, *SE*, represents the additional moment, force, or stress demand on the component being rated due to foundation movement. It is proposed that load cases (except fatigue) include the effects of settlement when it is considered significant and agencies have performed measurements of foundation movements, relative displacements, or connection distortion. For all load cases except fatigue, the rating factor equation in Eq.(4-1) can be revised to include the effects of settlement, as shown in Eq.(4-3),

$$RF_{sup} = \frac{C - \gamma_{DC}(DC) - \gamma_{DW}(DW) \pm \gamma_{P}(P) - \gamma_{SE}(SE)}{\gamma_{LL}\left(LL + IM\right)} \tag{4-3}$$

The definition of parameters in Eq.(4-3) is the same as in Eq.(4-1). At present, γ_{SE} is taken to be 1.0 which is consistent with LRFD specifications. The LRFD load factor of 1.0 is prescribed to be used with predicted settlement, whereas the proposed load rating would be based on measured settlements. Moulton et al. (1985) have suggested that a linear elastic analysis of loads from measured settlements will conservatively estimate demands (actual demands will be lower) due to creep and relaxation. Hence, it is expected that using a γ_{SE} of 1.0 will produce conservative load

ratings. Further research and test data would be required to determine appropriate γ_{SE} values for measured settlements that account for the variability of loads resulting from settlement, the variability of settlement measurement, and the effects of creep and relaxation.

Substructure Load Rating

Additional Loads on Substructures

In traditional load rating of superstructures, the primary operational demand results from dead and live loads. Loads from other sources, such as wind, water, ice, and earth pressure are not included in the load rating equations due to their relative insignificance. Earthquake loading is considered in the LFRD approach as an "Extreme Event" that does not coincide with operational loading.

Wind loading is evaluated in LRFD using 4 load cases: Strength III, Strength V, Service I, and Service IV. The Strength III and Service IV wind load cases have no live load and should be evaluated separately from load rating when deemed necessary. The Strength V and Service I operational (occurring with live load on the bridge) load cases use an 89-kph (55 mph) wind with factors of 1.35 and 1.0 on the live load, respectively. The authors have investigated the significance of these load cases on the load rating of substructure elements and have not identified an example in which they control the load rating. It is expected that these load cases can control the load rating for tall substructures where lateral deck loading can generate a large moment in the pier.

For abutments and wingwalls, lateral earth pressure loads are essentially permanent loads that need to be considered when evaluating demands. Pier elements in moving water have a lateral load applied to submerged elements. While lateral load during flooding can be considered an extreme event case, normal stream flow under operational conditions can impart significant loads

on affected bridge components. Ice loading due to extreme event ice forces has not been considered in this research. Table 4-3 presents LRFD factors for loading that are not typically considered in LRFR but are considered in this research.

Table 4-3: LRFD Load factors not typically used during LRFR load rating.

Load	Symbol in LRFD	Typical Factor in LRFD code
Settlement	SE	γ_{SE} = 1.0 (Strength I, II, III, IV, often avoided by limiting settlement)
Vertical Earth Pressure	EV	γ_{EV} = 1.00 to 1.35 (Retaining Walls and Abutments) γ_{EV} = 0.9 to 1.30 (Rigid Buried Structures) γ_{EV} = 1.0 (Stability)
Horizontal Earth Pressure	EH	γ_{EH} = 0.9 to 1.50 (Active earth pressure) γ_{EH} = 0.9 to 1.35 (Passive earth pressure)
Water Load	WA	γ_{WA} = 1.0 (All Strength, Service, and Extreme Event)

Water Loading

Water loading on bridge piers can act transversely or parallel to the direction of traffic. Water loads are excluded from superstructure load rating because superstructures experience water loads (for example during submergence) only during extreme flooding cases. In AASHTO (2014), the water loads are included in all strength, service, and extreme event load cases. A design flood, which is based on minimum return frequency (i.e. 100-year return period), is used for strength and service load cases, while a check flood, which is based on a 500-year return period, is used for extreme event load cases.

For the purposes of load rating, it is proposed that the normal stream flow (or expected maximum during the evaluation interval) be considered as load on the bridge. The proposed water load is determined by considering the current state of the bridge foundation in terms of scour and hydrological conditions. Many state DOTs already have requirements for scour vulnerability

evaluation, following HEC-18 (Arneson et al. 2012) that should not be superseded by the proposed load rating procedure.

Proposed Load Cases for Substructures

Due to the additional loads experienced by substructures, additions to Table 6A.4.2.2-1 are proposed and listed alongside the current LRFR factors in Table 4-4.

Table 4-4: Load cases applicable to LRFR factors for substructures

Limit State	Dead Load	Wearing Surface	Design Load		Legal Load	Permit Load	Settlement	Water Load	Vertical Earth Pressure	Horizontal Earth Pressure
			Inv	Oper						
	γ_{DC}	γ_{DW}	γ_{LL}	γ_{LL}	γ_{LL}	γ_{LL}	γ_{SE}	γ_{WA}	γ_{EV}	γ_{EH}
Strength I	1.25	1.50	1.75	1.35	1.30 to 1.45	-	1.0	1.0	γ_{EV}	γ_{EH}
Strength II	1.25	1.50	-	-	-	1.10 to 1.40	1.0	1.0	γ_{EV}	γ_{EH}
Service I	1.00	1.00	-	-	-	1.00	1.0	1.0	γ_{EV}	γ_{EH}
Service II	1.00	1.00	1.30	1.00	1.30	1.00	1.0	1.0	γ_{EV}	γ_{EH}
Service III	1.00	1.00	0.80	-	1.00	-	1.0	1.0	γ_{EV}	γ_{EH}

*INV = inventory, OPER = operating

The equation for load rating of substructures, including foundations, can be modified to include effects of earth pressure, water loading and settlement as in Eq.(4-4),

$$RF_{sup} = \frac{C - \gamma_{DC}(DC) - \gamma_{DW}(DW) - \gamma_{SE}(SE) - \gamma_{EH}(EH) - \gamma_{EV}(EV) - \gamma_{WA}(WA)}{\gamma_{LL}(LL + IM)} \quad (4\text{-}4)$$

It is proposed that γ_{SE} be equal to 1.0 for the reasons mentioned in superstructure load rating. It is also proposed that γ_{WA} be equal to 1.0 for this research, primarily to provide consistency with existing LRFD standards. Reliability-based factors would need to consider the variability of stream flow over the load rating interval, as well as the likelihood of those flows occurring simultaneously with heavy truck loading. It is expected that these values would be specific to

individual bridges, and calibration of these factors beyond the LRFD values is believed to be beyond the scope of this research. Furthermore, Turkstra (1970) has found that extreme values of loading occur when one load reaches its extreme while the others are near their expected mean (Nowak 1999). Since load rating is an attempt to consider the maximum permissible live load, it is rational to only consider the expected (non-factored) water load, especially if a conservative value is chosen.

Combined Axial-Moment Load Rating

Substructures will typically contain elements that are subjected to both axial forces and bending moments (eccentric loading). Determining the available resistance of a pier during eccentric loading is a more involved procedure that generally requires evaluation of both the moment capacity and axial capacity, or a simultaneous evaluation of both. The equations governing the available capacity of elements in eccentric axial loading can be found in AASHTO (2014) and vary depending on element type. Applicable limit states can be found in Section 5.7.4.5 of AASHTO (2014) for reinforced concrete elements, Section 6.9.2.2 for steel elements, and Section 8.10.1 for timber elements. Specific limit states can be found in Eq.(A-1) through Eq.(A-7) in Appendix A.

Since the aforementioned equations are more complex than those governing the capacity of elements loaded purely in compression or uniaxial bending, Eq.(4-4) cannot be used to load rate eccentrically loaded columns. Furthermore, since the dead load and live load will not necessarily have the same eccentricity, it is not possible to subtract the permanent load effects from the capacity and divide by the live load demands to determine a load rating. Instead, the proposed methodology determines the multiple of live load that can be applied until the failure criterion is

met. This is achieved by separately determining the permanent load effects and live load effects, including the axial load and moments about both axes. The resultant load effects are then a function of the multiple (*m*), as shown in Eq.(4-5) for axial load,

$$P(m) = \gamma_{DC}\left(P_{DC}\right) + \gamma_{DW}\left(P_{DW}\right) + \gamma_{SE}\left(P_{SE}\right) + \gamma_{WA}(P_{WA}) + \gamma_{EV}\left(P_{EV}\right) + \gamma_{EH}(P_{EH}) + (m)\gamma_{LL}(P_{LL}) \quad (4\text{-}5)$$

where P is the axial load, and the subscripts follow the previously described AASHTO conventions. Eq.(4-5) also applies to the two moments, M_x and M_y, which can also be written as functions of *m*. The relevant limit state equation can then be a function of *m* by using $P(m)$, $M_x(m)$, and $M_y(m)$. The multiple of live load (*m*) that causes the limit state to be reached is then analogous to the rating factor (RF) obtained from Eq.(4-4). Figure 4-1 depicts this methodology applied to a circular reinforced concrete column. The blue solid line is the factored interaction surface that represents failure, the star is the factored permanent load effects, the circle represents the point of failure, and the dashed line represents the load path the total load effects take as *m* is increased. The direction of the dashed line is a result of the eccentricity of the worst-case live loading, which is defined as the case where the lowest multiple causes the failure surface to be reached.

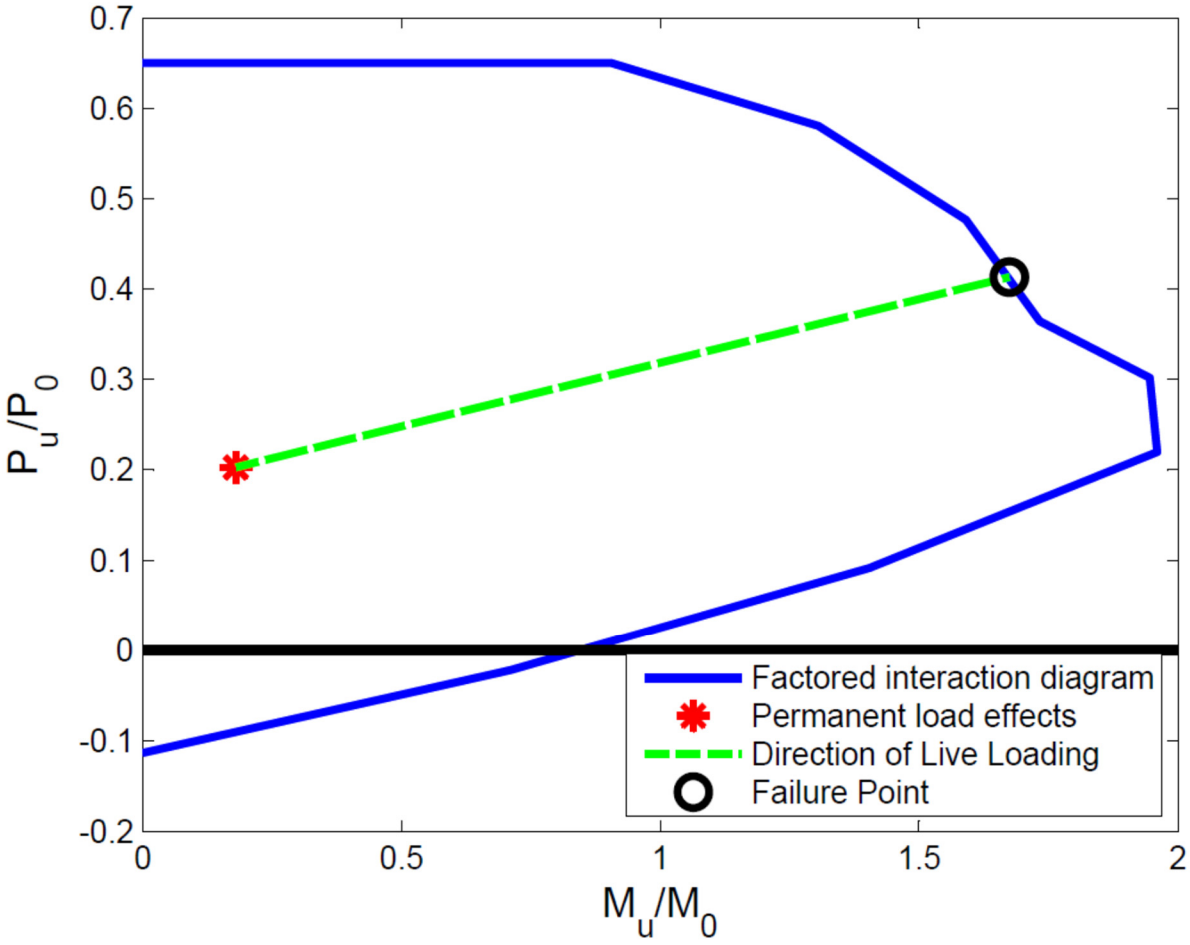

Figure 4-1: Path traveled between permanent loading and failure surface

The path shown in Figure 4-1 is only a 2D projection of the 3-dimensional path taken by the live load effects between the permanent load effects and failure. As such, the length of the line in 2-dimensional space is not particularly meaningful. When moment reversals (i.e. permanent load effects produce a moment with opposite sign of the live load moment) occur during live loading, a turn in the live loading line will be visible, as shown in Figure 4-2a. Figure 4-2b shows the cause of this, a moment reversal about the y-axis due the live load having the opposite sign as the dead load. It should be noted that although the path taken in Figure 4-2 appears longer than the

path taken in Figure 4-1, Figure 4-2 (in this case, although not generally) represents a lower load rating as the live load effects in Figure 4-2 are of greater magnitude.

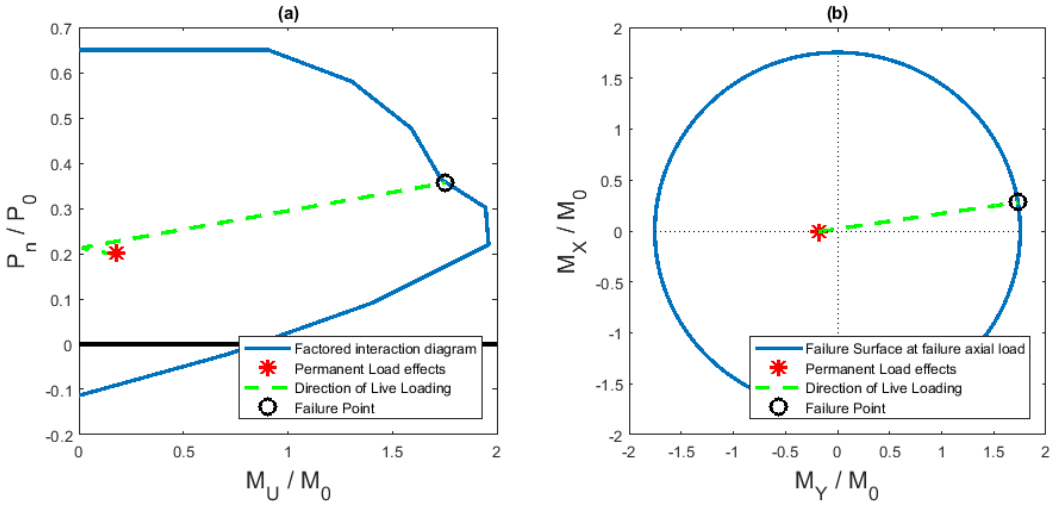

Figure 4-2: Live load loading path when stress reversal is present (a) in P_U-M_U space, and (b) in M_X-M_Y space

Substructure Functionality Index (SFI)

Many issues related to excessive bridge settlement will not be strength based, and therefore will not be directly dependent on the live loads. Since the live load forms the denominator of the rating factor equation, a rating factor cannot meaningfully characterize these issues. For these scenarios, a new form of load rating, defined herein as the *Substructure Functionality Index* (SFI), is proposed. The SFI is a positive number from 0 to 10, similar to the condition rating applied during bridge inspection. An SFI of 10 indicates that the bridge has experienced no differential movements, while an SFI of 0 indicates that the superstructure is no longer functional. If the settlement is greater than the allowable value, a negative SFI is mathematically possible. It is proposed that zero be the minimum value of SFI as it corresponds to a loss of functionality. The SFI can be applied to any connection or detail, but the index should be viewed as a rating on the substructure performance. The overall SFI of the bridge is governed by the lowest SFI of any

component. The SFI of each component will inherently account for the simultaneous movements of all foundation components. Unlike a load rating, the SFI is not intended in any way to estimate the magnitude of live load that can be safely applied. At low SFI's, the bridge still may be functional, though significant usability issues may exist. How detrimental a low SFI is will depend on the component being rated, details of the bridge, and how the limit criteria have been defined. Quantitatively, the SFI is expressed as:

$$SFI = \frac{\text{Allowable movement} - \text{Observed movement}}{\text{Allowable movement}} \times 10 \tag{4-6}$$

Allowable settlement can be calculated by the following three approaches. The most simplistic approach is to define "allowable" movement using existing AASHTO or state DOT guidelines. The "observed" movement should be estimated from field measurements. This method is likely to be overly conservative since guidelines are applicable to many bridges. These guidelines also do not typically restrict lateral movement, rotation, or consider the interaction of translation, rotation, and settlement. Hence, these limits will not be appropriate for foundations with several simultaneous movements.

The second approach to calculating allowable movement is to model the bridge including the foundation and subject the foundation elements to the observed movements. The distortion in various connections and details would then be the "observed movement", while the "allowable movement" can be determined from the capabilities of those connections or details (e.g., how far a girder can move before impacting an abutment, how much an elastomeric bearing pad can deform, how much a roller connection can rotate, etc.). This approach allows the inclusion of the effects of all measured or estimated movements into the SFI equation.

The third approach proposed is to measure the actual relative movement in a specific detail (e.g. girder translation relative to abutment or pier cap). This allows for direct and simple observation of the actual areas of concern, without worrying about modeling the entire bridge. The "allowable movement" would still need to be determined using the knowledge of the connection details and engineering judgement, but foundation movements would not necessarily need to be measured. The resulting SFI would still be a measure of total foundation performance, assuming foundation movements are the only source of deformations.

The SFI can be implemented into the traditional load rating paradigm by first determining which bridges are undergoing significant enough movement to warrant consideration of the impacts of settlement on functionality. On these bridges, critical details or connections can be identified for continuous ongoing monitoring. A limit to observable settlement, connection rotation, or differential movement can be defined following the above approaches. Observations of the settlement or connection distortion can be carried out with the regular inspection interval to provide an objective measure of the remaining functionality of the substructure. The SFI would be reported alongside the rating factor to indicate the severity of the current movement.

Modeling Techniques

Two different modeling techniques have been investigated in this paper. The first is a common approach where the foundation is not modeled alongside the rest of the superstructure and substructure. Instead, boundary conditions are applied to the model, often at the ground surface for interior bents or at the bearing location for abutments. In this modeling approach, observed settlements are applied directly to the boundary conditions as a separate load case. As long as the bridge behavior can be modeled elastically, the settlement load case can be added to the other

permanent loading on the bridge. This approach is described in greater detail in the "Three-Span Continuous Steel Girder Bridge" section.

The second design approach is to model the entire foundation, substructure, and superstructure in a single model. Pile-soil interaction in this approach is represented by nonlinear P-Y (lateral force-lateral displacement), T-Z (axial displacement-skin friction), T-θ (twisting-rotational resistance) and Q-Z (tip displacement-tip resistance) springs. A description of these springs and their governing equations can be found in the FB-Pier program manual (FB Pier 2015). This approach allows complete modeling of foundation elements, including modeling of soil behavior, and scour. For this modeling approach, the order the loads are applied is important as the soil springs are non-linear. In general, the model should be loaded with the dead and other permanent loads, then the settlement load, and lastly the live load. Only non-factored loads were used in the model, and the effects from each load were factored outside of the modeling. This modeling approach automatically includes the effects of settlements that occur from dead and live loading, although additional settlements can be modeled by converting the Q-Z tip spring to a fixed end and applying a displacement.

4.6 Field Examples

The application of the proposed integrated substructure-superstructure load rating approach has been demonstrated through two example bridges. Both bridges are in Pinellas County, FL, but have very different foundations and superstructures. One bridge is a 3-span continuous steel girder bridge with single column piers, while the other one is a 3-span slab bridge with 2 pile bent piers with 9 precast concrete piles (PCPs) each. The selection of these two bridges is expected to highlight different applications of the proposed methodology. The continuous girder

bridge is expected to experience load redistribution in the girders and tall pier columns due to foundation movement. In contrast, the simple span bridge is not expected to experience significant load redistribution due to uniform foundation movement. However, the piles within the pier bents are expected to experience load redistribution during scour or water loading.

Three-Span Continuous Steel Girder Bridge

I-275 Southbound in Pinellas County crosses over I-275 Northbound and 34th St. south with a 3-span, continuous girder bridge. There are five steel girders in composite action with a 190-mm (7.5 in) thick reinforced concrete deck. The girders are approximately 2.5m (99 in) deep with span lengths of 67 m, 70 m, and 62 m, (220 ft, 230 ft, and 203 ft) along the centerline. The bridge is curved with a radius of 537 m (1763 ft) and has a superelevation of 6.4%. The two intermediate bents in the bridge are hammerhead piers consisting of 2.1 m (7 ft) dia. concrete columns, longitudinally reinforced with 44 #11 bars. The piers are founded on a 2 m (6.5 ft) thick underground pile cap connected to 460 mm × 460 mm (18 in ×18 in) square PCPs, approximately 21.3 m (70 ft) long. The ends of the bridge are founded on reinforced concrete stub abutments supported by 8 PCPs each, ranging from 27.4 to 29 m long (90 to 95 ft). The soil conditions at all bents consist of 18.3 to 21.3 m (60 to 70 ft) of medium to dense sand with trace silt, underlain by a thin layer of soft clay above hard limestone.

A finite element model of the bridge (Figure 4-3) was created using the software package CSI Bridge. The girders, pier caps, and columns are modeled with frame elements. The deck is modeled with shell elements. The pile caps, piles, and soil are not modeled, and instead a fixity where movements can be prescribed is applied at ground surface. The model is linear elastic and the force redistribution from foundation movements are calculated in a separate load case.

References to the “outer” portion and the “inner” portion of the bridge refer to the outside and inside of the curvature, respectively.

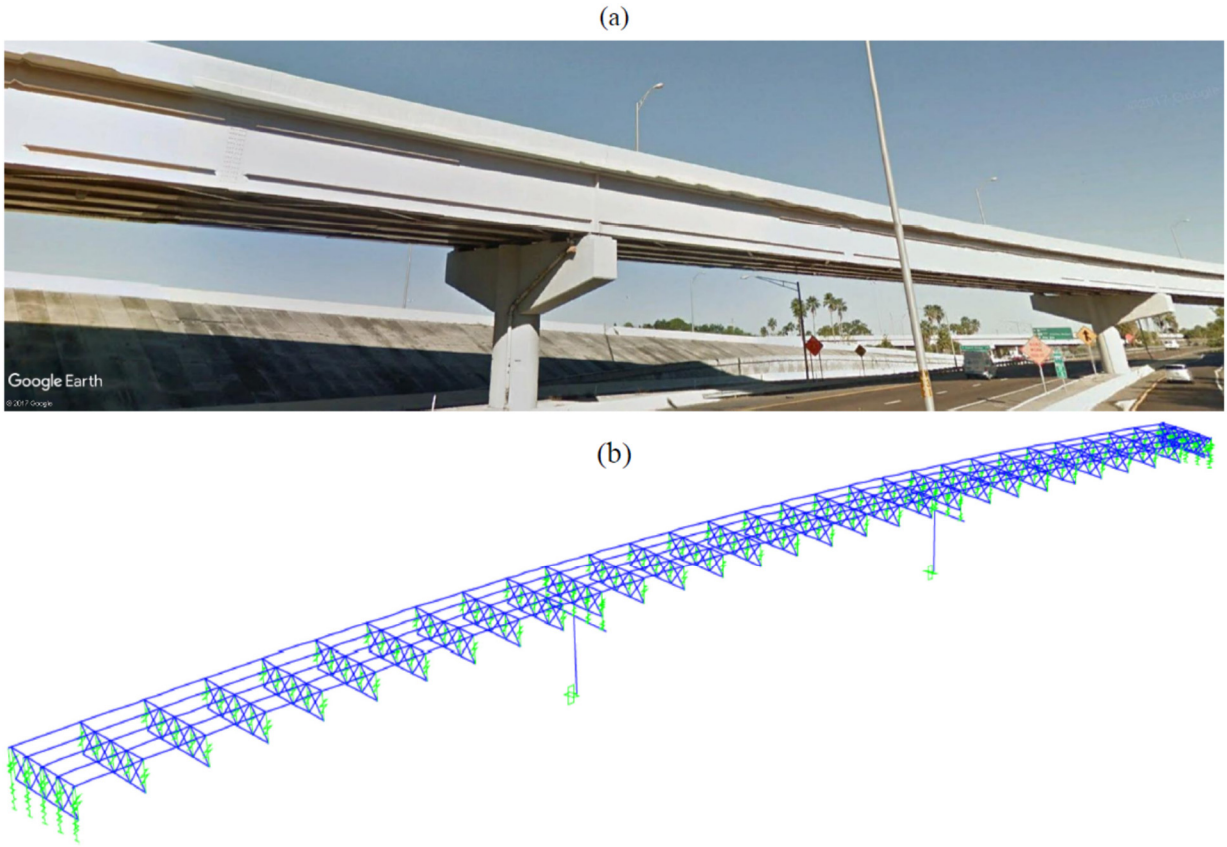

Figure 4-3: (a) Google Earth image of I-275 Bridge, and (b) *CSiBridge* model of I-275 Bridge

Two damage scenarios have been simulated using this bridge model. The first modeled damage scenario (SE-1) has 102 mm (4 in) of pure vertical settlement in a single pier, with no movement at the adjacent pier or abutments. The selection of 102 mm is arbitrary, but it is an amount of settlement expected to generate concerns while still being well below the limit of 0.004L (280 mm, 11 in) from AASHTO (2014). A second damage scenario (SE-2) considers a case where piles under one of the piers do not settle uniformly. In the simulated scenario, there is 51 mm (2 in) of settlement on the outer (with respect to girder curvature) edge of the pier, 102 mm (4 in) of settlement on the inner edge, and 25 mm (1 in) of translation in plane with the pier cap towards

the center of curvature. The second load case is applied to the model as 153 mm (3 in) of downward settlement, 51 mm (1 in) of horizontal translation, and 0.637° of transverse rotation at the base of the column. The load rating of the superstructure, the load rating of the pier column and SFI are calculated by considering these effects.

Superstructure Load Rating

Superstructure load rating was performed considering the two settlement cases (SE-1 and SE-2). The resulting negative moments over the adjacent pier and the girder negative moment capacities for three different conditions of girder (i.e., good, fair and poor) are shown in Table 4-5.

Table 4-5: Girder negative moments over adjacent pier for Strength I load case including settlement loads

	Factored Moments (kN.m)					Capacity (kN.m)		
Load Case	**DC**	**DW**	**SE-1**	**SE-2**	**LL**	**Good**	**Fair**	**Poor**
Girder 1	-8893	-6162	-920	-161	-4354	-31184	-29625	-26506
Girder 2	-10832	-7469	-1101	-479	-5396	-31184	-29625	-26506
Girder 3	-11349	-7765	-1197	-887	-5926	-31184	-29625	-26506
Girder 4	-9825	-6759	-1220	-1238	-5856	-31184	-29625	-26506
Girder 5	-7229	-6759	-1135	-1374	-5090	-31184	-29625	-26506

Figure 4-4 shows the rating factors for the negative moment region over the adjacent pier for the Strength I load case for all 5 girders, assuming poor condition with φ_c=0.85.

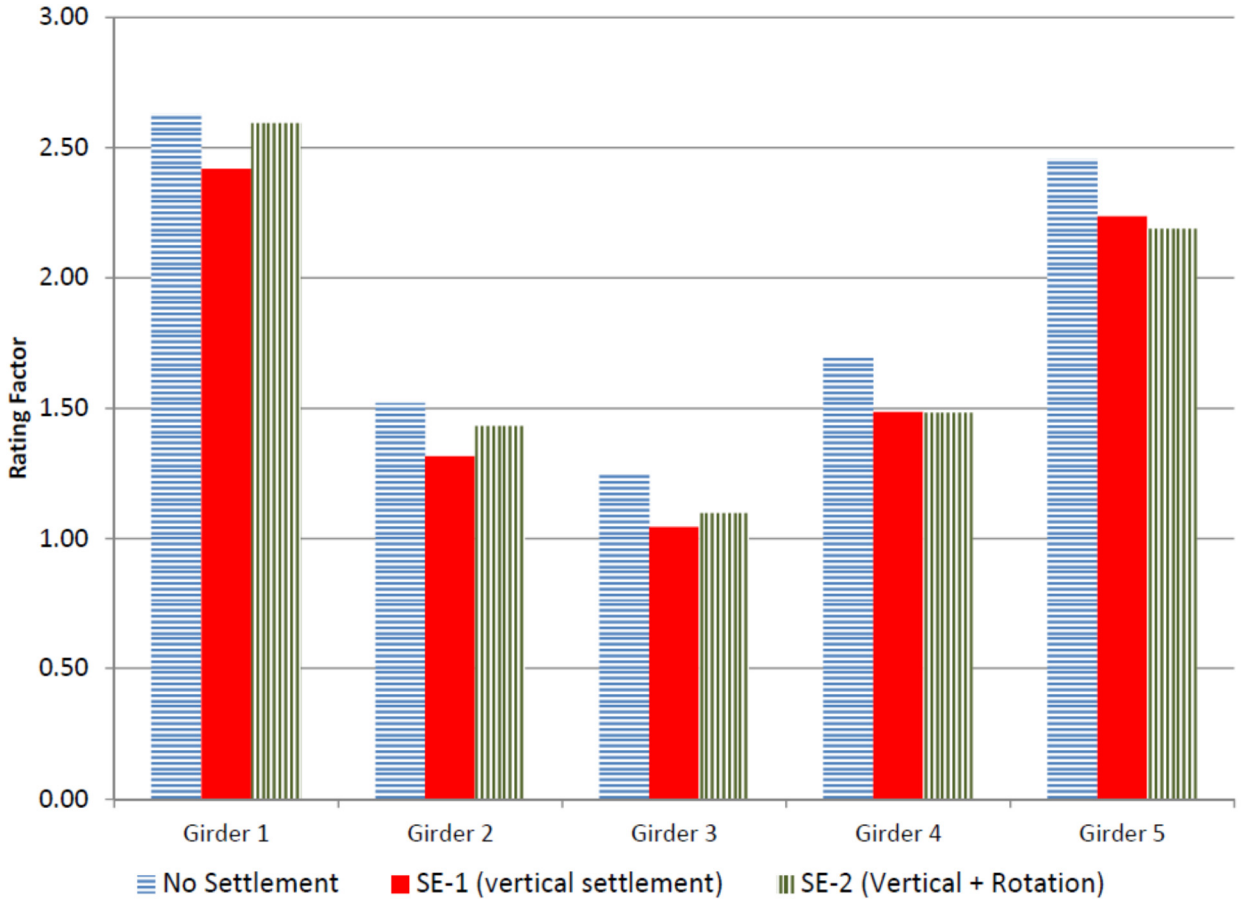

Figure 4-4: Rating factors for girders with no settlement, settlement scenario 1, and settlement scenario 2 for each girder in poor condition

The critical girder from Figure 4-4 is Girder 3, which has the lowest initial rating factor. In "good" condition, the rating factor for Girder 3 drops from 2.04 to 1.83 with 102 mm (4 in) of vertical settlement. In poor condition, this rating factor drops from 1.25 to 1.05. The load case with vertical settlement, rotation, and horizontal translation has a smaller impact than pure vertical settlement, except for Girder 5. Girder 5 still does not control the load rating of the superstructure when the foundation undergoes these movements. In the methodology presented by Sayed et al. (2013), the largest suggested settlement limit is 100 mm (4 in), indicating excessive conservatism. The proposed methodology allows the consideration of girder condition, non-vertical movement, and design and loading details.

Substructure Load Rating

The column in Pier 2 (Pier Column 2, PC2) has an initial load rating of 3.98. The first step in finding the failure condition is determining the critical live load effects (in this case, when the rating vehicle passes over Pier 2 on the inside lane, producing the maximum moment in the column). The live loads from the critical case are then multiplied by a factor, *m*, which is increased until the limit state equation is met. The total loads at failure can be found using Eq.(4-5), and the rating factor is the *m* that causes the limit state to be met. The direction of loading as *m* is increased is shown in P_u-M_u space by the dashed line in Figure 4-5, and the failure condition is shown by the circle. While this process can be solved closed-form, in the experience of the authors, a solution with 3 digits of precision can be converged on very quickly by trial and error (<10 iterations). The load rating procedure was then applied with both settlement cases, shown in Figure 4-6.

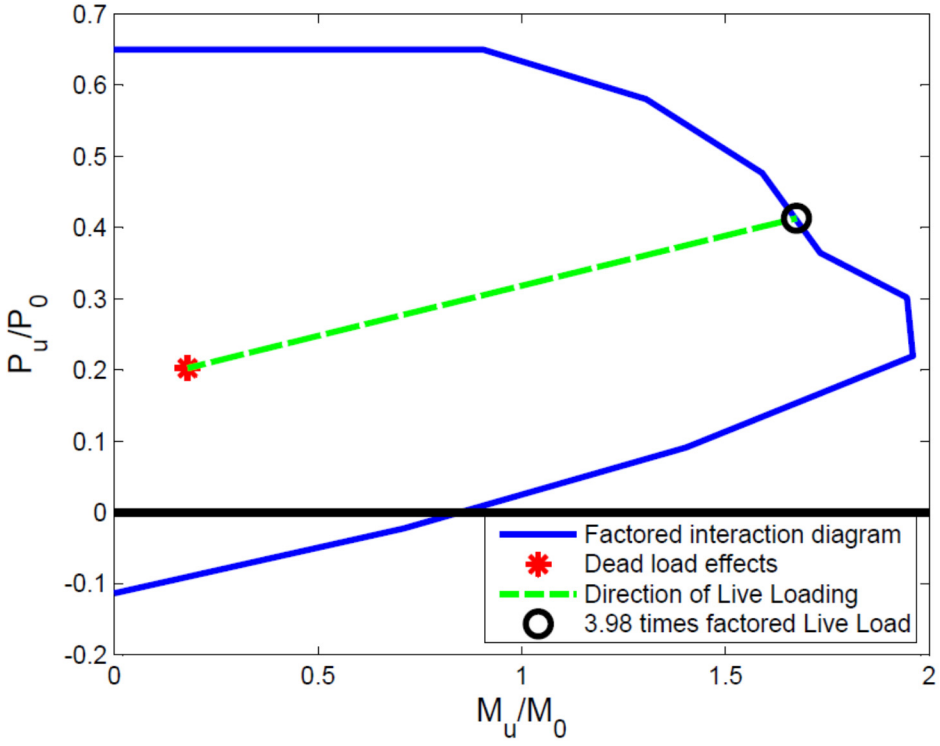

Figure 4-5: Load Rating of PC2 with no settlement

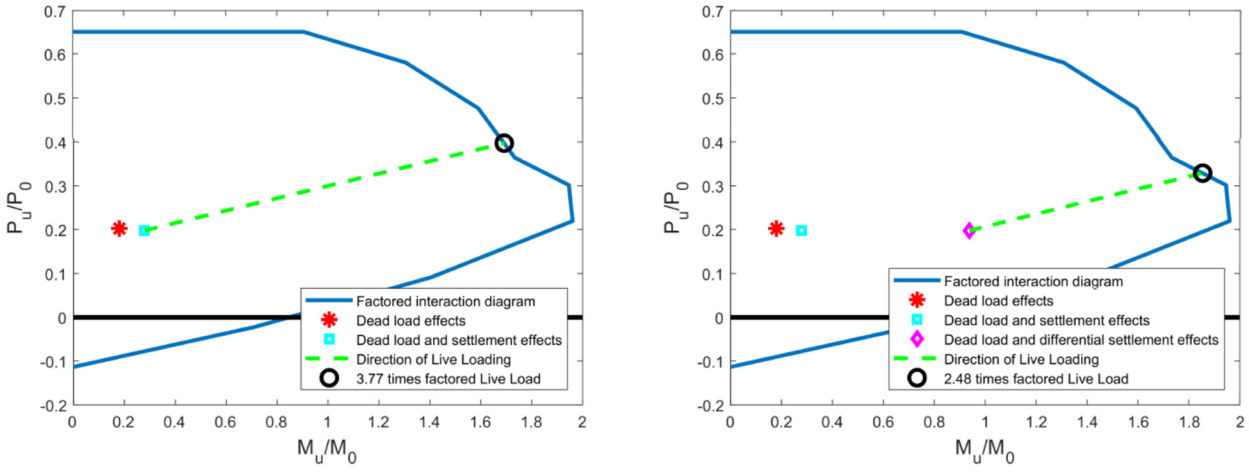

Figure 4-6: Load rating of PC2 during (a) settlement, and (b) settlement, rotation, and translation

Figure 4-6 shows the load rating of PC2 after settlement has occurred. The vertical settlement imposed in the first settlement load case lowers the rating from 3.98 to 3.77. The second settlement load case lowers the load rating to 2.48. All load ratings assume a column condition

factor of 1.0; a lower condition factor would require factoring of both the nominal moment resistance and nominal axial resistance when forming the interaction surface.

Substructure Functionality Index

The angular distortion criterion of 0.004L from AASHTO (2014) is applicable to the load case with vertical settlement only. Applying this criterion to this bridge gives:

$$0.004 \times 70\text{m} = 0.28\,\text{m} = 280\,\text{mm}\ (11\ \text{in}) \tag{4-7}$$

Using the 280 mm (11 in) limit from AASHTO (2014) for the SFI equation in Eq. (4-6) gives:

$$SFI = \frac{280\text{mm} - 102\text{mm}}{280\text{mm}} \times 10 = 6.36 \tag{4-8}$$

Another possible criterion includes limiting translation in the elastomeric bearing pads to 64 mm (2.5 in), which is approximately half of the thickness of the bearing pad. In the SE-1 load, five bearing pads connecting Pier 2 to the girders experience a maximum of 2.8 mm (0.11 in) of displacement (under the innermost girder) from the first settlement load case. During the second settlement load case, the middle girder experiences 89 mm (3.5 in) of displacement. These movements are translated to an SFI for the first and second settlement load cases in Eq. (4-9) and Eq. (4-10), respectively.

$$SFI_{SE1} = \frac{64\text{mm} - 2.8\text{mm}}{64\text{mm}} \times 10 = 9.56 \tag{9}$$

$$SFI_{SE2} = \frac{64\text{mm} - 89\text{mm}}{64\text{mm}} \times 10 \le 0 \tag{10}$$

These indices provide a simple measure of the remaining functionality of the substructure. It is important to note the differences between Eqs.(4-8) and (4-9) which are for the same load case. The 0.004L limit on vertical differential is based on total performance criteria including

strength and serviceability issues, so the SFI found from bearing pad deformation is not expected to match the SFI from the AASHTO (2014) limit. The SFI for the second settlement case in Eq. (4-10) shows that the movement observed at the bottom of the pier column has exceeded the functionality of the bearing pad. A real-life inspection could directly measure the bearing pad translation and not bother with estimation of foundation movement and modeling of the bridge.

Three-Span Prestressed Concrete Simple Span Bridge

State Road 595 crosses over Stevenson Creek, in Pinellas County, FL. It is a 3-span simple span bridge, with each span comprised of 18 rectangular prestressed concrete box beams. The girders are not spaced and are instead connected transversely using post-tensioned steel rods. A cast in place unit takes the place of a 19th girder and connects the two halves of the bridge. The asphalt wearing surface was placed directly onto the prestressed concrete sections. All three spans are 11.8 m (38 ft, 8 in) in length, for a total of 35.4m (116 ft) of bridge length. The interior piers are pile bents with a 760 mm (30 in) deep reinforced concrete pile cap supported by nine 460 mm (18 in) square prestressed concrete piles. The outer two piles on each bent are battered at 1/12 towards the outsides of the bent. The abutments are also supported on nine 460 mm (18 in) square prestressed concrete piles. The girders are connected to the piers and abutments by elastomeric bearing pads. The piles are driven approximately 1.2 m (4 ft) into soft limestone. Above the limestone is approximately 1.8 m (6 ft) of firm to stiff marine clay and above the clay is a 2.1 m (7 ft) deep layer of sand with shells. Previous scour analysis estimated a potential scour depth of 13 feet at this bridge.

Two models of this bridge were created with identical superstructures. The deck was modeled with shell elements with properties matching each of the girders. A discontinuity with

separate bearing pads on each side is provided over the piers. Prestressing steel for each girder is represented by a single tendon with the same total area and eccentricity as the total prestressing steel. The first model, shown in Figure 4-7, has the pile for each pile bent modeled to the top of ground surface, with a pin boundary condition preventing translation and rotation at the ground surface. Rotation was allowed at these connections to prevent over-constraining the model. A frame element was placed underneath the abutment bearing pads to allow for a prescribed abutment displacement to be input. This model was used to model two damage scenarios: 102 mm (4 in) of uniform vertical settlement of one of the pile bents, and 51 mm (2 in) of uniform horizontal movement of one of the abutments.

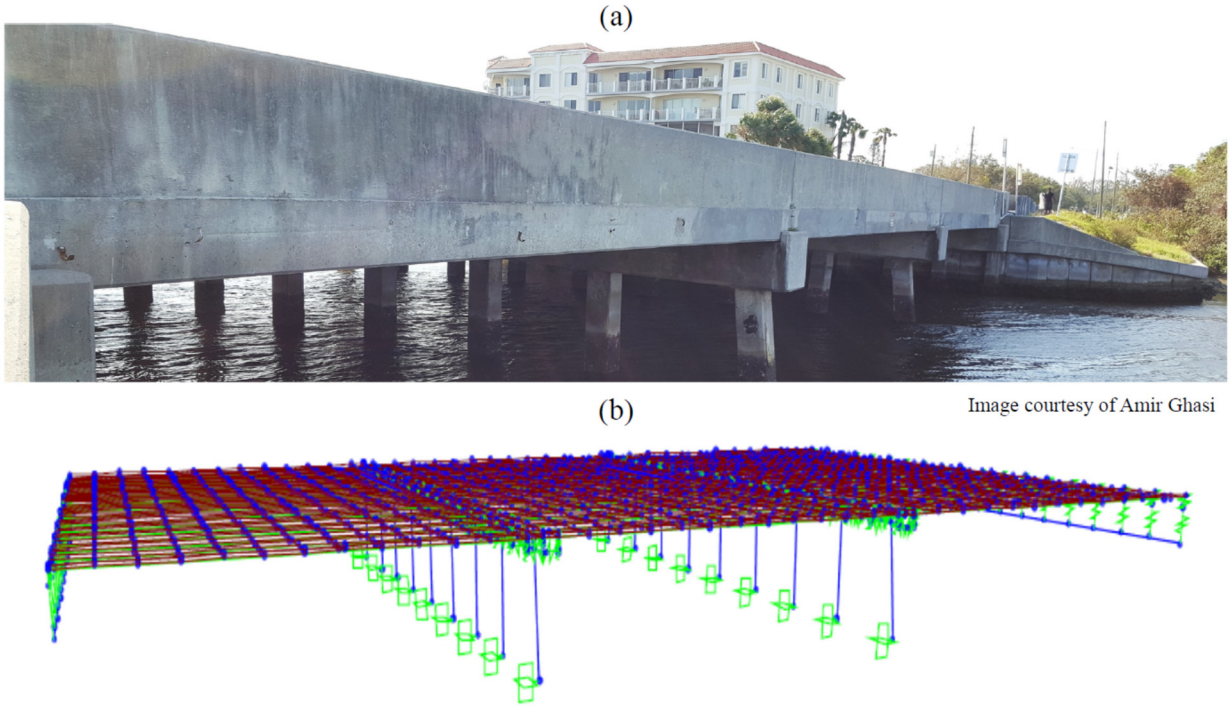

Figure 4-7: (a) SR 595 bridge, and (b) SR 595 bridge model with piles cut off at ground elevation

The second model is identical to the first model, except with the addition of the remaining portions of pile below ground surface. In this model, non-linear P-Y, T-Z, and T-θ springs were used to represent the soil conditions around the piles and Q-Z springs were used to represent the

tip resistance of the piles. This model was used to determine the loading on piles including scour and water flows at various scour depths.

Superstructure Load Rating

Since the SR 575 Bridge is a simple span bridge, vertical pier movement does not have a significant impact on the load rating of the bridge superstructure. The only moment transferred into the girders comes from the stiffness of the bearing pads restraining rotation. Since the abutments have neoprene bearing pads, the horizontal movement does not impart significant moment demands on the superstructure, outside of a small negative moment in the end region near the abutment. Only a slight longitudinal stress imparted on these girders, meaning load rating of the Strength I and Service I conditions will be relatively unaffected by foundation movement. Figure 4-8 shows the plot of the moment demands resulting from dead and wearing surface loads, HL-93 live load, vertical pier settlement, and horizontal abutment movement. As can be seen in Figure 4-8, the moment demands from pier settlement or abutment movement are insignificant when compared to live and dead load demands.

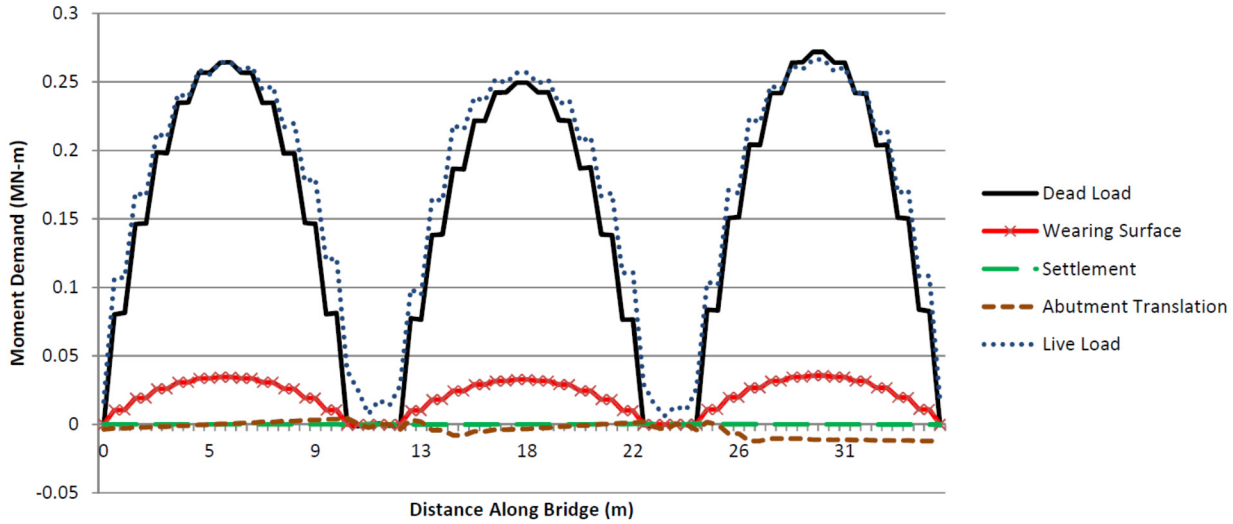

Figure 4-8: Moment demands from various load cases

Since the superstructure load rating was mostly unaffected by the substructure behavior, it was not investigated using the second model. The modeling technique that uses soil springs can used for superstructure load rating, although settlement would need to be applied to the bottom of the piles, requiring a fixed condition rather than a Q-Z spring.

Substructure Load Rating

Substructure load rating was only performed with the model including P-Y springs. This model allowed for the successive removal of non-linear springs, accompanied by a water load of 1.75 N/mm (0.12 K/ft) on the exposed underwater pile sections. The stream pressure was calculated in accordance with Eq. 3.7.3.1-1 of AASHTO (2014) and applied as a distributed load to the submerged pile sections above the ground surface. The piles were load rated using the limit state equation given by Eq. 5.7.4.5-3 of AASHTO (2014), shown in Eq.(4-11):

$$\left(\frac{M_{ux}}{M_r}\right)+\left(\frac{M_{uy}}{M_r}\right)\leq 1.0 \tag{11}$$

where M_{ux} and M_{uy} are the moments about the X and Y axes, respectively. M_r is the effective moment capacity considering the applied axial load. Eq. (4-11) is applicable for these piles as the factored axial load is less than 10% of the gross axial capacity. The rating factors were found by iterating the rating factor until the left side of Eq.(4-11) equaled 1.0.

The addition of water load to the exposed piles primarily caused a reduction in compressive loading on the upstream piles and an increase in compressive loading on the downstream piles. Since the piles on this bridge were lightly loaded in axial compression, the critical effect from water loads was on the piles where the axial load was reduced, as this reduction reduced the effective moment capacity. As scour increases, all pier piles experienced greater moment demands from the live load. The critical pile is the second pile from the upstream side of the bridge which experienced 11.2 kN (2.5 Kips) and 66.2 kN (14.9 Kips) reduction in compressive load from the water load in the as-built and fully scoured condition. The critical live load was a single truck passing over the pier in the lane farthest to the downstream side of the bridge, as this produced a tensile axial load and the largest moment on the critical pile. Table 4-6 provides the factored loads obtained for the critical pile in the non-scoured and fully scoured condition. Table 4-7 shows how the rating factor is affected by scour up to the maximum possible depth. The considered scour depths include removal of P-Y springs representing: half of the sand being scoured, all of the sand being scoured, the entire sand and half of the clay layers being scoured, and all of the clay and sand being scoured with only the soft limestone embedment remaining.

Table 4-6: Calculated factored loads without scour and with full scour

Load	No scour			2.44 m of scour			Full scour		
	P (kN)	M2 (kN.m)	M3 (kN.m)	P (kN)	M2 (kN.m)	M3 (kN.m)	P (kN)	M2 (kN.m)	M3 (kN.m)
DC + DW	-428.5	0.4	2.4	-474.3	0.2	3.8	-486.3	0.2	5.4
WA	11.2	-6.9	-0.9	57.7	1.1	-0.9	66.2	-4.5	-1.1
HL93+IM	50.6	-29.4	-170.1	110.3	-8.7	-251.5	113.1	-10.2	-358.0
Total	*-366.7*	*-35.9*	*-168.6*	-306.2	-7.5	-248.6	*-307.0*	*-14.5*	*-353.6*

Table 4-7: Rating factors for the critical pile with varying scour

Load Case	Rating Factor
No Scour, no water load	1.70
No Scour with water Load	1.65
1.27 m of scour	1.42
2.44 m of scour	1.28
3.47 m of scour	0.95
Maximum Scour to Limestone (4.88 m)	0.91

Substructure Functionality Index

The bearing pad distortion limit chosen for this bridge was 13mm (0.5 in). The maximum translational bearing pad distortion for the load case with 102 mm (4 in) of vertical pier settlement was 2 mm (0.082 in). The distortion in the bearing pads connecting to the abutment with 51 mm (2 in) of movement was 39.6 mm (1.56 in). The maximum bearing pad distortion observed from the model during the fully scoured condition with water loads was 1.78 mm (0.07 in). Table 4-8 provides a summary of the functionality indices based on bearing pad deformation.

Table 4-8: Functionality index based on bearing pad deformation for three damage scenarios

Damage Scenario	SFI
102 mm of vertical settlement under one of the piers	8.46
51 mm of abutment translation	0
Maximum scour and water loading on pier	8.63

4.7 Conclusions and Future Work

A framework for integrated superstructure-substructure load rating of bridges with foundation movements and an index to quantify functionality of bridges in the presence of foundation movement has been proposed and illustrated through two example bridges. It was shown through the example bridges that vertical settlement could substantially impact the load rating of superstructure and substructure elements. In the bridges studied, horizontal and rotational movements did not substantially impact the superstructure load rating but did reduce the substructure load rating and the proposed *Substructure Functionality Index* (SFI), which quantifies the amount of tolerable movement. Applying this methodology to bridges with noted settlement, scour, or substructure deterioration issues can allow bridge managers to objectively qualify foundation issues and inform management decisions. Load rating foundation capacity and performance can aid preliminary decision making when considering a foundation for reuse.

In conclusion, the primary findings of this research were:

- Load rating of superstructures may be non-conservative if foundation movement has occurred and is not considered.
- Foundation movement and additional loading sources like water or earth pressure may lower the load rating of foundation elements.

- The functionality of substructures can be objectively quantified through use of the *Substructure Functionality Index* (SFI)

Further investigation is needed into how the rating factor of various types of substructures, bearings, and superstructures depend on movement. Time dependent properties such as creep or relaxation should be investigated to determine the time dependency of settlement loads. For substructure load rating, investigation into the load rating of damage scenarios and strengthened components needs to be performed. Investigation should be performed to assess the appropriate inspection and rating interval for substructure movement, as well as the appropriate water flows to consider and their factors during that interval. Further investigation is also needed to identify components that will govern the substructure functionality index (SFI) of bridges undergoing foundation movement.

4.8 Acknowledgements

The research presented in this paper has been supported through the foundation characterization program of Federal Highway administration, contract no. DTFH61-14-D-00010/0002. Any opinions, findings, and conclusions or recommendations expressed in this paper are those of the authors and do not necessarily reflect the views of the Federal Highway Administration. The authors would also like to thank the Florida DOT for providing bridge plans, drawing, and scour evaluation reports for the examples used in this paper.

4.9 References

AASHTO. (2011). *Manual for Bridge Evaluation*. American Association of State Highway and Transportation Officials, Washington, D.C.

AASHTO. (2014). *LRFD Bridge design specifications*. American Association of State Highway and Transportation Officials, Washington, D.C.

ACI. (2015). *SP-17(14) Reinforced Concrete Design Handbook Volume 2*. (A. Taylor, T. H. III, and A. Nanni, eds.), American Concrete Institute, Farmington Hills, MI.

Andrawes, B. and Caiza, P. (2012) *Bridge Timber Piles Load Rating Under Eccentric Loading Conditions*. ASCE Journal of Bridge Engineering, Vol. 17, No. 4, pp. 700-710

Arneson, L. a., Zevenbergen, L. W., Lagasse, P. F., and Clopper, P. E. (2012). HEC-18 *Evaluating Scour at Bridges*. *Publication No. FHWA-HIF-12-003*, Federal Highway Administration.

Barker, R. M., Duncan, J. M., Rojiani, K. B., Ooi, P. S. K., Tan, C. K., and Kim, S. G. (1991). "Manuals for the Design of Bridge Foundations: Engineering Manual for Estimating Tolerable Movements of Bridges." *Transportation Research Board*, (343).

Bozozuk, M. (1978). "Bridge Foundations Move." *Transportation Research Record*, (678), 17–21.

Cai, C.S. and Shahawy, M. (2003), "Understanding Capacity Rating of Bridges from Load Tests", *Practice Periodical on Structural Design and Construction*, Vol. 8, No. 4, pp. 209-216.

Chajes, M.J., Mertz, D.R. and Commander, B. (1997), "Experimental Load Rating of a Posted Bridge", ASCE Journal of Bridge Engineering, Vol. 2, No. 1, pp. 1-10.

DiMillio, A. F. (1982). *Performance of Highway Bridge Abutments Supported by Spread Footings on Compacted Fill*. FHWA/RD-81/184 (NTIS PB83-201822).

Dupont, B., and Allen, D. (2002) *MOVEMENTS AND SETTLEMENTS OF HIGHWAY BRIDGE APPROACHES* Report No. KTC-02-18/SPR-220-00-1F Kentucky Transportation Cabinet, Frankfort, KY

FB-Pier (2015). *FB-MultiPier Manual*. Florida Bridge Software Institute, Gainesville, FL.

Florida Department of Transportation (FDOT). (2016) *Bridge Load Rating Manual.* Topic No. 850-010-035, Tallahassee, FL

Gao, L. *Load Rating Highway Bridges in Accordance With Load and Resistance Factor Rating Method,* First edition, Outskirts Press, Denver, Colorado, 2013.

Grover, R. A. (1978). "*Movements of Bridge Abutments and Settlements of Approach Pavements in Ohio.*" *Transportation Research Board*, (678), 12–17.

Illinois Department of Transportation (IDOT) (2014) *"Bureau of Local Roads and Streets Manual"* IDOT, Springfield, IL

Kim, K.H., Andrawes, B. (2017) "Load Rating of Deteriorated and FRP Retrofitted Bridge Abutment Timber Piles" ASCE Journal of Bridge Engineering, Vol. 22 No. 9

Maine Department of Transportation (MaineDOT). (2015) *"Load Rating Guide"* MaineDOT, Scarborough, ME

Massachussetts Department of Transportation (MassDOT). (2013) *LRFD Bridge Manual* MassDOT, Boston, MA

Mertz, D. (2005) "*Load Rating by Load and Resistance Factor Evaluation Method* " NCHRP 20-07, Task 122 Transportation Research Board

Modjeski and Masters, University of Nebraska, Lincoln, University of Delaware, and NCS Consultants, LLC (2015) "*Bridges for Service Life Beyond 100 Years: Service Limit State Design"* SHRP 2 Report S2-R19B-RW-1 *Transportation Research Board*

Moon, F., Romano, N., Masceri, D., Braley, J., Mertz, D.R., Samtani, N., Murphy, T., Lopez de Murphy, M. (2018) NCHRP Web-only Document 245: Bridge Superstructure Tolerance to Total and Differential Foundation Movements. NCHRP Project 12-103, Transportation Research Board, Washington, DC.

Moulton, L. K., GangaRao, H. V. S., and Halvorsen, G. T. (1985). *Tolerable movement criteria for highway bridges*. *Federal Highway Administration*, Report No. FHWA/RD-85/107, Washington, D.C.

Nowak, A. S. (1999). NCHRP 368 Calibration of LRFD Bridge design code NCHRP Report No. 368, Transportation Research Board, Washington, D.C.

Paikowsky, S. G., and Y. Lu. (2006) "Establishing serviceability limit state in the design of bridge foundations." Foundation Analysis and Design: Innovative Methods. (GSP 153) 49-58.

Sanayei, M., Reiff, A.J., Brenner, B.R., and Imbaro, G.R. (2016). "Load Rating of a Fully Instrumented Bridge: Comparison of LRFR Approaches" Journal of Performance of Constructed Facilities, Paper No. 04015019. doi:10.1061/(ASCE)CF.1943-5509.0000752

Sayed, S. M., Sunna, H. N., and Moore, P. R. (2013). "Load Rating of Pile-Supported Bridges Susceptible to Scour." Journal of Bridge Engineering, 18(5), 439–449.

Turkstra, C.J., (1970) "Theory of Structural Design Decisions", Study No. 2, Solid Mechanics Division, University of Waterloo, Waterloo, Ontario, Canada.

Wahls, H. . (1990). Design and construction of bridge approaches. National Cooperative Highway Research Program Synthesis Report 159. Transportation Research Board, Washington, D.C.

Walkinshaw, J. L. (1978). "Survey of Bridge Movements in the Western United States." *Transportation Research Board*, (678), 6–12.

Wang, Z., Chen, G., Kwon, O., Orton, S. (2011). "*Calibration of Load and Resistance Factors in LRFD Foundation Design Specifications.*" Report No. NUTC-R237, U.S. Department of Transportation, Washington, D. C.

Chapter 5 Existing Pile Capacity

This chapter features the contents of a manuscript by the following authors that has been formatted for publication in a peer-reviewed manual.

Determining the Capacity of Reused Bridge Foundations from Limited Information

Nathan T. Davis[1], Masoud Sanayei[2], Anil K. Agrawal[3] and Farrokh "Frank" Jalinoos[4]

[1]PhD Candidate, Dept. of Civil & Env. Engineering, Tufts University, Medford, MA 02155

[2]Professor, Dept. of Civil & Env. Engineering, Tufts University, Medford, MA 02155

[3]Professor, Dept. of Civil Engineering, The City College of CUNY, New York, NY 10031

[4]Research Structural Engineer, Federal Highway Administration, Office of Infrastructure R&D, McLean, VA 22101

Abstract

Reuse of bridge foundations often requires determining the capacity of existing foundations, including driven piles. These piles have a proven history of load carrying capacity but may lack test data from which the capacity can be obtained. In general, pile capacity can be estimated from the pile geometry and soil properties using empirical calculations. However, these produce highly uncertain results due to the variable nature of soil and pile driving methods. As a result, LRFD practice uses low resistance factors during for pile design based on these calculations that can produce inefficient designs, sometimes with lower capacity than the loading observed during the initial service life. This research proposes a novel reliability-based methodology to update the capacity of individual piles based on previously observed loading to the pile group. A likelihood function is developed that accounts for the probability that a single pile has low capacity given that the total group capacity was greater than the observed loading during its initial service life. The results are tabulated to show the increases to the LRFD resistance factors that are possible while maintaining the reliability index (and corresponding probability of failure) for standard LRFD designs.

Keywords: Bridge foundation reuse, deep foundations, in-service loading, capacity, reliability

5.1 Introduction

When an existing in-service bridge is being rehabilitated, widened, or replaced, significant economic advantages can be realized through alternatives that reuse substructure and foundation components (Boeckmann and Loehr 2016). Foundation reuse can be particularly beneficial for accelerated and low traffic-impact construction methods by maintaining the existing alignment and reducing construction activities. Many foundations that may be candidates for reuse are supported by driven piles, potentially with limited or non-existent test data, installation records,

and quality control. These foundations may have questions surrounding their durability, capacity, or integrity. This research proposes a novel approach to determining the geotechnical capacity, which can only be utilized when durability and integrity questions have been answered.

Modern construction of new foundations supported by driven piles will typically employ static or dynamic testing to determine the capacity of piles. Pile capacity estimation techniques, such as static analysis or dynamic analysis (based on driving criteria), typically provide highly variable estimations of pile capacity as shown by Paikowsky et al. (2004). These equations are frequently used for sizing piles and determining preliminary capacity but are assigned low resistance factors for design by the Load and Resistance Factor Design (LRFD) Bridge Specifications (AASHTO 2014), which can lead to highly inefficient designs. For reused foundations, the factored capacity determined using design equations may be less than the load previously applied to the bridge. A common formalized procedure for accounting for the previous loading history when estimating pile capacity doesn't currently exist.

This paper proposes a reliability-based methodology that updates resistance factors prescribed by the LRFD Bridge Specifications (AASHTO 2014) using the previous loading history. The proposed methodology considers the previous loading applied to the pile cap to determine the likelihood of one of the piles having a low pile capacity. A distribution of ultimate pile capacity is then updated considering this knowledge of previous loading. The updated distribution is used in a reliability analysis to produce designs with consistent probabilities of failure. A second methodology is explored that does not consider a pile capacity prediction method, but assigns a capacity based solely on the previously applied loading. The former

methodology is appropriate in situations where a capacity can be estimated using design equations, while the latter method does not require prior estimation of the pile capacity.

5.2 Background

The LRFD approach seeks to maintain a constant probability of failure for components by prescribing load and resistance factors based on the expected variation of load and resistances (Barker et al. 1991; Novak 1999). The LRFD Bridge Specifications (AASHTO 2014) provide resistance factors for the geotechnical capacity of driven piles that vary based on the calculation method used to determine that pile's capacity. These factors account for two main sources of pile capacity variability: the variation of pile capacities on a single site (on-site variation), and the inherent uncertainty associated with the prediction method. When pile capacities are based on the results of static testing to failure a resistance factor of 0.75 to 0.80 is recommended to account for on-site pile capacity variation. A slightly lower factor ranging from 0.65 to 0.75 is recommended for capacities derived from dynamic test data obtained during pile driving. For new foundations, one of these forms of testing is frequently employed. Static analysis methods, commonly used for preliminary pile sizing, predict capacity from empirical equations based on soil properties and produce highly variable results. When not augmented with test data, capacities derived from empirical equations require low resistance factors ranging from 0.25 to 0.50. In addition, pile driving formulae that estimate capacity on driving performance allow for resistance factors ranging from 0.10 to 0.50. The guidance found in AASHTO (2014) largely follows the recommendations of Allen (2005), who summarized prior work done by Paikowsky et al. (2004) and Barker et al. (1991) to determine resistance factors that provide a consistent probability of failure.

Ellingwood et al. (1980) conducted early research into calibrating load and resistance factors for structural components using reliability analysis. Six load cases were considered that included combinations of live, dead, wind, and earthquake loading. Ellingwood and Galambos (1982) detail this methodology and provide summaries of target reliabilities for various structural components. Moses and Verma (1987) applied reliability-based design principles to evaluate in-service bridges, including a methodology that load rated components by their reliability index.

Barker et al. (1991) applied reliability analysis to driven pile capacity using mean value first-order second-moment (MVFOSM) reliability analysis. This research calculated the required resistance factors for driven piles using then-current load-factor design (LFD), which used load factors of 1.3 and 2.17 for dead and live loads, respectively. It was observed that previous working stress design (WSD) codes provided reliability indices between 1.6 and 3.1, with long-span bridges having higher reliabilities due to a higher dead to live load ratio. Target reliabilities between 2.5 and 3.0 were suggested for axially loaded driven piles, although it was suggested that 2.0 to 2.5 may be appropriate due to the ductile nature of pile failure and the effects of group redundancy.

Novak (1999) studied the reliability of bridge structural components designed using LFD and ASD for spans of various lengths. Like Barker et al. (1991), it was shown that long-span bridges were typically built to higher reliabilities than short spans, due to the higher dead to live load ratio. A parametric study of the variability of dead and live loads on bridges was performed by Novak (1999), finding that these loads followed lognormal distributions with the biases and coefficient of variations (COVs) as listed in Table 5-1.

Table 5-1: Bias and COV of load prediction

	Bias of prediction (λ)	COV of distribution (σ/μ)
Live Loads	1.15	0.2
Dead Loads	1.05	0.1

Ayyub and Assakkaf (1999) have presented a method that uses the First Order Reliability Method (FORM), pioneered by Hasofer and Lind (1974), to determine partial safety factors (PSFs) for the loading and resistance of bridge components. This methodology allows for all required safety factors to be computed at once, or for the resistance factor to be computed, given predetermined load factors. Paikowsky (2004) followed this methodology to produce resistance factors for use in LRFD along with the dead and live load factors of 1.25 and 1.75, respectively. Paikowsky et al. (2004) followed the lognormal distributions presented in Nowak (1999) for dead and live loading on the bridge foundation.

To develop pile capacity distributions, Paikowsky et al. (2004) compiled test data on the performance of static analysis and dynamic capacity estimation methods. Static methods do not typically account for installation, while dynamic capacity estimation methods are primarily based on the details associated with driving, such as hammer energy, pile penetration, and driving criteria. The compiled test data consisted of hundreds of piles where the nominal capacity was calculated using static and dynamic capacity estimation methods and the ultimate capacity found through static testing to failure. From the results, a lognormal distribution of the ratio of ultimate capacity to nominal capacity was calculated for each prediction method. Target reliabilities of 2.33 for redundant piles (pile caps with 4 or more piles) and 3.0 for 3 or fewer piles were suggested.

Allen (2005) compared the resistance factors found by calibrating existing ASD practice (following Barker et al. 1991) with those found through reliability analysis (Paikowsky et al.

2004). From these results, recommendations were made for resistance factors to be used in LRFD analysis alongside dead and live load factors of 1.25 and 1.75, respectively. The recommended resistance factors were not generally the explicit result of a reliability analysis but were in line with the calibrated factors from Paikowsky et al. (2004). Hence, the proposed methodology will update the resistance factors provided by Allen (2005) and AASHTO (2014) using an updated reliability analysis that follows from the data compiled by Paikowsky et al. (2004).

Zhang and Tang (2002) have proposed a method for updating the reliability analysis proposed by Barker et al. (1991). This methodology uses Bayesian sampling to update the distribution of the mean pile capacity using load test results from individual piles. The original mean capacity distribution is derived from a prior distribution of pile capacities governed by the capacity estimation technique and an assumed on-site variance. A new resistance factor is found using the MVFOSM approach. Park et al. (2015) followed this approach to update resistance factors on a site with 10 individual pile tests.

Abdallah et al. (2015) also proposed a new updating strategy using individual pile tests. This strategy defines a lower bound of pile capacity that is utilized in a reliability analysis to update the required resistance factor. Huang et al. (2016) developed an approach to updating individual pile capacity without considering the distribution of the mean pile capacity. This methodology still relies on load tests of individual piles. Zhang et al. (2017) discuss the implications of Bayesian updating techniques on the geotechnical engineering practice. Several barriers to widespread usage of Bayesian methods were identified that included lack of available computer codes and unfamiliarity with Bayesian methods.

5.3 Proposed Methodology

To conform with the current code approach, the proposed methodology provides a method for updating the distribution of individual pile capacity on a site. This new distribution will be used in a reliability analysis to determine new resistance factors for driven piles considering the past loading on a bridge foundation. A major advantage of this approach is the results can be employed by practicing engineers by utilizing the prescribed resistance factors provided later in this paper.

Since the loading history considered in this research consists of loading on a set of piles simultaneously, it is useful to consider that set to be a "population" of piles in which each individual pile is simply a sample. Individually, these piles will all have the same PDF that links their ultimate capacity to predicted (nominal) capacity. However, it can be further assumed that the capacities of the piles will be related to each other. In the previous research from Paikowsky et al. (2004) and Zhang and Tang (2002), this relation has been defined as a coefficient of variation (COV) between individual piles on the site.

Previously observed loading on bridge foundations consists of a mixture of dead loads and live loads. During reuse, a portion of the existing dead load corresponding to the reused components will remain on the foundation. Another portion will be removed and replaced, and this replacement load may be lower or higher than the original dead load. Live loading can consist of operational trucks, past permit loading, or test trucks. Loading from past permitting or test trucks can be used to update pile capacity, as it can be observed that such loading didn't cause significant distress (such as excessive settlement), and the magnitude of the load is reported in permit documents. A computer model may be needed to determine how much of the load reaches each pile group. It cannot be known from this loading how much load was transferred into each

individual pile, as piles may have varying stiffness and the ductile nature of pile failure will cause a pile near failure to increasingly lose stiffness and transfer loads to the adjacent piles. It cannot necessarily be determined through observation that any individual pile failed or did not take up adequate load unless structural distress has occurred.

Instead, it can be determined from the previous loading that the *average* capacity of the piles being loaded is *at least* as great as the average load that was applied to that *population*. A population of piles refers to a group of piles that were similarly driven and similarly loaded during testing, some of which may be battered. Battered piles subjected to purely vertical load will experience greater axial loading than vertical piles, since the axial force in battered piles will contain a lateral component as well. However, this effect will be minor in comparison to the loading history, especially for low batter angles. The proposed approach of updating pile capacity by considering the average vertical load will yield a slightly conservative result, as it does not include any axial loading caused by lateral loads. The new resulting capacity will be the axial capacity of the all piles (including battered).

It would be impossible to measure the actual on-site variation between pile capacities without obtaining test data of individual pile capacities. However, statistical data has been compiled in the literature that attempts to quantify the on-site variance of pile resistance. Based on research by Kay (1976) and Evangelista et al. (1977), Zhang and Tang (2002) have adopted a blanket site variance of 0.20. Paikowsky et al. (2004) have classified sites into three categories of variability: low, medium, and high. Based on the research by Phoon and Kulhawy (1996), these three site categories were taken to have on-site pile capacity COVs of 0.15, 0.25, and 0.35, respectively. Selection of an appropriate variability for a site always requires engineering

judgment, since the actual variability of the site will depend on the soil variability, the variability of installation techniques, and various other factors that are difficult to quantify. This method is applicable to sites with any selected variability, though only sites with low, medium, and high (COVs of 0.15, 0.25, and 0.35) variabilities are presented in this paper.

5.4 Distribution of Individual Pile Capacity

Paikowsky et al. (2004) have considered the ratio of ultimate pile capacity to nominal capacity of an installed pile to be a random variable following a lognormal distribution. This distribution is defined by its bias (ratio of mean ultimate capacity to nominal capacity) and coefficient of variation (COV). Eq.(5-1) shows a lognormal distribution typically used to model individual pile capacity (Paikowsky et al. 2004; Novak 1999).

$$f_X = LN(\mu_x, \sigma_x) \tag{5-1}$$

Figure 5-1 shows an example distribution of pile ultimate capacity normalized by the capacity predicted by the β-method for an H-pile in clay where $\mu_x = 0.61$ and $\sigma_x = 0.37$. Due to the variability of this prediction method, a resistance factor of 0.25 is specified by AASHTO (2014) when pile capacity is determined only from its results.

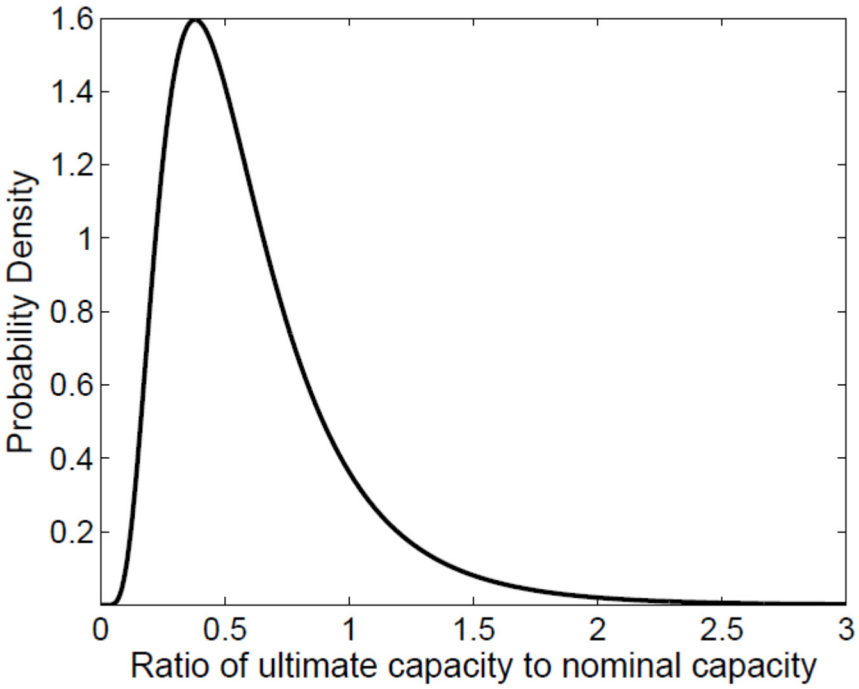

Figure 5-1: Distribution of ultimate pile capacity given a nominal capacity calculated using the β-method.

5.5 Population Capacity Distribution

For updating purposes, it is convenient to transform the parameters in Eq.(5-1) using the logarithmic transformations (Ang and Tang 1975) shown in Eq.(5-2) and Eq.(5-3).

$$\sigma_{x,\ln} = \sqrt{\ln\left(\sigma_x^2 + 1\right)} \tag{5-2}$$

$$\mu_{x,\ln} = \ln\left(\mu_x\right) - \frac{\sigma_{x,\ln}^2}{2} \tag{5-3}$$

Zhang and Tang (2002) have proposed a methodology to calculate the distribution of the population mean using the distribution of individual pile capacity and the expected on-site variability. The distribution of the mean is given by Eq.(5-4) for normally distributed pile capacity and site variability. The parameters governing the PDF of the population mean are given by Eq.(5-5) and Eq.(5-6).

$$f'(\mu) = N_\mu(\mu', \sigma') \tag{5-4}$$

$$\mu' = \mu_{x,\ln} \tag{5-5}$$

$$\sigma' = \sqrt{\sigma_{x,\ln}{}^2 - \sigma^2} \tag{5-6}$$

In Eq.(5-4), *f'(μ)* is the distribution of the population mean, which is normally distributed with respect to μ, with a mean of μ' and a standard deviation of σ', μ_x and σ_x are the mean and standard deviation of the individual piles, respectively, and σ is the assumed on-site variability. It is helpful to keep these distributions normalized with respect to both the nominal pile capacity and the number of piles so that the distribution represents the ratio of the population mean capacity to the predicted capacity. Figure 5-2 shows three possible distributions of population mean capacity corresponding to low, medium, and high variability sites for a site where the individual pile capacities follow the distribution in Figure 5-1 (which represents an H-pile in clay with capacity determined using the β-method).

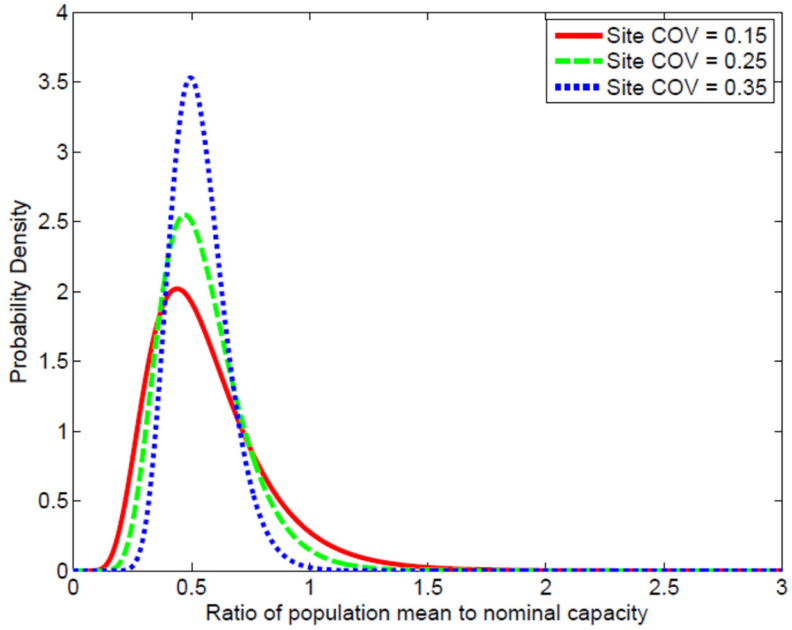

Figure 5-2: Three possible population mean distributions.

5.6 Updating Population Mean Capacity Distribution

Zhang and Tang (2002) have employed Bayesian sampling theory (Ang and Tang 1975) and have provided a new distribution of the population mean, given the results of a limited number of pile tests to failure. The new population is normally distributed (or lognormally distributed after conversion) and is given by Eq.(5-7),

$$f''(\mu) = N_{\mu}(\mu'', \sigma'') \tag{5-7}$$

where μ'' and σ'' are given by Eq.(5-8) and Eq.(5-9),

$$\mu'' = \frac{x(\sigma')^2 + \mu'\left(\frac{\sigma^2}{n}\right)}{(\sigma')^2 + \left(\frac{\sigma^2}{n}\right)} \tag{5-8}$$

$$\sigma'' = \sqrt{\frac{(\sigma')^2\left(\frac{\sigma^2}{n}\right)}{(\sigma')^2 + \left(\frac{\sigma^2}{n}\right)}} \tag{5-9}$$

In Eq.(5-8), x is the average test result (pile capacity) from an n-sized sample of piles. The novel aspect of this research is that no individual testing is required to be performed on piles. Instead, the distribution described by Eq.(5-7) will be utilized to determine the likelihood of the population mean capacity being as least as large as observed, considering all possible pile capacities for a single pile (n = 1). Hence, the distribution of the population mean can become a function of the individual capacity of an arbitrary pile, x, the mean and variance of individual pile capacity (μ_X and σ_X), and the on-site variance, σ, following Eq.(5-1) through Eq.(5-6).Figure 5-3 shows the PDF of the population mean (for the example case of H-piles in clay, β-method) for a

site variance (σ) of 0.15, given two possible values of individual pile ultimate capacity, x (shown as a percentage of the nominal capacity).

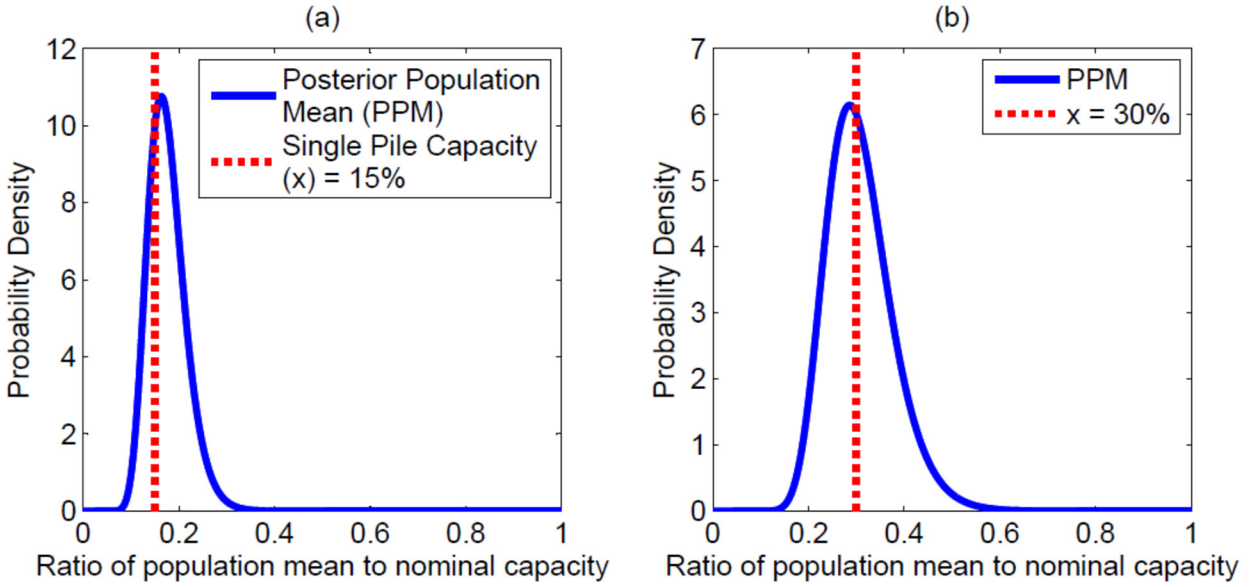

Figure 5-3: Distribution of population mean given (a) a pile with 15% of the nominal capacity, and (b) a pile with 30% of the nominal capacity.

5.7 Bayesian Updating of the Pile Capacity Distribution

Following Bayes' theorem (Ang and Tang 1975), an updated probability distribution can be obtained using

$$f_{updated}(x) = \frac{f_X(x)P(\varepsilon \mid x)(x)}{\int_{-\infty}^{\infty} f_X(x)P(\varepsilon \mid x)(x)dx} \tag{10}$$

where $f_{updated}(x)$ is the new PDF that describes the probability of a pile having a specific capacity, given the observations on past loading history. Here, $P(\varepsilon \mid x)$, commonly referred to as a likelihood function, represents the probability of observation ε being made, given x. $f_X(x)$ is the prior distribution of pile capacity, as shown in Figure 5-1. In this methodology, this specifically

refers to the likelihood that the population mean was *at least as large as* the observed loading for a given x, as shown in Eq.(5-11).

$$P(\varepsilon \mid x) = L(x) = P(f''(\mu \mid x) \geq past\ loading) \tag{5-11}$$

where $f''(\mu)$ is a function of x, as shown by Eq.(5-7), Eq.(5-8), and Eq.(5-9).

Figure 5-4a and Figure 5-4b show the population mean distributions (from Figures 3a and 3b) along with the maximum past loading, shown by a vertical dashed line. In these figures, the blue line represents the $f_{updated}(x)$ obtained in Eq.(5-10), and the shaded region represents the range of possible population means that are equal to or greater than the previously observed loading. The likelihood that this observed population mean could occur along with an arbitrary possible single pile capacity, x, is denoted by the shaded area and is noted in the legend of these figures as "Likelihood". The area of the shaded region is always between 0 and 1.0 and forms the likelihood function $L(x)$. Figure 5-4c and Figure 5-4d show these same distributions and likelihoods if a higher maximum past loading of 30% of the nominal capacity has been previously observed.

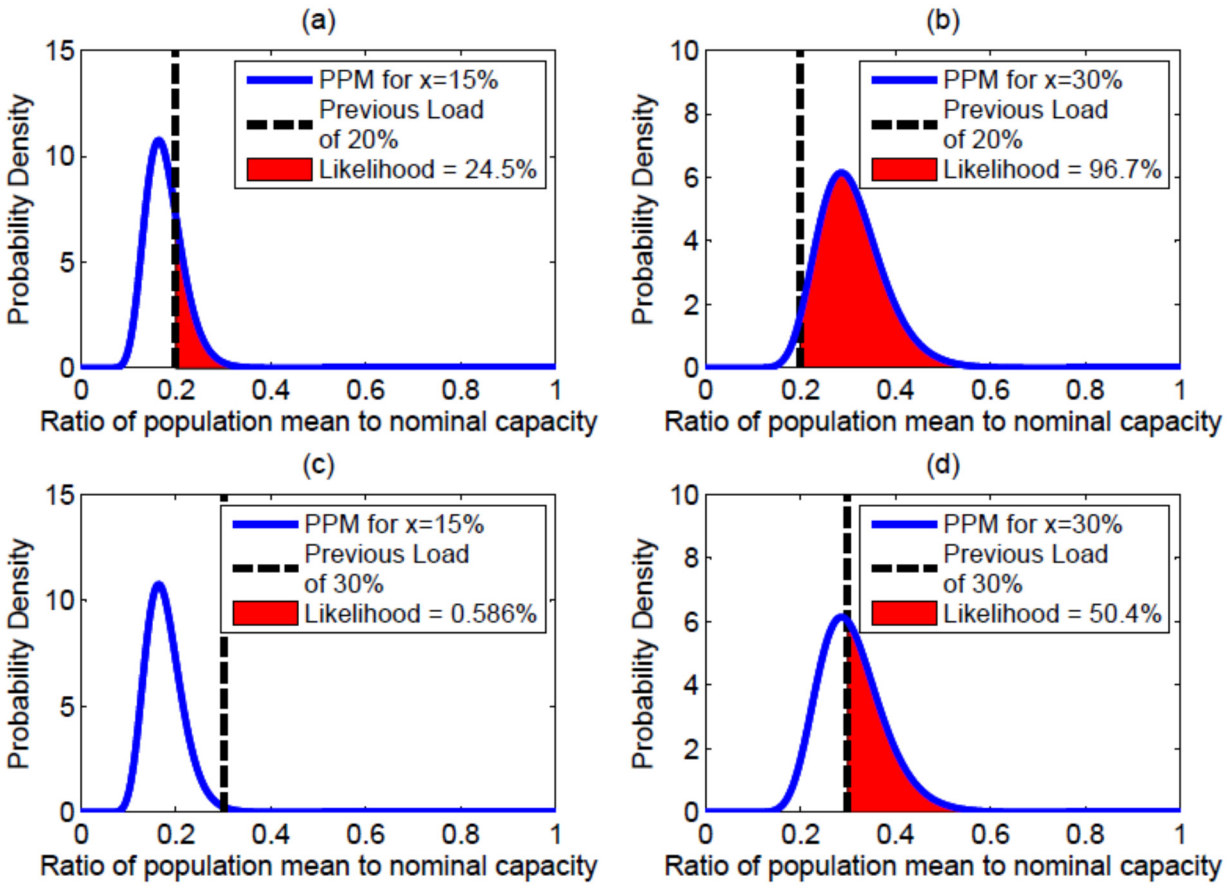

Figure 5-4: Distributions shown in Figures 3a and 3b with a past loading of 20% of the nominal capacity (a and b), and 30% of the nominal capacity (c and d).

As can be seen in Figure 5-4, the likelihood function generally decreases as x decreases, although the magnitude depends on the magnitude of the past loading. The likelihood function in Eq.(5-11) was numerically integrated using the MATLAB (MathWorks 2016) integral function to determine the constant that forms the denominator of Eq.(5-10). The equation for the posterior pile capacity PDF given in Eq.(5-10) was solved again using numerical integration. In practice, the primary difference between the prior and posterior distributions is the reduction in probability of low values of *x*. This can be observed by comparing the PDF of the prior distribution from Figure 5-1, with updated distributions considering a past loading of 20% and 30% of the nominal pile capacity, as shown in Figure 5-5.

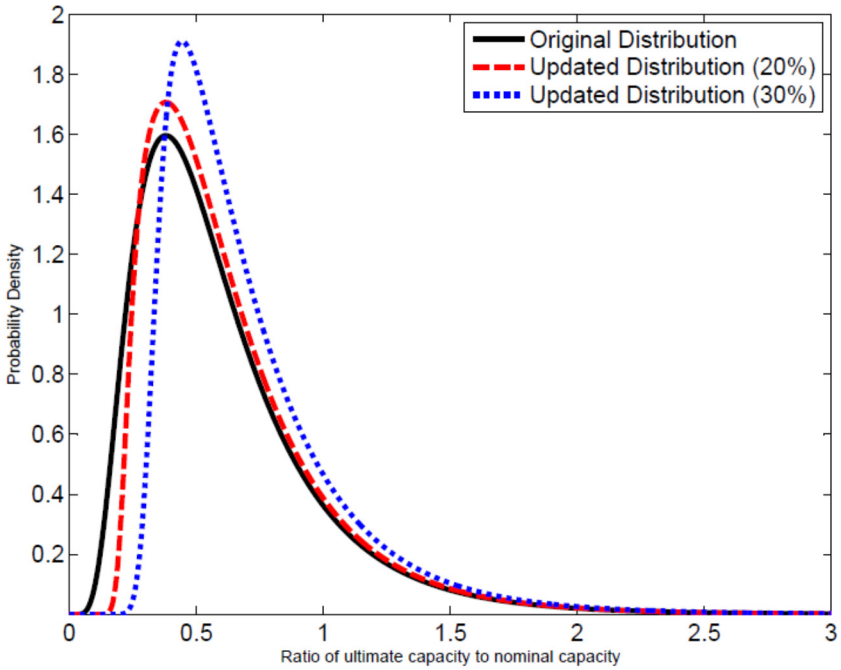

Figure 5-5: Original and updated distribution for pile subjected to previous loading.

The black solid line in Figure 5-5 shows the PDF of the ultimate capacity normalized with respect to the nominal capacity for a pile with its capacity predicted by the β-method. The dashed line in Figure 5-5 accounts for a past loading of 20% of the nominal pile capacity being applied to the pile population, on average. The dotted line accounts for a previous past loading of 30% of the nominal pile capacity. The updating process accounted for the unlikelihood of a single pile having an ultimate resistance far below that of the population mean and provides a new distribution that can be used to estimate the reliability of the pile with respect to future uncertain loading. The new distribution is numerical, rather than a defined distribution (i.e. lognormal).

5.8 Determining a New Resistance Factor

A new resistance factor is calculated using the updated pile capacity distribution described previously. A partial safety factor (PSF) formulation, as described by Ayyub et al. (2002) and

followed by Paikowsky et al. (2004) and Nowak et al. (1999), was used to find the resistance factor required to reach a target reliability index of 2.33. The PSF formulation can be used with an arbitrary limit state, and the limit state equation solved to derive this factor is given by Eq.(5-12):

$$g = R_{nom}x_1 - LL_{nom}x_2 - DL_{nom}x_3 \tag{5-12}$$

where R_{nom}, LL_{nom}, and DL_{nom} are the nominal resistance, live load, and dead load effects, respectively. Variables x_1, x_2, and x_3 in Eq.(5-12) represent the distributions that describe the ultimate pile capacity (updated), live loads, and dead loads, respectively, normalized with respect to their respective nominal values. The parameters governing the distributions of x_2 and x_3 are given in Table 5-1. To solve the general limit state equation in Eq.(5-12), LL_{nom} is set to be 1 and DL_{nom} is equal to the dead to live load ratio (Q_d / Q_L). This ratio is taken to be 2.5 for this analysis following Paikowsky et al (2004), although the methodology allows selection of any ratio. A reliability analysis following Hasofer and Lind (1974) is then performed with the value of R_{nom} iterated until the target reliability index is achieved. Since the load factors to be used on the live and dead loads are set by AASHTO (2014) to be 1.75 and 1.25, respectively, the formula for the appropriate resistance factor is given by Eq.(5-13) below,

$$\phi = \frac{1.75(1) + 1.25(\frac{Q_d}{Q_L})}{R_{nom}} \tag{5-13}$$

In Eq.(5-13), (Q_d / Q_L) is the ratio of dead load to live load and R_{nom} represents the nominal resistance value converged during the analysis. Since the updated distribution has a lower likelihood of the ultimate capacity being far lower than the nominal capacity, a lower R_{nom} is

required to achieve the same reliability index, leading to higher ϕ values. Figure 5-6 shows the calculated required resistance factor for various levels of past loading observed. This figure is only for a single distribution, denoted as "Original ϕ value" given by Paikowsky et al. (2004), and does not correspond to a specific resistance factor given in the LRFD Bridge Specification (AASHTO 2014).

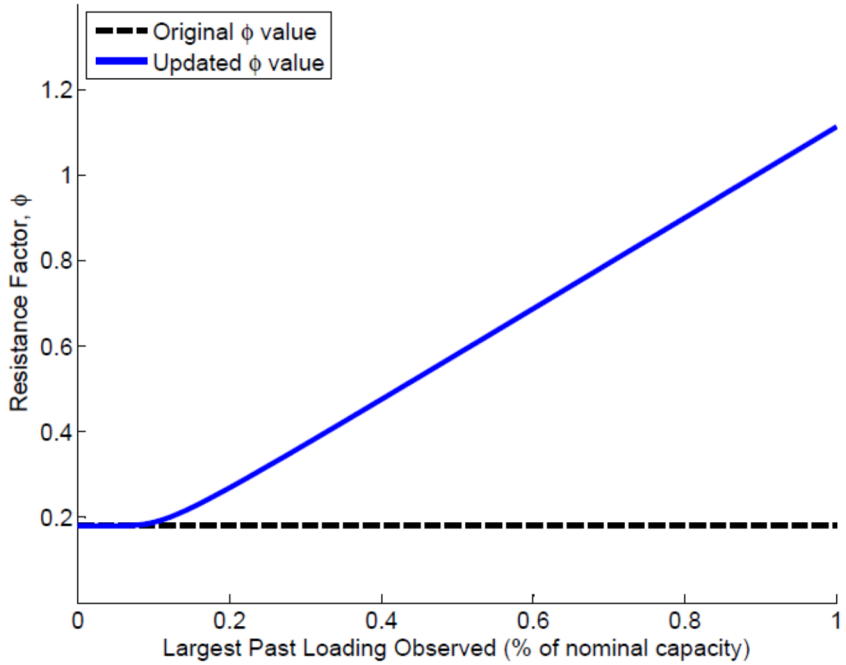

Figure 5-6: Updated Resistance Factor, ϕ, versus the largest load supported by pile group

Figure 5-7 shows the resistance factor as a function of largest previously applied loading for three cases of site variability. "Original ϕ value" in this figure refers to constant value of ϕ as per Paikowsky et al. (2004). The increase in resistance factor ϕ, with an increase in the largest previously applied loading becomes lesser as the site variability COV increases from 0.15 to 0.35. Nevertheless, benefit of higher value of resistance factor ϕ due to consideration of the largest previously applied load for all three site variabilities are obvious from Figure 5-7.

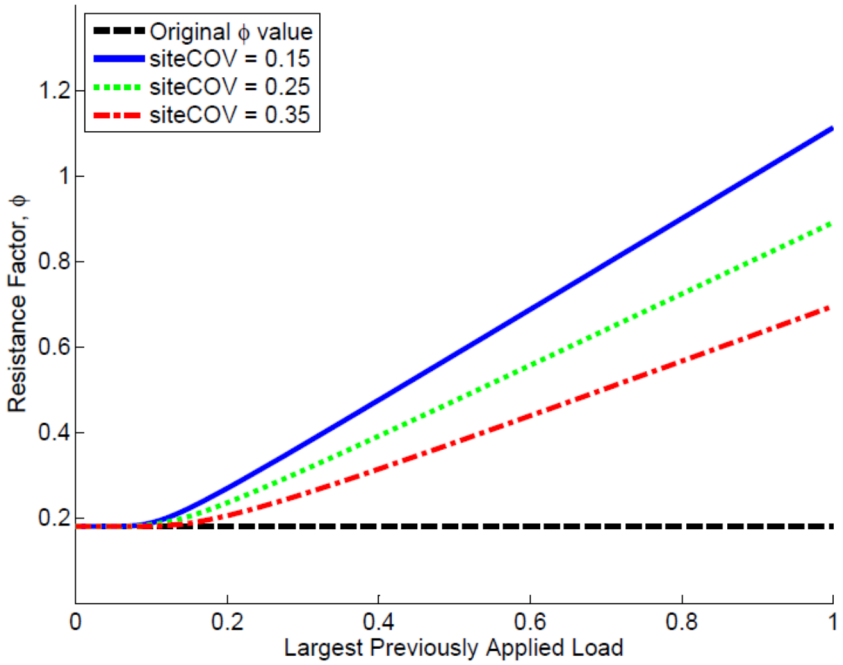

Figure 5-7: New resistance factor using varying site COVs

5.9 Impact of Uncertainty in Previously Applied Loading

A sensitivity analysis has been performed to understand the impact of uncertainty in the previously applied loading on the proposed methodology. An updated resistance factor, ϕ, was found considering 2 scenarios: the actual previous loading was deterministic, but higher or lower than estimated; and the previously loading was treated as a single probabilistic value with a variety of possible variances. The updated resistance factor (ϕ) for both analyses determines the resistance factor (ϕ) that is required to meet the target reliability (2.33), considering the actual (not estimated) loading. This procedure is useful for determining how sensitive the results are to inaccurate estimations of past loading. Figure 5-8(a) shows the impact of the previously applied loading being higher or lower than that expected for the β-method example on a site with an in-site coefficient of variation of 0.15 (the blue top line in Figure 5-7). Figure 5-8(b) shows the impact of a probabilistic loading being used to update the required resistance factor (ϕ) to maintain a reliability of 2.33 for the β-method example. This analysis finds the likelihood function shown graphically

in Figure 5-4 using a second reliability analysis that determines the probability of the group capacity being greater than the applied load. This greatly increases the computational time, as the methodology provided by Hasofer and Lind (1974) needs to be computed for many possible values of individual pile capacity, *x*, to numerically determine the integral in the denominator of Eq.(5-10).

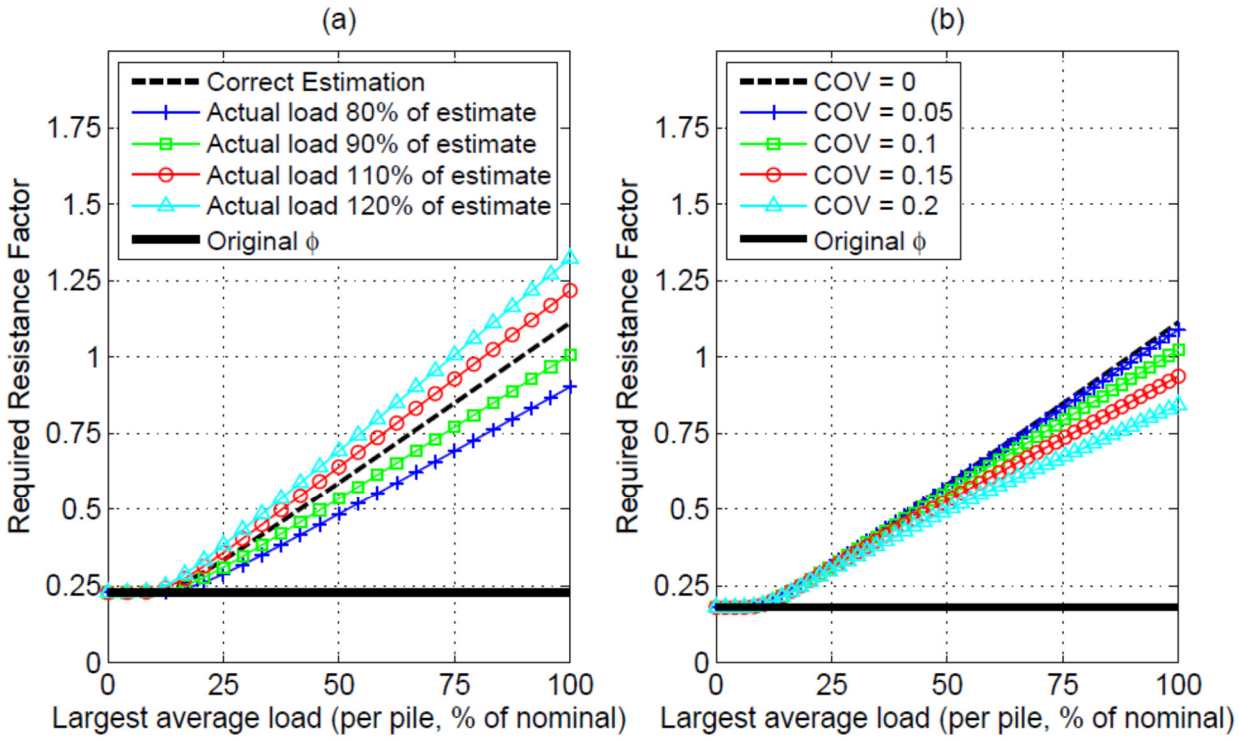

Figure 5-8: Updated resistance factors for test loads of various biases and variances

From Figure 5-8, a biased estimate of the previous loading applied impacts the updated curve even at very low loads (relative to nominal pile capacity). As expected, if the actual applied load is lower than estimated, a lower resistance factor (ϕ) is required to maintain a reliability index of 2.33, and a higher resistance factor (ϕ) maintains this index if the load was underestimated. Thus, an underestimate of the previous loading is a conservative choice. If the previous loading is treated as probabilistic, there is little impact at low previous loads relative to nominal pile

capacity). If the coefficient of variation of the previous load is 0.2 (the value typically used for live loads), then the reduction to the required resistance factor (ϕ) roughly matches that of a 20% reduction in deterministic load. However, permit loads are expected to have a much lower uncertainty than typical live loads due to reporting requirements and verification of truck weights. It is therefore recommended that the previous loading be treated as a deterministic load with an appropriately conservative estimate of load be used as the updating load. The level of conservatism should account for Figure 5-8. This allows use of Table 5-2 in the next section for updating purposes, rather than implementation of the entire methodology.

5.10 Application of Findings to LRFD Code

The statistical data on pile capacity distributions presented by Paikowsky et al. (2004) are divided into 41 static capacity prediction methods and 14 dynamic prediction methods. Each separate distribution will produce a new resistance factor, which may vary from the code prescribed resistance factor. The LRFD Bridge Specifications (AASHTO 2014) lump these into 7 resistance factors for static capacity calculation methods, 3 for dynamic calculation methods, and 4 for dynamic and static testing. The resistance factor obtained for each pile distribution do not necessarily match the corresponding LRFD resistance. Therefore, it is necessary to normalize Figure 5-6 to the prior code factor obtained for the various distributions in Paikowsky et al. (2004) that fit into that category.

For example, the α-method has a code prescribed resistance factor of 0.35 in clay and mixed soils. Paikowsky et al. (2004) list 11 different distributions for driven piles in clay, each with their own calibrated ϕ factor (ranging from 0.24 to 0.54, with an average of 0.38). To Apply the updating procedure, the curve shown in Figure 5-6 is obtained for each of these distributions

and normalized by dividing by the non-updated (prior) ϕ factor for each distribution (the dashed black line in Figure 5-6). The new curve represents the multiple of ϕ (as a function of permit load magnitude) that can be used while maintaining a minimum reliability of 2.33. To combine the various distribution provided in Paikowsky et al (2004) into the LRFD (AASHTO 2014) categories, the Paikowsky et al. (2004) data is aggregated into the respective design categories. A weighted average (to number of piles used in the statistical data) is taken of this collection of curves to find the percent increase in ϕ allowable that maintains the target reliability. The updating curve for the α-method is given in Figure 5-9.

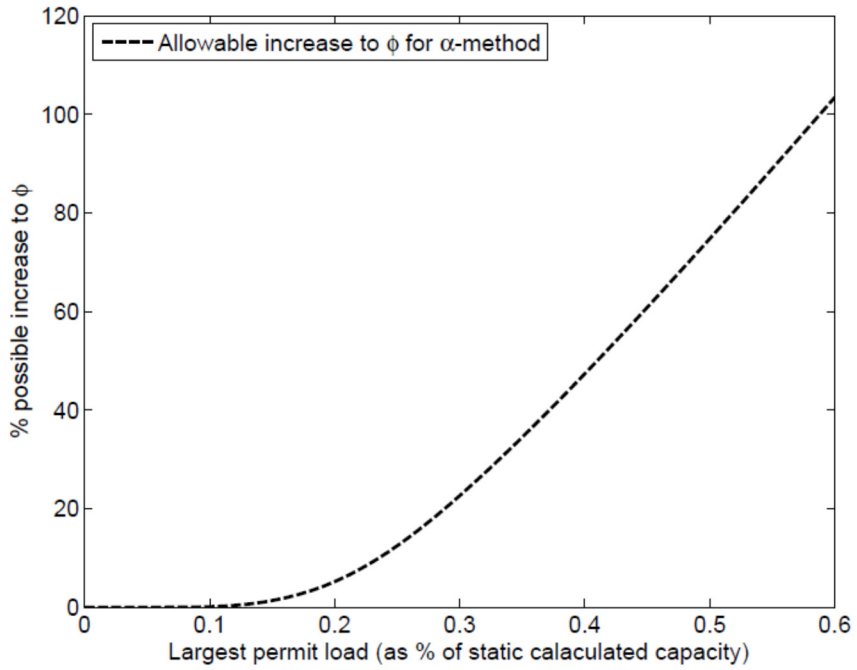

Figure 5-9: Updating curve for piles with capacities calculated using alpha method (site COV = 0.15)

This updating procedure is performed for all prediction methods where a prior distribution is obtainable. Table 5-2 provides the LRFD resistance factor alongside updated resistance factors using the above described methodology and a site variance of 0.15 (the same table for site variance of 0.25 and 0.35 are available in the supplemental data). The maximum past load should be a

conservative estimate of the average past load applied to each pile from all sources (accounting for the effects of load variance in Figure 5-8). The updated resistance factor for each method maintains a reliability index of 2.33 for each individual pile.

Table 5-2: Updated pile resistance factors for LRFD (low variability).

	Condition/Resistance Determination Method	Resistance Factor (LRFD)	Updated resistance factor Maximum past load (% of nominal)					
			10%	20%	30%	40%	50%	60%
Dynamic	WEAP	0.50	0.50	0.53	0.64	0.78	0.92	1.07
	FHWA-modified Gates	0.40	0.40	0.41	0.46	0.55	0.64	0.75
	ENR formula	0.10	0.11	0.14	0.19	0.24	0.30	0.35
Static	α-method	0.35	0.35	0.37	0.43	0.52	0.61	0.71
	β-method	0.25	0.25	0.28	0.34	0.41	0.49	0.58
	λ-method	0.40	0.40	0.43	0.50	0.59	0.70	0.81
	Nordlund/Thurman Method	0.45	0.45	0.45	0.47	0.54	0.62	0.70
	SPT-method	0.30	0.30	0.32	0.34	0.40	0.46	0.53
	CPT-method	0.50	0.50	0.50	0.50	0.52	0.57	0.63
	End bearing in rock	0.45	-	-	-	-	-	-

From Table 5-2, it is evident that that the updating methodology does not have a consistent effect on piles with capacities predicted from various methods. For piles with capacities predicted using wave equation analysis, it is possible to get a resistance factor above 1, higher than either the predicted capacity or previously applied load. This is due to the WEAP prediction method having a high bias of 1.656, and a high COV of 0.724. The updated PDF has an especially high likelihood of values greater than the predicted value, which is reflected in the updated reliability analysis. It may be desirable in practice to limit the capacity to the previous average loading applied. Conversely, the CPT-method is least suited to this updating method, although an increase

of 20% in the capacity is possible when the pile group withstood loading of 60% of the nominal capacity. The static capacity calculation methods can all have their resistance factors raised substantially, especially in low-COV populations. Piles that are end bearing in rock cannot be updated using this methodology, as little statistical data on these piles is available.

5.11 Determining Capacity without prior distribution

In some cases, obtaining a prior distribution of pile capacity may not be possible due to limited or unreliable subsurface information. For driven piles end bearing on rock, statistical data on capacity estimation is not readily available. For these scenarios the first methodology cannot be employed, and a second methodology is proposed to verify the capacity of existing piles, given only the previous loading history or the magnitude of test loads applied to the group of piles being investigated. The test load or previous loading occurs in conjunction with dead loads, earth pressure loads, and other permanent loads acting on the pile group being considered. The magnitude of the test load or previous load is defined as the *excess population mean (epm)*, or the average excess pile capacity beyond those permanent loads. This load is considered to be the average excess capacity of the pile group, although individual pile capacities will vary from each other and may be greater or lower than average.

A PDF of the excess capacity of an individual pile is obtained by assuming the piles of a single population are lognormally distributed with parameters μ and σ, obtained from Eq.(5-14) and Eq.(5-15). For this methodology, previously applied load or a test load is treated as deterministic, but all other loads acting on the pile (during current service life or reuse) can be assumed to be probabilistic. The total distribution of excess pile capacity is then given by Eq.(5-16),

$$\sigma^2 = (siteCOV^2 + 1) \tag{5-14}$$

$$\mu = -\frac{1}{2}\sigma^2 \tag{5-15}$$

$$excess\ pile\ capacity = epm * x_{epc} \tag{5-16}$$

where *epm* has been defined as the magnitude of the test load or previous load. In Eq.(5-16) $x_{epc} = LN(\mu,\sigma)$, a lognormal distribution with parameters μ and σ. A limit state equation is assembled in Eq.(5-17) for just the live loading to determine the nominal live loading that achieves the target reliability index,

$$G = epm * x_{epc} - LL_{nom} * x_{LL} \tag{5-17}$$

where LL_{nom} is the nominal live load and x_{LL} is the lognormal distribution of live loads described in Table 5-1. Following Ayyub and Assakkaf (1999), a reliability analysis can be performed using Eq.(5-17) with LL_{nom} iterated until the target reliability is reached. The allowable live load capacity (C_{LL}) (LRFD capacity beyond what is used for dead loads) is then found using Eq.(5-18). The total geotechnical capacity of the piles can be calculated by considering the Strength I limit state, as shown in Eq.(5-19). Since AASHTO (2014) uses capacities calibrated to this limit state for all limit states, this capacity is also considered to be applicable to all limit states.

$$C_{LL} = 1.75 * (LL_{nom}) \tag{5-18}$$

$$C_{tot} = 1.75(LL_{nom}) + 1.25(DL_{nom}) + \sum \gamma_P (P_{nom}) \tag{5-19}$$

In Eq.(5-19), DL_{nom} is the nominal dead load acting on the pile, P_{nom} are other nominal permanent loads acting on the pile, and γ_P are the load factors for those loads. Figure 5-10 shows the ratio of C_{LL} to the test load magnitude or largest permit load for a target reliability of 2.33.

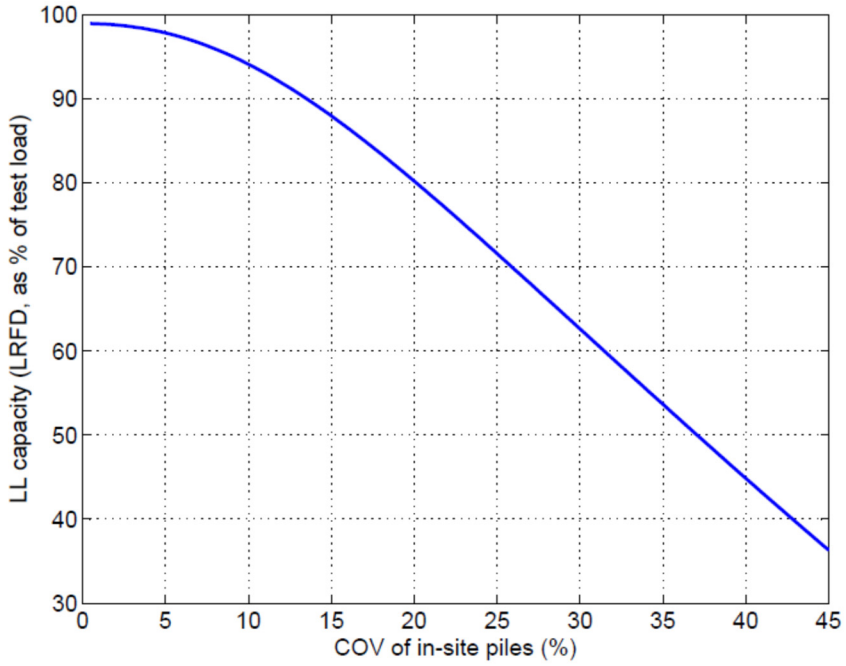

Figure 5-10: LL capacity of existing piles for various site COVs

To account for modified loading after reuse, a new limit state function is proposed to estimate the reliability of the piles after removal and replacement of the dead load, as shown in Eq.(5-20)

$$G = (epm)x_{epc} + DL_{rem}x_{DL,1} - DL_{new}x_{DL,2} - LL_{nom}x_{LL} \tag{5-20}$$

In Eq.(5-18), DL_{rem} is the dead load that will be removed and DL_{new} is the dead load that will be added during reuse. These two numbers can sum to zero if the total dead load acting on the piles does not change during reuse. The change in dead load, however, will cause a reduction in available live load capacity, as both the removed and new dead loads are variable. Figure 5-11

presents the factored LL capacity as a function of the test load or previously applied load, normalized with respect to the magnitude of the existing dead load for a site COV of 0.15.

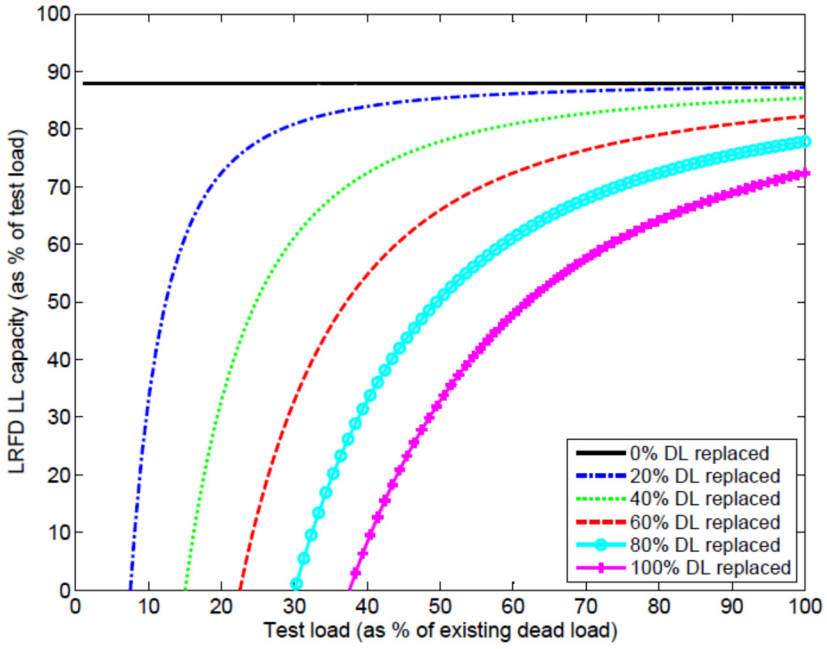

Figure 5-11: LL capacity as function of proof load for various magnitudes of DL replacement

It should be noted that this approach is able to explicitly include changes in the dead load during reuse in Eq.(5-18). It reduces to the live load testing shown in Figure 5-10 (for the 0.15 COV point) when there is no change in dead load. In case of increase in the dead load of the bridge because of bridge repurposing, this approach can also be used to design the maximum increase in the dead load that will allow the reuse of the bridge foundation. Then the design of superstructure can be optimized through analysis, modeling and innovative materials to limit increase in the dead load to this maximum allowable increase for reuse. Figure 5-12 shows plots for a pile foundation where 20% of the existing dead load was removed and replaced. In this figure, 5 different options are plotted: 2 with decreased new load, 2 with increased new dead load, and one that maintains the nominal dead load (although with uncertainties introduced by the swapping of 20% of the dead

load). The y-axis in Figure 5-12 shows the live load capacity (on top of new dead load) as a percentage of the test load applied to the original bridge. Note that the black line in Figure 5-12 is identical to the blue line (20% replaced) in Figure 5-11.

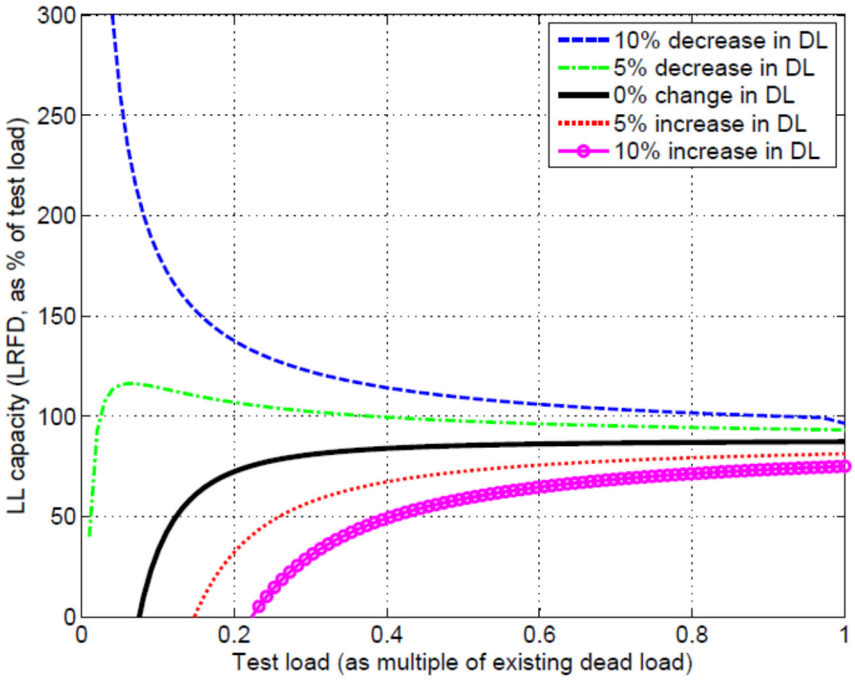

Figure 5-12: LL capacity of piles given changes to DL

5.12 Examples

Route 2A Bridge: Haynesville, ME

The Route 2A Bridge in Haynesville, ME is a 3-span steel girder bridge supported by mass concrete stub abutments and solid wall piers (Krusinksi 2015). Both piers and abutments are founded on driven timber piles installed through a loose silty sand layer that ranges in thickness from 4.6 to 10.4 m (15 to 34 ft). Both piers and one of the abutments were driven into a dense glacial till layer as indicated by borings and historical records of pile cutoff elevations. The 2nd abutment was believed to be terminated in the silty sand layer. The nominal pile capacity was calculated to be 329 kN (74 kips) per pile, including only 31 kN (7 kips) of end bearing resistance.

The nominal capacity is based on the Nordlund method for side resistance and the Thurman method for end bearing capacity. The factored capacity was found to be 147 kN (33 kips), nearly the same as the allowable strength design non-factored load capacity of 142 kN (32 kips) per pile found in historical records. Using the updated resistance factors in Table 5-2 and assuming low variability between the piles (COV = 15%), the resistance factor can be updated to include the maximum past loading, as shown in Figure 5-13. From this figure, the new LRFD capacity for each individual pile in the pile group (with on-site COV of 15%) is given as a function of the total loading, including dead loads and previous permit loading.

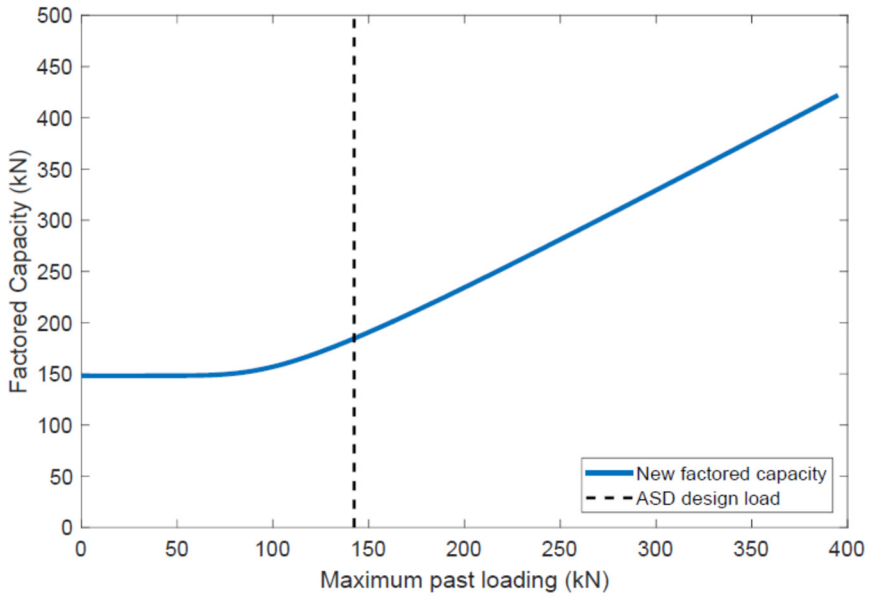

Figure 5-13: New factored capacity as a function of maximum past loading

Since the factored geotechnical capacity of 147 kN (33 kips) was not sufficient for design, the pile cap was excavated, and a single pile was load tested with a hydraulic jack. The pile failed at 534 kN (120 kips) of load, allowing for a factored capacity of 374 kN (84 kips). To achieve this factored capacity using this method, a loading of approximately 347 kN (78 kips) per pile would need to be applied to the abutments, for a total of 8,327 kN (1,872 kips) on the entire 24-pile

abutment. This is approximately 2.4 times the ASD design load of 3,416 kN (768 kips) on this abutment.

Jackson Road over Route 2: Lancaster, MA

The Jackson Road Bridge in Lancaster, MA (GTR 2014) was considered for replacement due to the age of the superstructure and accelerated deterioration. The two abutments and center pier of the original bridge were founded on timber piles. No load test data was available for the piles, although extensive driving logs, including details of the pile hammer, blow counts, and end-of-drive penetration were found in the documentation for the bridge. A range of possible capacities for each pile was determined using wave analysis, which were then compared to the expected future loading on each individual pile. It was determined that the total geotechnical capacity of the foundation was sufficient, but with several piles being overloaded when compared to their factored geotechnical capacity. The bridge was reconstructed with geofoam being used to replace the abutment soil. The replacement of this soil with geofoam lowered the loading on the overloaded pile enough to reuse the pile without modification.

A resistance factor of 0.5 is prescribed by the LRFD Bridge Design Specifications (AASHTO 2014) for use on piles with their capacity determined using wave analysis. Had the previous loading been considered, a higher resistance factor and LRFD capacity could be specified while maintaining a reliability index of 2.33 for the piles. A plot of the resistance factor that achieves a target reliability of 2.33 versus the maximum past loading is shown in Figure 5-14. From this figure, the required resistance factor to maintain the target reliability is plotted against possible values of the maximum previously applied loading, in kN.

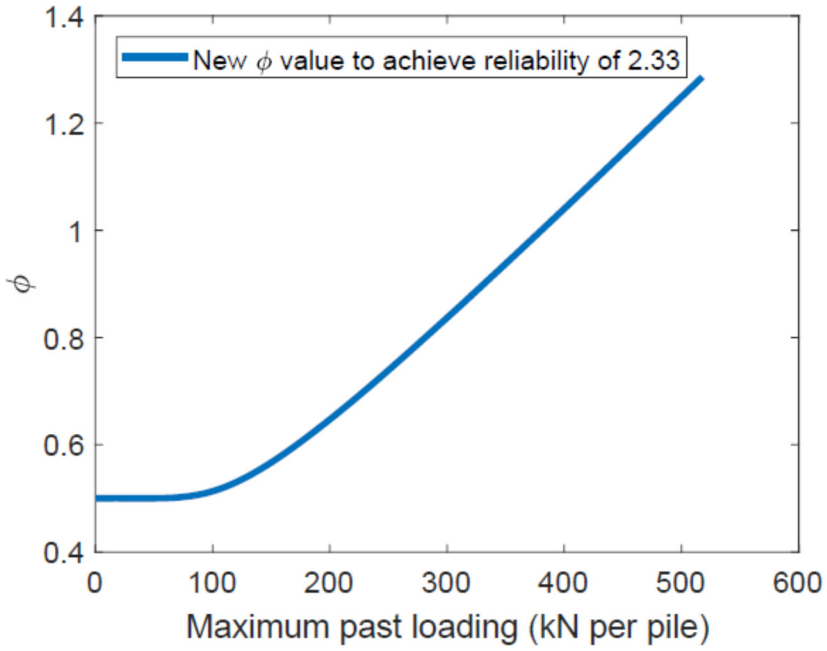

Figure 5-14: Updated resistance factors based on past loading

Route 1A Viaduct, Bath ME

The Route 1A viaduct in Bath, ME (Haley and Aldrich 2013) consisted of 19 piers and abutments, supported by a mixture of driven steel H-piles and spread footings bearing on rock. The H-piles were visually examined to be in good condition. The parallel seismic testing ensured that the piles were driven to the top of bedrock. The piers were reused with the original foundations with the pile capacity considered to be governed by the structural capacity of the piles. Without making any assumptions about the soil or rock conditions, each group could be analyzed for capacity based solely on the maximum previous loading. Assuming a 30% replacement of dead load on the bridge, a graph of total pile capacity versus total previous load can be made, as shown in Figure 5-15. This figure provides the total LRFD capacity of the individual piles in the foundation as a function of the total previously applied loading.

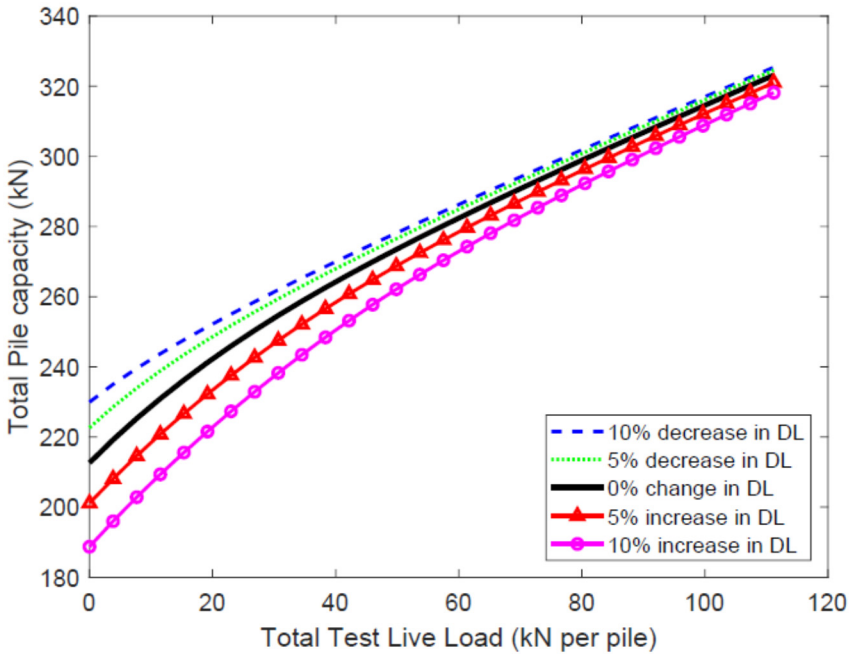

Figure 5-15: Capacity versus test load for Pier 5

5.13 Conclusions

The proposed methodology allows engineers to consider previous loading on pile groups when determining the capacity of a single pile. By considering the maximum previous loading applied to an entire pile group, a higher resistance factor for individual pile geotechnical capacity can be used by the design engineer while maintaining a constant reliability index. The use of a higher resistance factor and capacity may allow the design of a reused foundation to forego expensive strengthening, load reduction techniques, or individual pile testing to ensure piles have adequate capacity. A second methodology is provided that allows engineers to determine the capacity of a pile, given no data except the average loading held by the piles previously. This methodology is useful for determining the capacity of piles bearing on rock with no available static test data. This method effectively applies a resistance factor that ranges from 0.5 to 0.9 on the live load capacity, as determined through placement of a known weight. The effective code factor on dead loads is determined considering the amount of load removed and replaced, and the total

change in dead load. The capacity obtained using this method can be applied to other load cases, although the capacity determined does not consider past earthquake or wind loading.

5.14 Future Work

Further work is needed to determine appropriate probabilistic distributions for lateral earth pressure loading and other loading. Inclusion of past earthquakes, downdrag, and other loading can be considered as other sources of previous loading, as well as potential sources of future loading. Hazards like downdrag and scour that reduce the pile length available for resistance can also be considered. This method can be adapted to be used with sensors, such as strain gauges, to measure the forces going into individual piles. Further statistical data can be gathered on the resistance of piles end bearing in rock. This methodology can be further explored to include measurements of bridge movement during loading or unloading. Research is needed into determining the impacts of group effects from closely spaced piles. The methodology can be adapted to include data from embedded sensors at the base of the piles to determine the amount of strain being transferred to the pile tip.

5.15 Acknowledgements

The research presented in this paper has been supported through the foundation characterization program of Federal Highway administration, contract no. DTFH61-14-D-00010/0002. Any opinions, findings, and conclusions or recommendations expressed in this paper are those of the authors and do not necessarily reflect the views of the Federal Highway Administration.

5.16 References

AASHTO (American Association of State Highway Transportation Officials). (2014) AASHTO LRFD Bridge Design Specifications, Customary U.S. Units, 7th Edition. AASHTO, Washington, D.C.

Abdallah, Y., Najjar, S. Saad, G. (2015) Impact of Proof Load Test Programs on the Reliability of Foundations. IFCEE 2015, March 17-21, 2015. San Antonio, Texas.

Allen, T. M. (2005). Development of Geotechnical Resistance Factors and Downdrag Load Factors for LRFD Foundation Strength Limit State Design, FHWA-NHI-05-052, Federal Highway Administration, U.S. Department of Transportation, Washington, DC.

Ang, A. H-S., and Tang, W. H. (1975). *Probability Concepts in Engineering Planning and Design*, Vol 1, Basic Principles. John Wiley & Sons, New York.

Ayyub, B., and Assakkaf, I. (1999) LRFD Rules for Naval Surface Ship Structures: Reliability-Based Load and Resistance Factor Design Rules. Naval Surface Warfare Center, Carderock Division, U.S. Navy.

Barker, R., Duncan, J., Rojiani, K., Ooi, P., Tan, C., and Kim, S. (1991) NCHRP Report 343: Manuals for the Design of Bridge Foundations. TRB, National Research Council, Washington, DC.

Collin, J. G. and Jalinoos, F. (2014). "Foundation Characterization Program: TechBrief #1—Workshop Report on the Reuse of Bridge Foundations." Publication FHWA-HRT-14-072, Federal Highway Administration, Washington, D.C.

Ellingwood, B., Galambos, T. (1982). Probability-Based Criteria for Structural Design. Structural Safety, Vol.1, pp. 15–26.

Ellingwood, B., Galambos, T., MacGregor, J., and Cornell C. (1980) Development of a Probability-Based Load Criterion for American National A58. National Bureau of Standards Publication 577. Washington, DC.

Evangelista, A., Pellegrino, A., and Viggiani, C. (1977). "Variability among piles of the same foundation." *Proceedings of the 9th International Conference on Soil Mechanics and Foundation Engineering,* Tokyo, 493-500.

Geosciences Testing and Research, Inc. (GTR) (2014). "Jackson Road over Route 2 Evaluation of Existing Timber Pile Capacity Report. Letter Report to Lin Associates Incorporated.

Haley and Aldrich (2013). Preliminary Geotechnical Design Report U.S. Route 1 Viaduct Bridge Rehabilitation MAINEDOT WIN 19273.00 Bath, Maine. Maine Department of Transportation, Augusta, ME

Hasofer, A. M., and Lind, N. C. (1974). An Exact and Invariant First-Order Reliability Format. Journal of Engineering Mechanics, Vol. 100. No. EM1, pp. 111–121.

Huang, J., Kelly, R., Li, D., Zhou, C., Sloan, S. (2016) Updating reliability of single piles and pile groups by load tests. Computers and Geotechnics, Vol. 73 pp. 221 to 230.

Kay, J. N. (1976). "Safety factor evaluation for single piles in sand." *Journal of Geotechnical Engineering,* ASCE, 102(10), pp. 1093-1108.

Kusinksi, L. (2015). *Geotechnical Report for Haynesville Bridge U.S. Route 2A over Mattawamkeag River Haynesville, ME* Fed No. STP-2050(900)X Maine Department of Transportation Augusta, ME

MathWorks, Inc. (2016) MATLAB and Statistics Toolbox Release 2016b, Natick, Massachusetts

Moses, F., and Verma, D. 1987. NCHRP Report 301: Load Capacity Evaluation of Existing Bridges. TRB, Washington, DC.

Nowak, A. (1999). Calibration of LRFD Bridge Design Code., NCHRP 368, Transportation Research Board, Washington, D.C., 20001

Paikowsky, S., Birgisson, B., McVay, M., Nguyen, T., Kuo, C., Baecher, G., Ayyub, B., Stenersen, K., O'Malley, K., Chernauskas, L., O'Neill, M. (2004). Design (LRFD) for Deep Foundations. NCHRP REPORT 507, Transportation Research Board, Washington, D.C., 20001

Park, J.H., Chung, M., Huh, J. (2015) Reliability Based Resistance Factor Calibration and Implementation of Axially Loaded Piles. *Proceedings of the 25th International Ocean and Polar Engineering Conference. Kona, HA, USA.*

Phoon, K. K. and Kulhawy, F. H. (1996) Practical reliability-based design approach for foundation engineering, Transportation Research Record, 1546, 94–99.

Phoon, K. K., Kulhawy, F. H., and Grigoriu, M. D. (2003). "Development of A Reliability-Based Design Framework for Transmission Line Structure Foundations." Journal of Geotechnical and Geoenvironmental Engineering, Vol. 129, No. 9, pp. 798 - 806.

Withiam, J. L., Voytko, E. P., Barker, R. M., Duncan, J. M., Kelly, B. C., Musser, S. C., & Elias, V. (1998). Load and resistance factor design (LRFD) for highway bridge substructures. Report FHWA HI-98-032. Federal Highway Administration, Washington, DC.

Yang, Luo. (2006) "Reliability-based design and quality control of driven piles." PhD Dissertation, University of Akron, Akron, OH

Zhang, J., Boothroyd, P., Calvello, M., Eddleston, M., Grimal, A.C., Iason, P., Luo, Z., Najjar, S., Rodriguez-Marek, A., Straub, D., Uzielli, M., Wang, Y., Walter, H. (2017) Bayesian Method: A natural Tool for processing Geotechnical Information. Joint TC205/TC304 Working Group on "Discussion of statistical/reliability methods for Eurocodes".

Zhang, L., and W. Tang. (2002) "Use of Load Tests for Reducing Pile Length." Deep Foundations, ASCE, Reston, VA 993-1005

Chapter 6 Conclusions

6.1 Overarching Research Conclusions for Foundation Reuse

A primary conclusion of this research is that foundation reuse is a viable technology that will increase in usage due to reduced costs. The viability of this technology has been evidenced by numerous case studies where existing bridge foundation elements were reused successfully for lower costs than projected for new foundation construction. The novel research conducted in support of the *Foundation Reuse for Highway Bridges* report (Agrawal et al. 2018) identified specific approaches that can facilitate management decisions associated with foundation reuse consideration. The research presented in this dissertation identified a methodology for identifying the behavior and parameters of a foundation system and detecting changes to that system over time. A load rating methodology for foundations was capable of accounting for foundation movement, changes to substructure components, and geo-hazards such as scour. A methodology was proposed to update the capacity of piles determined from empirical equations. Overall, the novel methodology investigated contribution to the conclusion that many techniques for managing foundation reuse are available but have not been codified into existence due to a previous lack of research activity and interest in reuse-specific technologies.

6.2 Contributions of Research in Foundation Reuse

The novel research contained in this dissertation has several notable contributions. The foundation identification technique proposed in Chapter 3 provides a methodology for modeling actual foundation behavior for estimating foundation parameters. The proposed method is capable of being adapted into a long-term monitoring scheme that can be used to identify changes to the foundation system and its behavior. The estimation of foundation parameters can potentially be used to identify unknown parameters of foundations, such as soil shear modulus, foundation depth,

and material properties. With some further extensions, the methodology may be capable of distinguishing between various foundation types.

The load rating procedure proposed in Chapter 4 is believed by the author to be the most comprehensive research into the load rating of foundations conducted to this point. Other research investigating load rating was discussed in Chapter 4 that was limited in scope or incapable of assessing very common issues encountered with foundations. The proposed method can account for preexisting settlement, possible future settlement, deterioration of substructure components, functionality issues (opening of expansion joints, over-rotation of bearings, knocking, etc.), and superstructure strength issues resulting from settlement-induced loading.

The pile capacity updating methodology proposed in Chapter 5 provides a novel method for determining pile capacity when test data is not available. Reuse cases had been observed where the lack of test data for the foundation limited capacity estimation techniques to methods with low resistance factors that typically produce inefficient designs. The proposed methodology demonstrated that the consideration of past loading allowed for new probabilistic distributions to be created that accounts for previous loading on a group of driven piles. Including this past loading was demonstrated to allow for high resistance factors while maintaining the LRFD prescribed target reliability.

Overall, this research resulted in a thorough documentation of the state of practice in foundation reuse, provided by the *Foundation Reuse for Highway Bridges* (Agrawal et al. 2018). This manual provides an in-depth resource for practicing engineers and bridge owners interested in evaluating aging bridge foundations for reuse consideration. As little previous research exists

for reused bridge foundations in the US, this resource helps identify the standard of care that is commonly used for reused foundations.

6.3 Future Work

Various avenues of future research have been identified throughout the research conducted in this dissertation. The foundation identification technique proposed in Chapter 3 can be extended to help identify scour, determine foundation type, and provide a near real-time (based on how data is aggregated) monitoring capability. To identify scour and determine foundation type, the method will need to be extended with a statistical analysis of observed data. The statistical analysis will need to account for the variation observed in the acquired data and the sensitivity of various parameters to the outcome of the method.

The load rating methodology proposed in Chapter 4 requires further investigation prior to widespread implementation in the National Bridge Inspection Standards (NBIS). Since the NBIS needs to be suitable for all types of bridge, it should be further investigated how the load rating of superstructures subjected to foundation movement changes by superstructure type and material. Long-term effects such as creep and relaxation were ignored in the present research, but inclusion of these effects may substantially increase the amount of tolerable movement determined during application of this methodology. Further investigation to assess damage scenarios and strengthened components when performing load rating of substructure components would provide a more holistic view of the load rating procedure for foundation elements. To enact the use of the substructure functionality index (SFI), functional limits for various components should be research and compiled.

The pile capacity updating methods presented in Chapter 5 also has further work that can be performed to verify the adequacy and applicability of the methodology. The method as proposed does not account for uncertainty behind earth pressure loading on multiple rows of piles and other probabilistic sources of loading. The method has not yet been extended to include sources of previous loading such as earthquakes, scour, downdrag, and liquefaction. Investigation into how these loads when previously applied to a foundation can impact the reliability analysis and understanding of current pile capacity can improve the updating procedure. This method can also be extended to include use of data from sensors, such as measured foundation movements, strain measurements from individual piles or foundation elements, and other potential sources of information. Further research would be required to extend this methodology to piles in closely spaced groups with non-trivial amounts of pile group interaction.

6.4 References

Agrawal, A.K., Jalinoos, F., Davis, N.T., Hoomaan, E., Sanayei, M. (2018) *Foundation Reuse for Highway Bridges*. FHWA Office of Research, Development, and Technology. McLean, VA 22101

Appendix A

Integrated Superstructure-Substructure Load Rating for Bridges with Foundation Movements-Supplemental Data

Reinforced Concrete Piers

For reinforced concrete piers, the combined axial and moment capacity is calculated through the use of an interaction diagram, as outlined in ACI (2015). For circular piers, since the cross-section is radially symmetric, biaxial bending moments about two axes can be resolved into a resultant bending moment (M_u), as shown in Eq.(S1),

$$M_U^2 = M_x^2 + M_y^2 \tag{A-1}$$

This resultant moment is then used with the interaction diagram in Figure 1 with the ultimate axial force to determine if the section has enough capacity.

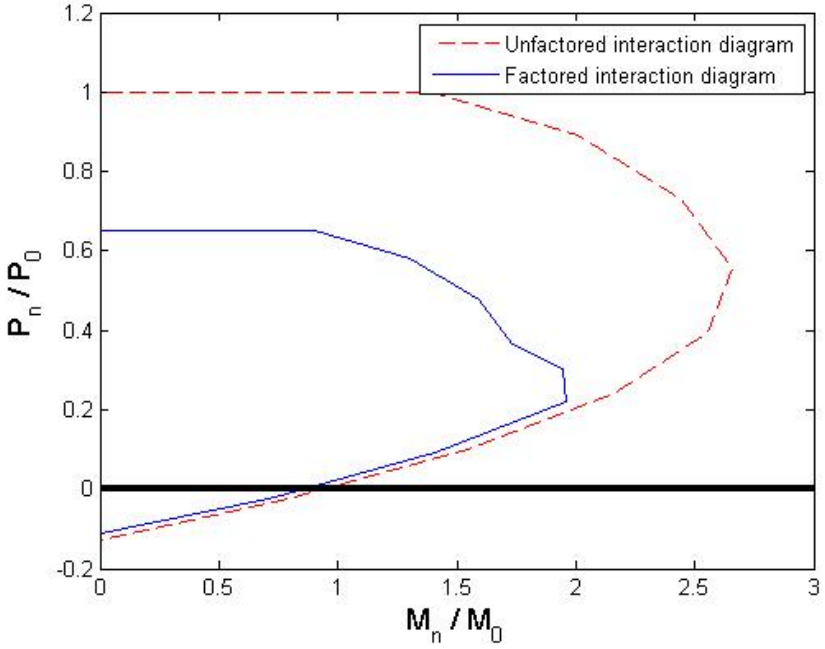

Figure A0-1: Interaction diagram for uniaxial bending

For rectangular columns, the interaction surface becomes more complex. In this case, section 5.7.4.5 of AASHTO (2014) allows for one of two approximate equations to be used. When the column has significant axial load ($P_n \geq 0.10\phi f_c' A_g$), factored total axial resistance (P_{rxy}) can be calculated by Eq. (S2),

$$\frac{1}{P_{rxy}} = \frac{1}{P_{rx}} + \frac{1}{P_{ry}} - \frac{1}{\phi P_o} \tag{A-2}$$

where P_o is given by Eq. 5.7.4.5-2 of AASHTO (2014), ϕ is the LRFD resistance factor, P_{rx} is the factored total axial resistance only considering e_y, and P_{ry} is the factored total axial resistance only considering e_x. When $P_n < 0.10\phi f_c' A_g$, the capacity is defined by the following equation,

$$\frac{M_{ux}}{M_{rx}} + \frac{M_{uy}}{M_{ry}} \leq 1.0 \tag{A-3}$$

where M_{rx} and M_{ry} are the nominal moment capacities in the x and y directions, respectively.

Steel Piers

There are two conditions prescribed by the AASHTO (2014) for steel columns undergoing combined flexure and axial loads. If $P_u/P_r < 0.2$, P_u being the factored applied axial load and P_r being the factored resistance, then the capacity is estimated by Eq.(S4) below,

$$\frac{P_u}{2P_r} + \left(\frac{M_{ux}}{M_{rx}} + \frac{M_{uy}}{M_{ry}} \right) \leq 1.0 \tag{A-4}$$

However, if $P_u/P_r > 0.2$, the capacity is estimated by Eq.(S5) below,

$$\frac{P_u}{P_r} + \frac{8.0}{9.0}\left(\frac{M_{ux}}{M_{rx}} + \frac{M_{uy}}{M_{ry}} \right) \leq 1.0 \tag{A-5}$$

where M_{rx} and M_{ry} are the nominal moment capacities in the x and y directions, respectively.

Timber Piers

Section 8.10.1 of the AASHTO (2014) states the following two conditions must be satisfied for all timber members

$$\frac{P_u}{P_r} + \frac{M_u}{M_r^*} \leq 1.0 \tag{A-6}$$

$$\frac{M_u - \frac{d}{6} P_u}{M_r^{**}} \tag{A-7}$$

Where $M_r^* = F_b S$, and M_r^{**} is the factored resistance adjusted by all applicable adjustment factors except CV.

Appendix B

Determining the Capacity of Reused Bridge Foundations from Limited Information- Supplemental Data

Table B0-1: Updated pile Resistance factors for LRFD (low variability)

	Condition/Resistance Determination Method	Resistance Factor (LRFD)	Updated resistance factor Maximum past load (% of nominal):					
			10%	20%	30%	40%	50%	60%
Dynamic	WEAP	0.50	0.50	0.53	0.64	0.78	0.92	1.07
	FHWA-modified Gates	0.40	0.40	0.41	0.46	0.55	0.64	0.75
	ENR formula	0.10	0.11	0.14	0.19	0.24	0.30	0.35
Static	α-method	0.35	0.35	0.37	0.43	0.52	0.61	0.71
	β-method	0.25	0.25	0.28	0.34	0.41	0.49	0.58
	λ-method	0.40	0.40	0.43	0.50	0.59	0.70	0.81
	Nordlund/Thurman Method	0.45	0.45	0.45	0.47	0.54	0.62	0.70
	SPT-method	0.30	0.30	0.32	0.34	0.40	0.46	0.53
	CPT-method	0.50	0.50	0.50	0.50	0.52	0.57	0.63
	End bearing in rock	0.45	-	-	-	-	-	-

Table B0-2: Updated pile Resistance factors for LRFD (medium variability)

	Condition/Resistance Determination Method	Resistance Factor (LRFD)	Updated resistance factor Maximum past load (% of nominal):					
			10%	20%	30%	40%	50%	60%
Dynamic	WEAP	0.50	0.50	0.52	0.59	0.69	0.79	0.91
	FHWA-modified Gates	0.40	0.40	0.40	0.43	0.48	0.55	0.62
	ENR formula	0.10	0.10	0.13	0.17	0.21	0.25	0.29
Static	α-method	0.35	0.35	0.36	0.39	0.44	0.51	0.58
	β-method	0.25	0.25	0.27	0.30	0.35	0.41	0.47
	λ-method	0.40	0.40	0.42	0.46	0.51	0.58	0.66
	Nordlund/Thurman Method	0.45	0.45	0.45	0.46	0.49	0.53	0.59
	SPT-method	0.30	0.30	0.31	0.32	0.35	0.39	0.44
	CPT-method	0.50	0.50	0.50	0.50	0.50	0.50	0.53
	End bearing in rock	0.45	-	-	-	-	-	-

Table B0-3: Updated pile Resistance factors for LRFD (high variability)

	Condition/Resistance Determination Method	Resistance Factor (LRFD)	Updated resistance factor Maximum past load (% of nominal):					
			10%	20%	30%	40%	50%	60%
Dynamic	WEAP	0.50	0.50	0.51	0.54	0.60	0.68	0.76
	FHWA-modified Gates	0.40	0.40	0.40	0.40	0.42	0.46	0.51
	ENR formula	0.10	0.10	0.12	0.15	0.18	0.21	0.24
Static	α-method	0.35	0.35	0.35	0.36	0.38	0.42	0.47
	β-method	0.25	0.25	0.26	0.27	0.30	0.34	0.37
	λ-method	0.40	0.40	0.40	0.43	0.46	0.50	0.55
	Nordlund/Thurman Method	0.45	0.45	0.45	0.45	0.45	0.47	0.50
	SPT-method	0.30	0.30	0.31	0.31	0.32	0.34	0.36
	CPT-method	0.50	0.50	0.50	0.50	0.51	0.52	0.54
	End bearing in rock	0.45	-	-	-	-	-	-